Acylation of Therapeutic Peptides

Interaction with Lipid Membranes and its Implications in Oral Delivery

Trier, Sofie; Andresen, Thomas Lars; Henriksen, Jonas Rosager; Jensen, Simon Bjerregaard

Publication date:
2016

Document Version
Publisher's PDF, also known as Version of record

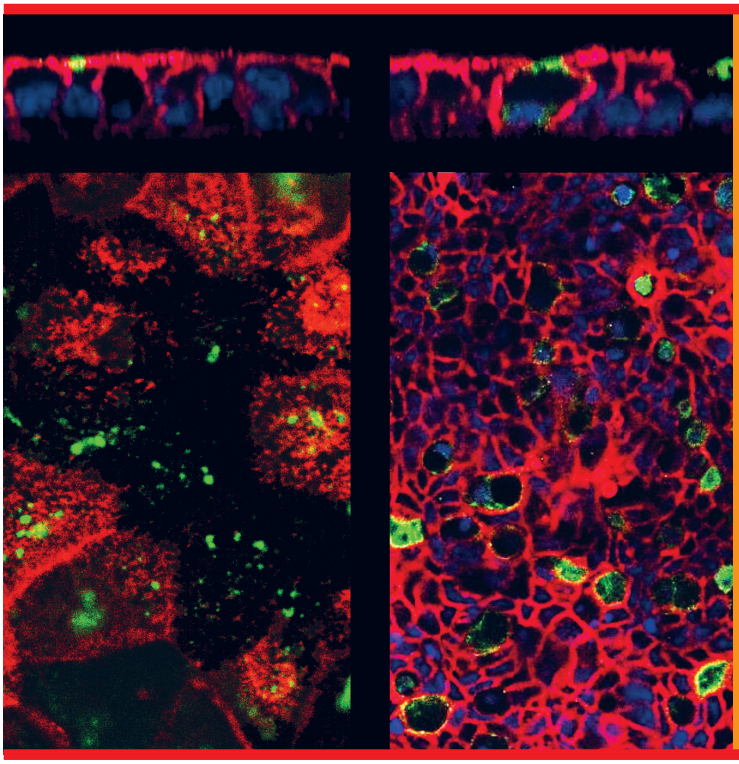

Acylation of Therapeutic Peptides

Interaction with Lipid Membranes and its Implications in Oral Delivery

Sofie Trier
PhD Thesis June 2016

DTU Nanotech
Department of Micro- and Nanotechnology

Acylation of Therapeutic Peptides

Interaction with Lipid Membranes and its Implications in Oral Delivery

PhD thesis
June 2016

Sofie Trier

Supervised by Thomas L. Andresen, Ulrik L. Rahbek, Holger M. Strauss, Lars Linderoth and Simon Bjerregaard.

Acylation of Therapeutic Peptides - Interaction with Lipid Membranes and its Implications in Oral Delivery

This thesis was typeset using LaTeX. Figures were generated in Prism, Gnuplot, GIMP and Inkscape.

Technical University of Denmark
Department of Micro- and Nanotechnology
Ørsteds Plads
Building 345E
DK-2800 Kongens Lyngby
Denmark

Novo Nordisk A/S
Global Research
Novo Nordisk Park 1
DK-2760 Måløv
Denmark

Preface

This thesis is submitted as part of the requirements for obtaining the PhD degree at the Technical University of Denmark (DTU). The thesis is the results of an industrial PhD project at DTU and Novo Nordisk A/S, which was funded by the Danish Innovation Fund (previously named the Danish Research and Innovation council) and Novo Nordisk. The project was supervised by Professor Thomas L. Andresen (university supervisor), Senior Scientist Holger M. Strauss (main company supervisor), Principal Scientist Simon Bjerregaard (company co-supervisor), Senior Director Ulrik L. Rahbek (company co-supervisor) and Team manager Lars Linderoth (company co-supervisor). The work was carried out partly at the Department of Micro- and Nanotechnology, DTU Nanotech, in the Colloids and Biological Interfaces Group, and partly in Novo Nordisk, in the Biophysics and Characterization, Oral formulation, Protein and peptide chemistry, and ADME (Absorption, Distribution, Metabolism and Excretion) departments. The project commenced in January 2012 and, following various detours, was concluded in the summer of 2016. In a two-month period from April to May 2012 I visited the lab of Professor Chi Wu at the Chinese University of Hong Kong. In two roughly 7-months periods I was on maternity leave (August 2013 - February 2014 and June 2015 - January 2016), and a short while before the expected project conclusion I assumed a position in Novo Nordisk, which caused a delay in the thesis writing.

There are many people who have helped me throughout this project. First and foremost, I am grateful to all my supervisors for giving me the opportunity to join their groups and departments, and for providing valuable guidance and help throughout the course of the project. At DTU, the Colloids and Biological Interfaces Group created an interesting and helpful working atmosphere, and I would particularly like to thank Jonas Henriksen and Kasper Kristensen for helpful guidance and discussions along the way. I also thank Hsih-Yin Tan for a great collaboration on the microfluidic caco-2 setup. At Novo Nordisk, the aforementioned departments have welcomed me into their inspiring working groups, where numerous people have helped me during the project. Particularly, Lisette G. Nielsen, Trine Moghaddam, Tine T. Mellergaard, Anette Heerwagen, Gitte Hedelund and Stephen Buckley helped with cell culturing and experiments; Anja Knudsen aided in peptide synthesis and purification; Anette Koch, Henning Gustafsson, Berit Bergerud, Marie Ø. Pedersen, Andrew J. Benie, Per-Olof Wahlund and Jesper S. Pedersen aided with biophysical characterization.

In connection with my stay in Hong Kong, I would like to thank Professor Chi Wu for giving me the opportunity to visit his lab and for providing accomodations during the stay. Additionally, I would like to express my gratitude to his group members (particularly Zhoujun Dai) for welcoming me and ensuring a memorable stay in the amazing city of Hong Kong.

Last, but not least, I would like to thank my family, friends, and my husband Anders for their support and patience during the twists and turns of the project.

Abstract

Oral administration of therapeutic peptides could benefit millions of chronically ill people worldwide, through easier and less stigmatized therapy, and likely improve the long-term effects of currently widespread disease mismanagement. However, oral peptide delivery is a formidable task due to the harsh and selective gastrointestinal system, and development has lacked far behind injection therapy.

Peptide acylation is a powerful tool to alter the pharmacokinetics, biophysical properties and chemical stability of injectable peptide drugs, primarily used to prolong blood circulation, but it is not widely studied in an oral context. As acylation furthermore increases interactions with the lipid membranes of mammalian cells, it offers several potential benefits for oral delivery of therapeutic peptides, and we hypothesize that tailoring the acylation may be used to optimize intestinal translocation.

This work aims to characterize acylated analogues of two therapeutic peptides by systematically increasing acyl chain length in order to elucidate its influence on membrane interaction and intestinal cell translocation *in vitro*. The studied peptides are the 33 amino acid Glucagon-like peptide-2 (GLP-2) , which promotes intestinal growth and is used to treat bowel disorders such as inflammatory bowel diseases and short bowel syndrome, and the 32 amino acid salmon calcitonin (sCT), which lowers blood calcium and is employed in the treatment of post-menopausal osteoporosis and hypercalcemia. The two peptides are similar in size and structure, but oppositely charged at physiological pH. Both peptides were acylated with linear acyl chains of systematically increasing length, where sCT was furthermore acylated at two different positions on the peptide backbone.

For GLP-2, we found that increasing acyl chain length caused increased self-association and binding to lipid and cell membranes, whereas translocation across intestinal cells displayed a non-linear dependence on chain length. Short and medium chains improved translocation compared to the native peptide, whereas long chain acylation displayed no improvement in translocation. This indicates an initial translocation benefit for shorter chains through increased interaction with the cell membrane, which reverts to a hindrance for long chains, i.e. the analogues get stuck in the cell membrane. Co-administration of a paracellular absorption enhancer was found to increase translocation similarly for each analogue while retaining acyl chain length dependence. A transcellular enhancer displayed increased synergy with the long chain acylation, consistent with increased membrane fluidization 'liberating' bound peptide, although medium chain acylation remained optimal overall. The results indicate that rational acylation of GLP-2 can increase its *in vitro* intestinal absorption, alone or in combination with permeation enhancers, and are consistent with the initial project hypothesis.

For sCT, an unpredicted effect of acylation largely superseded the anticipated membrane interactions; i.e. acylated sCT acted as its own *in vitro* intestinal permeation enhancer. Acylated analogues permeabilized lipid membranes, causing drastically increased peptide permeability through reversible cell effect similar to transcellular permeation enhancers. The effect likely stems from a synergy between the positive peptide charge and membrane-active acyl moiety, supported by its pH-dependency, whereby the effect increased with decreasing pH and concomitant charge increase. The extent of permeation enhancing effect was highly dependent on acylation chain length and position, with highest peptide permeability for short chain N-terminal acylation or

medium/long chain Lys18 acylation, whereas permeability and cell membrane binding appeared correlated only for some analogues. However, prolonged heating and/or solution storage of certain acylated sCT analogues caused aggregation in physiological buffer solutions, potentially forming fibril-like structures. Lys18 acylation appeared superior to N-terminal acylation, most clearly exemplified by the short chain analogues, however, no systematic dependence on acylation chain length was apparent. All analogues could be monomerized by addition of cyclodextrin, however, their separate permeability enhancing effects were reduced in the mixtures, and the additive was not investigated further. Thus, acylation of sCT for oral delivery purposes may not be indiscriminately applicable, and requires rational choices of acylation details and/or additives.

Further investigations of the most cell-permeable sCT analogues unveiled quite distinct permeation enhancer effects, ranging from high membrane binding / high permeability and non-specific enhancing effect on model compounds, to very low membrane binding / high permeability and very limited unspecific permeation enhancer effects, i.e. selective and efficient translocation.

Peptide receptor potency was retained for GLP-2 analogues following acylation, whereas sCT analogues displayed substantially reduced potency, depending on acylation position and length.

Overall, rational acylation of the studied peptides can increase *in vitro* intestinal permeability, modestly for GLP-2 and drastically for sCT, and might benefit oral delivery. GLP-2 results provide a well-founded predictive power for future peptide analogues, whereas sCT results hold great promise for future analogues, albeit with a larger uncertainty in predictions.

Resumé

At kunne administrere terapeutiske peptider oralt ville gavne millioner af kronisk syge mennesker verden over, igennem lettere og midre stigmatiserende behandling, og forbedre forebyggelsen af komplikationer og følgesygdomme som følge af utilstrækkelig sygdomsregulering. Men oral peptid-behandling er en udfordring på grund af det skrappe og selektive tarmsystem, og udviklingen har haltet langt efter præperater til injektion.

Acylering af peptider er et kraftfuldt værktøj til at ændre farmakokinetik, biofysiske egenskaber og kemisk stabilitet af injicerede terapeutiske peptider. Det bliver primært brugt til at forlænge cirkulationstiden i blodet, men er ikke så velundersøgt i orale sammenhænge. Idet acylering ydermere øger interaktionen med mammale cellers lipidmembraner, kan det give adskillige fordele for oral administrering af terapeutiske peptider, og vi foreslår at skræddersyede acyleringer kan bruges til at optimere absorption i tarmsystemet.

Dette projekt har til formål at karakterisere acylerede analoger af to terapeutiske peptider, ved systematisk at forøge acylkædelængden og undersøge effekten på binding til lipidmembraner og translokation igennem tarmceller *in vitro*. Det første peptid er det 33 aminosyre lange Glucagon-like peptide-2 (GLP-2), som fremmer tarmvækst og kan bruges til at behandle tarmlidelser såsom inflammatoriske tarmsygdomme og patienter med for kort tarm. Det andet peptid er det 32 aminosyre lange lakse calcitonin (sCT), som sænker calcium-niveauet i blodet og kan bruges til at behandle post-menopausal osteoporose og hypercalcæmi. De to peptider er sammenlignelige i størrelse og struktur, men har modsat ladning ved fysiologisk pH. Begge peptider blev acyleret med lineære acylkæder med systematisk stigende længde, hvor sCT desuden blev acyleret i to forskellige positioner på peptidet.

For GLP-2 fandt vi at stigende acylkædelængde forårsagede stigende selv-associering og binding til lipid- og cellemembraner, medens absorption igennem tarmceller afhang ikke-lineært af acyleringslængde. Korte og mellemlange acylkæder forbedrede translokationen sammenlignet med det native peptid, hvorimod langkædet acylering ikke gav nogen forbedring. Dette indikerer en indledningsvis translokationsfordel for kortere kæder grundet forøget interaktion med cellemembranen, som udvikler sig til en hindring for længere kæder idet peptidet sidder fast i cellemembranen. Inklusion af en paracellulær absorptionsenhancer forøgede translokationen sammenligneligt for hver analog, dvs. afhængigheden af acyleringslængde blev bibeholdt. En transcellulær absorptionsenhancer udviste synergi med langkædet acylering, konsistent med at membran-fluidisering kan 'befrie' membranbunden peptid, omend medium kædelængde forblev optimal overordnet set. Resultaterne illustrerer at rationel acylering af GLP-2 kan forøge tarmabsorption *in vitro*, alene eller i kombination med absorptionsenhancere, og er i tråd med projekthypotesen.

For sCT fandt vi en uventet effekt af acylering som til dels fortrængte de forventede membraninteraktioner, idet acyleret sCT opførte sig som en *in vitro* absorptionsenhancer. Acylerede analoger permeabiliserede lipidmembraner, og forårsagede drastisk forøget peptid-permeabilitet igennem reversible effekter på cellelaget i stil med transcellulære absorptionsenhancere. Effekten skyldes sandsynligvis en synergi mellem den positive peptidladning og membran-aktive acylkæde, hvilket understøttes af pH-afhængigheden, hvorved effekten voksede ved faldende pH og ledsagende ladningsforøgelse. Omfanget af enhancer-effekten var særdeles afhængig af acyleringskædelængde og -position, med størst peptid-permeabilitet for kort-kædet N-terminal acylering

eller medium/langkædet Lys18 acylering, men hvor membranbinding og permeabilitet kun var korreleret for nogle analoger. Længerevarende opvarmning eller håndtering i opløsning af nogle sCT analoger medførte aggregering i fysiologiske bufferopløsninger, potentielt i fibril-lignende strukturer. Lys18-acylering fremstod bedre end N-terminal acylering, mest tydeligt eksemplificeret for de kort-kædede analoger, men ingen systematisk afhængighed af acylkædelængden var tydelig. Alle analoger kunne monomeriseres ved tilsætning af cyclodextrin, men deres seperate absorptionsenhancer-effekter blev reduceret i blandingerne, og kombinationen blev ikke yderligere undersøgt. Altså er acylering af sCT til oral administration ikke nødvendigvis uvilkårligt anvendeligt, og kræver rationelle valg af acyleringsdetaljer og/eller tilsætningsstoffer.

Yderligere undersøgelser af de mest celle-permeable sCT analoger afslørede meget forskelligartede absorptionsenhancer-effekter, rangerende fra høj membranbinding / høj permeabilitet og uspecifik enhancer-effekt på modelstoffer til meget lav membranbinding / høj permeabilitet og lav uspecifik enhancer-effekt, altså selektiv og effektiv peptidtranslokation.

Peptidets receptor-aktivering var intakt efter acylering for GLP-2 analoger, hvorimod sCT analoger udviste mærkbart reduceret potens, afhængig af acyleringslængde og -position.

Overordnet set kan rationel acylering af de undersøgte peptider forøge *in vitro* tarmabsorption, moderat for GLP-2 og drastisk for sCT, og kan muligvis give en fordel i oral administration. GLP-2 resultaterne giver et velfunderet forudsigelsesgrundlag for fremtidige analoger, medens sCT resultaterne virker lovende for fremtidige analoger, omend forbundet med en større usikkerhed.

Contents

Chapter 1

Introduction

1.1 Why study oral peptide delivery?

Millions of people worldwide suffer from severe chronic diseases that require frequent administration of biomacromolecules, which for the vast majority involves injections. Although development of the treatment in itself is profound and life-changing, injecting oneself is a both physical and mental barrier, not least for the many chronically ill children. In fact, writing 'ill' hints at one of the problems, i.e. the stigma associated with injections, which mars the otherwise normal lives these modern medications have allowed patient to live. Sadly, this is one of the causes for otherwise treatable diseases being mismanaged. Swallowing a tablet is for many people much less invasive, but entry through the oral route is a formidable task for therapeutic peptides, due to the harsh and selective gastrointestinal system.

1.2 Thesis scope

So what does oral peptide delivery have to do with lipid membranes and acylation?

This work focuses on how therapeutic peptides cross the intestinal barrier to enter circulation, particularly how modifying them with a fatty acid chain affects this crossing. Peptide acylation is a powerful tool to alter the pharmacokinetics, biophysical properties and chemical stability of injectable peptide drugs, primarily used to prolong blood circulation, but is not widely studied in an oral context. The hydrophobic character of the acyl chain motivated a focus on interactions with the lipid membranes surrounding intestinal cells, where both cell models and artificial lipid membranes are employed as sketched in fig. 1.1. Cell models are most biologically relevant and are well correlated with *in vivo* results, whereas artificial membranes allow more well-controlled and quantitative studies, and the project attempts to bridge the gap between these two disciplines. Conducting the project in an interface between several scientific disciplines gives rise to both possibilities and challenges, and the aim is a high level of consistency in experimental procedures (e.g. peptide concentrations and solution buffers) whenever possible. This encompasses preferably using the methods and techniques that work in the chosen experimental conditions, as opposed to changing experimental conditions to fit each technique, even if it signifies discontinuing otherwise well-used characterization methods.

The project follows a circular setup, to accommodate synthesis and characterization of several families of acylated peptides, depending on the obtained result. Furthermore, investigations of two different peptides with similar acylations are incorporated, in order to separate the effects of acylation and backbone.

Understanding the effects of acylation may allow future rational design of orally delivered peptide drugs.

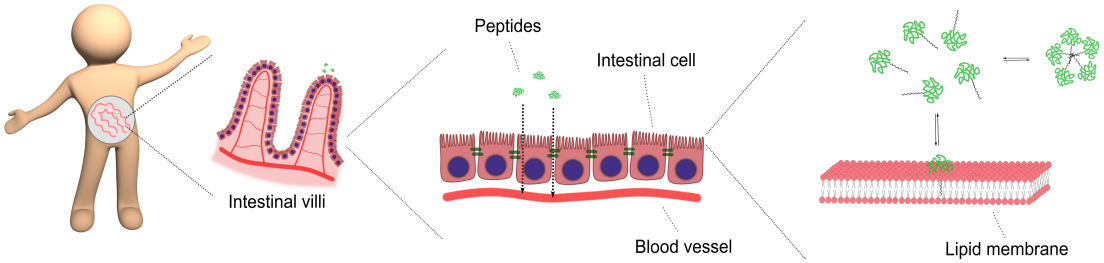

Figure 1.1: Study objective cartoon. A very popular scientific sketch to introduce how the membrane interaction and in vitro permeability of acylated peptides are investigated using an intestinal cell model and model lipid membranes.

1.3 This thesis at a glance

The thesis consists of one introductory chapter, two published papers, one manuscript in preparation, a section with additional results, a collaboration project, and a final concluding chapter. The introductory chapter, Chapter 2, introduces the core concepts of the project and briefly reviews the state of the quite diverse research fields. More specific literature reviews are included in the papers and manuscripts. Chapter 2 also contains a more elaborate discussion of the thesis scope than provided above. Chapter 3 concerns the first peptide GLP-2, and contains the first published paper along with some additional comments. It was written for a quite broad, open-access journal, and features fairly comprehensive introductions to several of the core techniques used in this thesis, therefore a separate section describing these techniques is not included. Chapter 4 concerns the second peptide sCT, and contains a published paper, a manuscript, and a section with additional results which will later be collected in a manuscript. Chapter 5 briefly decribes a collaboration project aiming at developing a microfluidic setup for *in vitro* studies like those employed in this project, where the resulting manuscript in preparation is appended in appendix C. The final concluding chapter, Chapter 6.1, summarizes the findings of the thesis and briefly discusses future directions of research.

1.4 Publications

Research papers

1. S. Trier, L. Linderoth, S. Bjerregaard, T.L. Andresen and U.L. Rahbek. Acylation of Glucagon-like peptide-2: interaction with lipid membranes and in vitro intestinal permeability. PLOS ONE 9 (2014) e109939.

2. S. Trier, L. Linderoth, S. Bjerregaard, H.M. Strauss , U.L. Rahbek, T.L. Andresen. Acylation of salmon calcitonin modulates *in vitro* intestinal peptide flux through membrane permeability enhancement. Eur J Pharm Biopharm. 2015;96: 329–37.

3. S. Trier, L. Linderoth, S. Bjerregaard, H.M. Strauss, T.L. Andresen and U.L. Rahbek. Acylated salmon calcitonin and dimethyl-β-cyclodextrin – self-association and *in vitro* intestinal permeability. *Manuscript under preparation; to be submitted.*

4. H-Y. Tan, S. Trier, M. Dufva, J.P. Kutter and T.L. Andresen. A multi-chamber microchip platform for studying drug transport across tissue barriers. *Manuscript under preparation; to be submitted.*

Conference contributions

S. Trier, L. Linderoth, S. Bjerregaard, H.M. Strauss, T.L. Andresen and U.L. Rahbek. Acylation of Glucagon-like peptide-2: interaction with lipid membranes and *in vitro* intestinal permeability. Poster presented at Liposome Research Days 2014, August 2014, Copenhagen.

Miscellaneous

A Danish popular scientific article was awarded 2nd prize in the Industrial PhD and Post Doc association 2014 communication competition, awarded by the Danish minister of research, and published at the popular scientific site *Videnskab.dk*.

Chapter 2

Background

2.1 Therapeutic peptides

Peptide therapeutics have assumed an increasingly important role within disease management, e.g. diabetes, oncology, metabolic, cardiovascular and infectious diseases, and constitute a substantial fraction of recent FDA approved drugs [3, 31]. Although macromolecular drugs ($\geq$ 1000 g/mol) are generally highly selective and efficacious, e.g. production, stability/solubility and delivery route is far more challenging than small molecules, and development has lacked behind. The most well known use of a therapeutic peptide is probably type 1 diabetes, where insufficient insulin production in patients is compensated by external administration of the peptide. Although this thesis focuses on other peptides, insulin deserves mentioning as it has been pivotal in driving peptide technology forward, due to the wide (and fast increasing) spread of diabetes.

Initially, insulin injection therapy was based on native insulin of animal origin, i.e. the peptide was purified from animal tissue. Gene technology enabled recombinant production of human insulin, which vastly improved large-scale manufacturing and availability, and further allowed modifications of the native peptide. Modern insulin analogues feature amino acid substitutions, truncation and/or attachment of non-peptide moieties, thereby improving production, storage stability, physico-chemical properties and physiological stability. In contrast to small molecules, where synthetic large-scale production was feasible early on, peptide synthesis is often too low-throughput and costly for drug production, although relevant for research purposes (see section 2.2).

The two therapeutic peptides studied in this thesis, GLP-2 and sCT, will be introduced in section 2.5.

As a brief note on terminology, the words peptide and protein are not always clearly defined, and often appear to overlap. In some texts the distinction is made at 50 amino acids in length, whereas others note that proteins are more structured. Here, therapeutic peptides signify small proteins (30-50 aa) with specific biological function and solution structure.

2.2 Peptide synthesis and characteristics

Single amino acids are readily available, but combining them into peptides through the amide bonds is tricky for large peptides, due to the many possible combinations of reactive groups, increasing with increasing peptide length. Peptides are synthesized by coupling the carboxyl group or C-terminus of one amino acid to the amino group or N-terminus of another. To avoid unintended reactions with 'the other' carboxyl / amine group or side chain functional groups, so-called protecting groups are usually necessary, where two different types can be used (orthogonal protecting groups, e.g. acid labile and base labile). The standard method is Solid Phase Peptide Synthesis (SPPS), where peptide chains are built from the C-terminal end on functionalized resin beads, through repeated cycles of N-terminal deprotection-wash-coupling-wash. The

'immobilization' of peptides allows easy filtration, where liquid-phase reagents and by-products of synthesis are flushed away. The finished peptide can be cleaved from the bead, followed by side chain deprotection and purification on preperative HPLC. The repeated coupling steps can be automated, where coupling yields are optimized by adding amino acids in major excess in optimized coupling reagents, and speed can be increased by heating, e.g. microwave-assisted SPPS, allowing synthesis of peptides up to around 100 aa. However, certain amino acids and combinations of neighboring amino acids are more troublesome, e.g. due to steric considerations increasing racemization, which can sometimes be alleviated by using di- or tri-amino acid building blocks, by reducing temperature or optimizing coupling reagents, or in severe cases require alteration of the peptide sequence. [85]

The amino acid sequence constitute the peptide primary structure, whereas the secondary/tertiary/quaternary structure is dynamic and depends on the peptide surroundings. Intra- or inter-peptide disulfide bonds form between two cysteines and intra-peptide hydrogen bonding determines organization into α-helix or β-sheet motifs. Electrostatic or hydrophobic interactions can cause peptide self-association into oligomers, which is highly dependent on solvent, peptide concentration, pH, temperature and ions. Most peptides exert their biological function as monomers, and either the secondary structure is required for function or it changes upon interaction with the target receptor or membrane. [34, 85]

2.3 Peptide acylation

Physiological peptide levels change slowly in response to tightly controlled feed-back loops, and a sudden increase in peptide concentration upon external administration can be inefficient or even harmful, particularly for insulin. The blood circulation time of peptides can be prolonged by modification with a fatty acid, motivated by a naturally occurring post-translational modification and fatty acid's affinity to long-circulating albumin. The resulting acylated (or lipidated) peptide can piggy-back on serum albumin, which is present in large amounts in the blood, thus preventing clearance and prolonging the circulation time [39, 54]. Acylated insulin can further be tailored to yield highly prolonged release following subcutaneous injection, through slowly dissolving multihexamers [45, 89].

The acylation technology (sketched in fig. 2.1) has expanded from insulin to other peptides, including several marketed drugs [51, 58, 96, 105]. It has further been shown to improve peptide enzymatic stability, likely due to reduced affinity for the highly specific enzymes [26, 35, 105]. Acylation often affects peptide solubility and self-association behavior, which in turn can alter secondary structure and solution stability (the latter in both directions) [12, 78, 97].

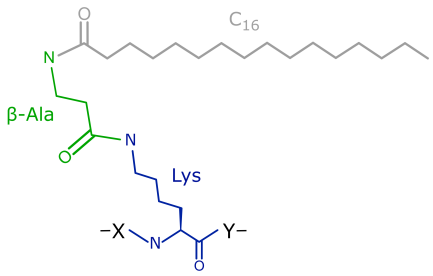

Figure 2.1: Acylation example. Carboxylic acids (e.g. hexadecaonic/palmitic acid as shown in grey) can be attached to peptides at the $\epsilon-$amino group of lysine (blue) or peptide N-terminal, possibly through a linker or spacer to increase flexibility (e.g. $\beta-$alanine as shown in green).

Alteration of therapeutic peptides generally carries the risk of reducing potency, so the acyl chain placement must be tailored to the peptide, e.g. by considering the structure-function

relationship of the peptide, i.e. which parts of the pepide are crucial for receptor binding and activation [35, 59, 88, 106]. A different approach to avoid impaired function is the prodrug strategy, where the acylation is reversibly attached, and is slowly cleaved off in a biological environment [20, 105].

As a brief note regarding the large-scale production of acylated peptides, the peptide backbone (precurser) can be produced recombinantly, and later modified synthetically with the acyl chain. [37, 85]

2.4 Oral delivery of peptides

Attempting to deliver peptides orally entails circumventing a well-functioning digestive system, which is intended to digest peptides and proteins from our food, and only allow entry of the harmless and useful building blocks. This thesis merely aims to investigate a small part of this formidable problem, but we will briefly describe some of the major challenges and possible solutions.

(It should be noted that oral peptide delivery is a very active research field, and a plethora of excellent reviews and book chapters describe it in far greater detail than attempted here [15, 19, 64, 80].)

Macromolecules may be protected through the esophagus and stomach by enteric coating of the dosage forms, and released as pH increases in the small intestine (i.e. the duodenum, jejunum and ileum), a technology which has been applied successfully to some peptides. [1, 14, 17, 70] The small intestine constitutes a highly metabolic environment, featuring numerous intestinal enzymes [17], but peptides may be protected by adding enzyme inhibitors to formulations [86, 95, 99, 100] or possibly through acylation as described in the previous section.

The mucosal lining of the intestine is tightly sealed to avoid unspecific absorption, and passive permeation of large, hydrophillic peptide drugs is limited [19, 48, 69]. This challenge is the focus of the thesis, and will be discussed further in the next section. For completeness sake it should be mentioned that after absorption, peptides are challenged by first-pass metabolism in the liver and clearance from the blood stream (depending on where in the body they exert their function) [33]. Incidently, hepatic entry is similar to endogenous insulin, and may thus be beneficial for this peptide, compared to the high systemic levels ensuing from subcutaneous injections. [107]

2.4.1 Intestinal absorption of peptides and in vitro models

Firstly, a brief note on the words absorption and permeation, which are used as synonyms here, but in some texts are used to distinguish between active and passive translocation across the cell layer. This work focuses on passive translocation, and features no attempts at shuttling peptides across via intestinal transporters [40]. Conversely, peptide transport most often describes passive permeation, which may be slightly misleading for newcomers to the field.

The passive translocation routes through the epithelial cell monolayer of the intestine are sketched in fig. 2.2. The transcellular route is efficient for small, hydrophobic molecules, whereas the larger hydrophilic peptides are generally believed to enter primarily through the paracellular route (albeit very inefficiently). [15, 19]

Intestinal absorption is often assessed *in vitro* by measuring drug translocation across monolayers of the human colon cancer cell line (caco-2). Although the cell line stems from the colon, it appears closer to the small intestine in regard to tightness and protein expression and is a good predictor of oral bioavailability [9, 42]. The experimental caco-2 setup is described in detail in [42], and as applied in this work in paper 1 (e.g. fig. 6). As a brief practical note, caco-2 cell lines change over time (e.g. with increasing passage number), and differ widely between different research labs [40]. One should be cautious in comparing literature values for e.g. permeability, and in our investigations (performed in the same lab, but over the course of several years) we used various internal standards to bridge permeability values. It should further be noted that caco-2 cell monolayers are a very simple model of the intestinal barrier, devoid of mucus-production,

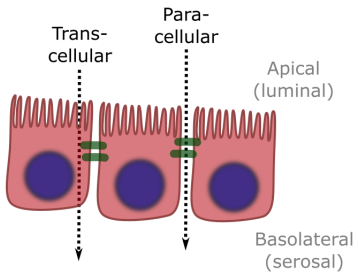

Figure 2.2: Intestinal translocation. Schematic illustration of passive permeation pathways through epithelial cells, from the apical side (corresponding to luminal or inner side in the intestine) to the basolateral side (corresponding to the serosal side, connecting to the circulatory system). The transcellular route entails crossing the outer cellular membrane twice and diffusing through the cytosol, whereas the paracellular route requires crossing the tight junction protein complex (green) sealing the cell boundaries. Inspired by fig. 3.1 in [17].

spatial effects, lymphoid tissue, and possibly several barrier/carrier proteins [40]. The relevance of mucus in peptide absorption is debated [15, 74, 76, 80], and more complex systems have been developed with mucus-producing HT29-MTX-E12 goblet cells alone [32, 71], cocultured with caco-2 cells in various ratios [61, 102], or even as triple cocultures [7]. Interestingly, the appended collaboration manuscript concerning caco-2 cells in a microfluidic setup feature some indications of caco-2 mucus-production, possibly due to the shear forces exerted on the cells (also previously observed for a similar microfluidic setup [49]). The complexity and biological similarity can be increased further in the *ex vivo* Ussing chamber model, where cell monolayers are substituted by rat intestinal tissue [24, 76], but this method is labor-intensive and requires continuous supply of rat intestines (which obviously involves sacrificing the animals).

Both *in vitro* and *ex vivo* models lack many natural variations in GI tract conditions, influenced e.g. by food and water consumption, which can affect peptide solubility and stability. Several more complex buffers have been used to mitigate this, e.g. fasted/fed state simulated intestinal fluid (FaSSIF/FeSSIF), which include bile salts and phospholipids [50], but such increased complexity may interfere with the delicate peptide-membrane interactions studied in this project.

Increasing peptide permeation The most prominent strategy to increase peptide absorption across the intestine is the co-addition of absorption enhancers that reduce the intestinal tightness. Absorption enhancers are a diverse class of compounds, that function either through a detergent-like unspecific destabilization of the cell membrane(s) or more specific interaction with surface proteins, inducing cellular mechanisms that effectuate an opening of the paracellular space between the cells (i.e. at the tight junction proteins) [11, 60, 101]. Often, the mechanism of action is not entirely clear, and may be a mix of both pathways. Some enhancers were initially used to increase the drug solubility, but were later found to have an independent effect on the epithelium [29, 43, 64].

The cellular effects of absorption enhancers can be quite profound, and most are cytotoxic at high concentrations. The concentration dependent cytotoxicity differs widely for different enhancers, and the concentration window for function without toxicity is often quite narrow [11, 101]. However, mucosal cells *in vivo* may be more resilient as they are replenished quite rapidly, and oral dosing with absorption enhancers is safe and efficacious in many instances [64].

The gut is a crowded place, and unintended absorption of harmful compounds due to unspecific reduction of epithelial tightness must be avoided. In many cases permeation enhancers can be optimized regarding specificity for their peptide payload, and quickly reversible effects.[15]. Other approaches include advanced delivery systems, e.g. mucoadhesive chitosan devices [36, 72, 91], nanoparticles [2, 29, 81, 84, 93], liposomes [29, 87] or combinations thereof [62, 66]. Alter-

Table 2.1: Peptide characteristics

Name	Size (aa)	Weight (g/mol)	PI	Sequence
GLP-2	33	3766	4	HADGSFSDEMNTILDNLAARDFINWLIQTKITD
sCT	32	3455	10.5	CSNLSTCVLGKLSQELHKLQTYPRTNTGSGTP-NH_2

Details: sCT contains a disulfide bridge at aa 1-7.

natively, the peptide itself can be modified with complex moieties, e.g. a cell-penetrating peptide motif [31] or vitamin B12 conjugation to attempt transporter-mediated active translocation [4]. The risk of reduced peptide potency following these modifications may be alleviated by the prodrug approach, whereby the added moiety is cleaved off after absorption [15].

2.4.2 Acylation and oral delivery

The majority of reports regarding acylated peptides have focused on subcutaneous injection, whereas the potential for oral administration remains an emerging field. Acylation has been shown to increase intestinal permeability and/or oral bioavailability of a few peptide drugs [21, 94, 96, 106], but mechanistic insights and optimization is sparse. *In vivo* experiments in live animals are limited, whereas experiments with cells and model lipid membrane allow more expansive investigations (although model systems are never as powerful as *in vivo* tests, which should always be kept in mind).

2.4.3 Acylation and interaction with lipid membranes

Intestinal absorption may benefit from the peptide (or parts of it) to be sufficiently hydrophobic to allow partitioning into lipid bilayers, but not to get stuck there. The hydrophobicity was traditionally measured as the octanol/water partitioning coefficient [82], but model lipid bilayers closer mimic the cell membranes, and can provide more detailed information concerning peptide membrane interactions [13, 52, 82]. Model lipid membranes come in many forms, where spherical, nano-sized bilayer liposomes are versatile tools to study interaction with peptides in solution, e.g. through fluorescence spectroscopy. If the peptide contains a tryptophan, which fluorescence depends on the polarity of the micro-environment, peptide membrane interaction (and peptide self-association) can be measured label-free [56]. Alternatively, the peptide can be modified with a fluorescent moiety, although this may affect the peptide properties. If the peptide perturbs the membrane upon insertion, it may be investigated by encapsulating a water-soluble fluorophore in the liposome (although this was not part of the original study objective, we will see its relevance in chapter 4).

Liposome partitioning studies are quite well-established for membrane-active peptides, such as antimicrobial peptides [57], where acylation has been shown to alter peptide interaction with lipid membranes more profoundly than expected from the increased hydrophobicity [30, 41]. Even small changes in acylation chain length was shown to affect membrane partitioning and thereby antimicrobial efficacy [30, 41], however such mechanistic studies remain rare in an oral delivery context, particularly in combination with *in vitro* investigations.

2.5 Peptides studied in this thesis

The two peptides (see table 2.1) are chosen partially as model peptides to study the impact of acylation on oral delivery potential, but also due to their biological activity and relevance as oral drug candidates.

GLP-2 and sCT are similar in size, whereas they are oppositely charged at physiological pH. GLP-2 is mainly unstructured in solution, where the native peptide is not expected to be

membrane active and spontaneously insert into lipid membranes, although these properties are not well established [25]. sCT contains a disulfide bridge (aa 1-7) and reportedly some alpha helix secondary structure in solution [6], and there are reports of membrane insertion, possibly as an amphipathic alpha helix [27, 65, 67, 68]. An amphipathic structure is partially consistent with parts of the peptide sequence's alternating hydrophobic and hydrophilic residues, illustrated e.g. by Kyte-Doolittle plots [55] (see fig. A.1 in appendix A).

GLP-2 is secreted in the intestine upon nutrient ingestion, and most importantly promotes intestinal growth and function [28, 73, 92]. It has (quite recently) been used to treat bowel disorders (e.g. Crohn's disease and short bowel syndrome) where it is administered as subcutaneous injections of the native peptide, possibly with minor amino acid substitutions [44, 95]. The plasma half-life of GLP-2 in humans is limited to a few minutes [38] due to renal clearance and enzymatic cleavage at the N-terminus (aa 1-2) by dipeptidyl peptidase-4 (DPP-IV) [38, 90], substantially decreasing the receptor potency [38]. A GLP-2 analogue with an A2G amino acid substitution, which is more stable towards DPP-IV is currently in clinical trials [44], but to the best of our knowledge, no previous attempts at developing oral GLP-2 have been reported. However, as GLP-2 elicits its function in the intestine, the oral entry route may be beneficial, and could in fact circumvent some of the usual complications in oral delivery.

Calcitonin is secreted in the thyroid in response to excess calcium in serum, and functions to reduce bone breakdown [22]. Human calcitonin is physically and chemically unstable in solution [10], so therapeutic use is based on salmon calcitonin (sCT), which is efficiently recognized by the human calcitonin receptor and circulates longer [23, 77]. sCT has long been used to treat osteoporosis and hypercalcemia, with parenteral or intranasal administration [79]. However, oral administration of sCT is extensively studied and tablet formulation development is far advanced, where the majority of reports employ native sCT in combination with oral permeation enhancers, carrier molecules or enzyme inhibitors [2, 8, 14, 16, 46, 47, 77].

Motivation for peptide modifications Reports of GLP-2 modifications are sparse, but acylation at aa 17 was previously reported in [78], along with interchanging of Lys/Arg (i.e. natural Lys30 changed to Arg, Leu17 changed to Lys and acylated, resulting in no net charge change), which motivated the GLP-2 analogues in this project. A D3E mutation was introduced to avoid racemization at the aa 2-3 Ala-Asp sequence.

The potency of sCT is highly dependent on the C-terminus [79], whereas the role of the N-terminal cysteine bridge and the central a-helix motif is somewhat unclear [6]. 2K PEGylation at Lys18 of sCT [103] or dual acylation with long chains at the sulfide bridge in a reversible or permanent manner was well tolerated regarding potency [20, 21, 96]. To accomodate Trp-fluorescence studies for sCT analogues as performed for GLP-2 analogues (employing its native Trp), a Y22W mutation was initially introduced in the sCT backbone.

In the present work, both peptides were acylated with linear acyl chains, either short (c8, i.e. using octanoic acid), medium (c12) or long (c16). The acylation was placed at aa 17 in GLP-2, and at aa 18 or the N-terminus in sCT. These systematic analogue series allow investigations into the effects of the acyl chain length, backbone charge and acylation placement, on the peptide-membrane interaction and *in vitro* intestinal permeability. Such results may enable elucidating potential general trends of peptide acylations on membrane translocation properties.

Chapter 3

Results for GLP-2

3.1 Paper 1

The following section contains paper 1, as typeset by the journal, as well as the supplementary information available online.

Summary The paper investigates a systematic series of acylated GLP-2 analogues, with c8, c12 or c16 acyl chains at the artificial Lys17.

The results demonstrate that increasing acyl chain length causes increased self-association and binding to lipid and cell membranes, whereas translocation across intestinal cells displays a non-linear dependence on chain length. Short and medium chains improve translocation compared to the native peptide, whereas long chain acylation display no improvement in translocation. This indicates an initial translocation benefit for shorter chains through increased interaction with the cell membrane, which reverts to a hindrance for long chains, i.e. the analogues get stuck in the cell membrane. This interpretation is supported by the effects of co-administered para- and transcellular enhancers, which increases translocation irrespective of acyl chain length for the former, whereas the latter display increased synergy with the long chain acylation, however, with the c12-acylation remaining optimal. Thus, rational acylation of GLP-2 can increase its intestinal absorption, alone or in combination with permeation enhancers, and the absolute quantification of liposome binding (partitioning coefficient 1300 M^{-1} for c12-GLP-2) may be used to predict the optimal acylation chain length for other acylation types or peptides.

OPEN ACCESS Freely available online

PLOS ONE

Acylation of Glucagon-Like Peptide-2: Interaction with Lipid Membranes and *In Vitro* Intestinal Permeability

Sofie Trier[1,2], Lars Linderoth[2], Simon Bjerregaard[2], Thomas Lars Andresen[1], Ulrik Lytt Rahbek[2]*

1 Dept. of Micro- and Nanotechnology, Center for Nanomedicine and Theranostics, Technical University of Denmark, Kgs. Lyngby, Denmark, **2** Diabetes Research Unit, Novo Nordisk, Maaloev, Denmark

Abstract

Background: Acylation of peptide drugs with fatty acid chains has proven beneficial for prolonging systemic circulation as well as increasing enzymatic stability without disrupting biological potency. Acylation has furthermore been shown to increase interactions with the lipid membranes of mammalian cells. The extent to which such interactions hinder or benefit delivery of acylated peptide drugs across cellular barriers such as the intestinal epithelia is currently unknown. The present study investigates the effect of acylating peptide drugs from a drug delivery perspective.

Purpose: We hypothesize that the membrane interaction is an important parameter for intestinal translocation, which may be used to optimize the acylation chain length for intestinal permeation. This work aims to characterize acylated analogues of the intestinotrophic Glucagon-like peptide-2 by systematically increasing acyl chain length, in order to elucidate its influence on membrane interaction and intestinal cell translocation *in vitro*.

Results: Peptide self-association and binding to both model lipid and cell membranes was found to increase gradually with acyl chain length, whereas translocation across Caco-2 cells depended non-linearly on chain length. Short and medium acyl chains increased translocation compared to the native peptide, but long chain acylation displayed no improvement in translocation. Co-administration of a paracellular absorption enhancer was found to increase translocation irrespective of acyl chain length, whereas a transcellular enhancer displayed increased synergy with the long chain acylation.

Conclusions: These results show that membrane interactions play a prominent role during intestinal translocation of an acylated peptide. Acylation benefits permeation for shorter and medium chains due to increased membrane interactions, however, for longer chains insertion in the membrane becomes dominant and hinders translocation, i.e. the peptides get 'stuck' in the cell membrane. Applying a transcellular absorption enhancer increases the dynamics of membrane insertion and detachment by fluidizing the membrane, thus facilitating its effects primarily on membrane associated peptides.

Citation: Trier S, Linderoth L, Bjerregaard S, Andresen TL, Rahbek UL (2014) Acylation of Glucagon-Like Peptide-2: Interaction with Lipid Membranes and *In Vitro* Intestinal Permeability. PLoS ONE 9(10): e109939. doi:10.1371/journal.pone.0109939

Editor: Miguel A. R. B. Castanho, Faculdade de Medicina da Universidade de Lisboa, Portugal

Received May 23, 2014; **Accepted** September 11, 2014; **Published** October 8, 2014

Data Availability: The authors confirm that all data underlying the findings are fully available without restriction. All relevant data are within the paper and its Supporting Information files.

Funding: ST was partially funded by The Danish Agency for Science, Technology and Innovation, and TLA was funded by the Technical University of Denmark. The funder Novo Nordisk A/S provided support in the form of salaries for authors ST, LL, SB and ULR, but did not have any additional role in the study design, data collection and analysis, decision to publish, or preparation of the manuscript. The specific roles of these authors are articulated in the 'author contributions' section.

Competing Interests: ST, LL, SB and ULR are employed by Novo Nordisk A/S, and LL, SB and ULR are shareholders in Novo Nordisk A/S. Funding does not alter the authors' adherence to all PLOS ONE policies on sharing data and materials.

* Email: ulyr@novonordisk.com

Introduction

Acylation of peptides with fatty acids is a naturally occurring post-translational modification, which has inspired alteration of therapeutic peptides for drug delivery. Acylation prolongs the systemic circulation half-life of otherwise rapidly cleared peptide drugs, through increased enzymatic stability [1–3] and binding to - and piggy-backing on - serum albumin [4]. An additional effect of acylation is increased peptide self-association and aggregation, which has been employed to ensure prolonged release of peptide drugs following subcutaneous injection [5]. Acylation can be performed without disrupting the peptide's biological potency [6], and has been employed for a multitude of therapeutic peptides [2,4,7,8], including several marketed drugs (e.g. insulin and Glucagon-like peptide-1).

The increased enzymatic stability of acylated peptides is particularly beneficial for oral administration, due to the highly metabolic environment in the stomach and intestine [9]. Another requirement for oral drug delivery is adequate absorption through the intestinal epithelial barrier, which is a major challenge for large, hydrophillic peptide drugs [10]. A widely used method for predicting oral absorption *in vivo* is *in vitro* quantification of translocation across monolayers of the human colon cancer cell line (Caco-2), which has been shown to correlate well with oral bioavailability [11,12]. Acylation has previously been shown to increase intestinal permeability of peptide drugs [6,7,13], but detailed investigations of systematic acyl variations are lacking,

which would benefit rational new designs of peptide drugs. The *in vitro* intestinal translocation studies can be further supplemented by measurements of peptide binding to model lipid membranes [14–16] in order to investigate the influence of membrane binding of acylated peptides on cellular membrane translocation.

Glucagon-like peptide-2 (GLP-2) is a 33 amino acid peptide, which is secreted from the human intestine following nutrient intake [17,18]. Therapeutically, GLP-2 stimulates intestinal growth and is employed in the treatment of inflammatory bowel diseases (e.g. Crohn's disease) and short bowel syndrome (e.g. following intestinal surgery) [19,20]. The plasma half-life of GLP-2 in humans is limited to a few minutes [21] due to extensive renal clearance and rapid enzymatic degradation by dipeptidyl peptidase-4 [21,22]. Furthermore, GLP-2 is presently administered as subcutaneous injections, which compromises patient comfort and compliance, in particular for chronic diseases like Crohn's. It would be highly beneficial to enable oral administration, and the combined effects of prolonged circulation time, improved enzymatic stability and intestinal permeability may render acylated GLP-2 a suitable candidate for oral drug delivery. Currently, however, there are no reports on the intestinal permeability or oral drug delivery potential of acylated GLP-2.

In the present study we synthesized and characterized acylated analogues of GLP-2, with systematically increasing acyl chain length, in order to investigate the effect of the acyl chain on membrane interaction and *in vitro* intestinal permeability. This was achieved by combining investigations of the interaction with lipid membranes and translocation across an intestinal cell model, as outlined in fig. 1.

We hypothesize that the acylation chain length can be optimized for translocation across the intestinal barrier, i.e. a moderate interaction with the lipid cell membrane is beneficial for translocation, whereas a stronger interaction may impair translocation. Acylation is expected to confer membrane affinity to GLP-2, as the native peptide is not membrane active. In this regard, GLP-2 was employed as a model peptide, however, the results may be applicable for development of a rational acylation strategy for other peptide drugs.

Absorption enhancers are often employed to increase oral peptide absorption, which makes it interesting to investigate how these affect the translocation of acylated peptides [23]. In the present study we included two enhancers with different enhancing mechanism, in order to investigate the effect of the enhancing mechanism. Ethylene glycol-bis(β-aminoethyl ether)-N, N, N, N-tetraacetic acid (EGTA) is a paracellular enhancer which increases transport between the cells by opening of the tight junctions [24], and sodium dodecyl sulfate (SDS) is a transcellular enhancer which increases transport through the cells at low concentrations, predominantly by fluidizing the cell membrane [25].

We hypothesize that the effect of paracellular enhancers will not be influenced by acylation, whereas the effect of transcellular enhancers that directly interact with the cell membrane may depend on the peptide-membrane interaction, through altered membrane affinity and/or dynamics of membrane insertion.

Materials and Methods

Materials

Resin and natural amino acids were purchased at Novabiochem (Germany). c8, c12 and c16 carboxylic acids, Fmoc-beta-Alanine and native GLP-2 were provided by Novo Nordisk A/S. Palmitoyloleoylglycerophosphocholine (POPC) was purchased from Avanti Polar Lipids (USA). HEPES, Ovalbumin (OVA, from chicken egg white) and other standard chemicals were purchased from Sigma-Aldrich (Denmark). DMEM medium, l-glutamine and penicillin/streptomycin was purchased from Lonza (Switzerland). HBSS buffer, fetal bovine serum (FBS), nonessential amino acid and other standard cell culture products were purchased from Gibco (Denmark). Radioactively labeled [^{3}H]mannitol, scintillation fluid (Microscint-40), luciferase substrate (SteadyLite) and 96-well plates for luciferase assay (CulturPlate, black) were purchased from PerkinElmer (USA). 12 well Transwell plates for Caco-2 cell monolayers (polycarbonate, 12 mm, pore size 0.4 μM) were purchased from Corning Costar Corp. (USA). GLP-2R BHK cells were provided by Novo Nordisk (the cloning was previously described by Thulesen et al. [26] and Sams et al. [27]) and Caco-2 cells (HTB-37) were purchased from ATCC.

Peptide synthesis

The peptides were synthesized by automated Fmoc based SPPS, using a preloaded Fmoc-Asp(OtBu)-Wang polystyrene LL resin in 0.25 mmol scale on a CEM Liberty microwave peptide synthesizer (CEM Corporation, NC) using standard protocols, with a modified coupling temperature of 50°C [28]. Fmoc deprotection was carried out in 5% piperidine and 0.05 M HOBt in NMP.

The acylation was conjugated to the lysine side chain by incorporation of lysine as Lys(Mtt), which allowed chemical modification using the standard coupling procedures stated above, following Mtt removal. The Mtt group was removed by washing the resin with DCM and suspending the resin in neat (undiluted) hexafluoroisopropanol for 20 minutes followed by washing with DCM and NMP. After synthesis the resin was washed with DCM, and the peptide was cleaved from the resin by a 3 hour treatment

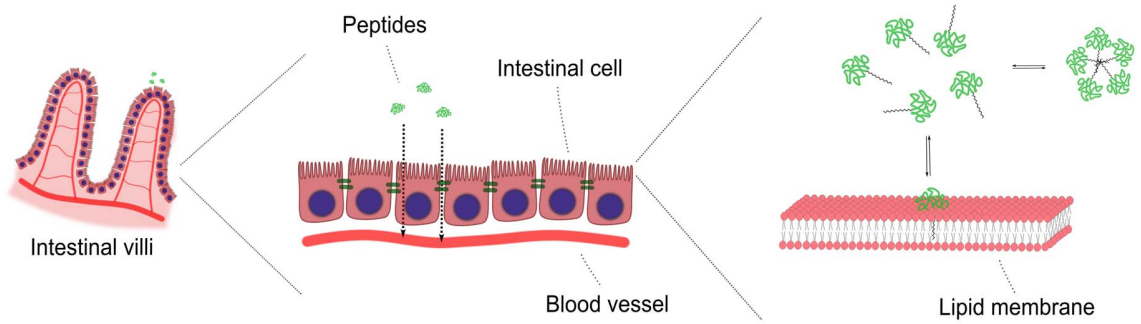

Figure 1. Schematic illustration of the study objective. The membrane interaction and *in vitro* permeability of acylated GLP-2 is investigated using an intestinal cell model and model lipid membranes.
doi:10.1371/journal.pone.0109939.g001

with $TFA/TIPS/H_2O$ (95/2.5/2.5) followed by precipitation with diethylether. The peptide was dissolved in a suitable solvent (e.g. 1:1 $MeCN : H_2O$) and purified by preparative HPLC on an XBridge c18 column (Waters), using a gradient from 10% MeCN/Buffer (10 mM TRIS and 15 mM $(NH_4)_2SO_4$, pH 7.3) to 50% MeCN over 40 min, flow rate 60 mL/min. The fractions were analysed by a combination of UPLC and LCMS methods, and the appropriate fractions were pooled and transferred to TFA salt for lyophilization, using a gradient from 10% MeCN/0.1% TFA/MQ to 60% MeCN. The peptides were finally quantified using a chemiluminescent nitrogen detector, as previously described by Fujinari et al. [29].

The isoelectric point of GLP-2 is approximately 4, with a theoretical charge of -4 at neutral pH, and the analogues are expected to be very similar.

Liposome preparation and characterization

POPC lipid films were prepared by evaporation from chloroform:methanol (9:1 v/v) using a gentle nitrogen flow. The residual organic solvent was evaporated in vacuum overnight and the lipid films were rehydrated to 25 mM in HEPES buffer (10 mM HEPES, 150 mM NaCl, pH 7.4) at room temperature with frequent vigorous agitation for 1 hour. The multilamellar lipid suspensions were subjected to 10 cycles of freeze-thawing (isopropanol/dry-ice and $40^{\circ}C$ water bath) and extruded to 100 nm liposomes by passing it 21 times through a 100 nm polycarbonate filter in a manual extruder (Avanti Polar Lipids). [30]

The liposome hydrodynamic size after extrusion was measured in a ZetaPALS Zeta Potential Analyzer (Brookhaven Instruments Corporation), after dilution to 50 μM in sterile filtered HEPES buffer. In all experiments the liposome diameter was 130 ± 5 nm with PDI 0.1.

The lipid concentration in liposome suspensions after extrusion was determined by phosphorous analysis, as previously described by Rouser et al. [31]. Briefly, the phospholipid sample was degraded with heat and perchloric acid, reacted with ammonium molybdate and reduced by ascorbic acid. Absorbance of the resulting molybdenum oxides (molybdenum blue) was measured at 812 nm, and lipid sample concentration was determined from a phosphate standard row. All samples were measured in triplicates. A typical final concentration after extrusion at 25 mM was 22.5 ± 0.1 mM.

Tryptophan fluorescence measurements

Peptide self-association. Fluorescence measurements were carried out using an OLIS SLM8000 fluorescence spectrometer equipped with excitation and emission monochromators and polarizers. Tryptophan was excited at 280 nm and emission scans were aquired from 300 to 400 nm with 2 nm step size, 2 s integration time and slit widths 16 nm. Quartz cuvettes with an excitation pathway of 10 mm and an emission pathway of 4 mm were used with 1 mL sample volume. Peptide samples in the concentration range 0.5–100 μM were prepared directly in the cuvette from 100 μM stock solutions in sterile filtered HEPES buffer. Temperature was maintained at $37^{\circ}C$ via an external water bath, and the solutions were mixed by magnet stirring in the cuvette.

The recorded spectra were fitted to obtain the peak position and intensity, as described by Burstein et al. [32], using an iterative least-squares fit (built-in in Gnuplot). Self-association of the peptides causes a blue-shift and increase in tryptophan maximum fluorescence, due to increased hydrophobicity near the tryptophan residue, and the blue-shift is used as an indicator of self-association.

Liposome partitioning. Fluorescence measurements were conducted similarly to self-association experiments, with integration time 4 s, slit widths 8 nm (excitation) and 16 nm (emission) and polarizers set to 90° (excitation) and 0° (emission).

The peptide solution was prepared directly in the cuvette and was subsequently titrated with a 20 mM liposome suspension. The peptide was used at a concentration (2 μM) below its self-association concentration, to avoid any signal from self-association.

The fluorescence was initially measured as full wavelength scans (300–400 nm), where the wavelength yielding the largest change with liposome addition was identified (344 nm). Subsequently, the fluorescence was measured as time-scans at 344 nm, and the fluorescence after each liposome addition measured for 5 minutes (increased and stabilized rapidly) and averaged over the last 3 minutes. It was verified that the fluorescence did not change substantially after the 5 minute measurement (up to 1.5 h).

Liposome partitioning model

The membrane partitioning model is described in detail by Etzerodt et al. [33]. Briefly, the tryptophan fluorescence after the *i'th* addition of liposome (F_i) depends on the lipid concentration after the *i'th* addition ($C_{lip,i}$) and the partition coefficient (K) through:

$$F_i = F_0 + (F_{inf} - F_0) \cdot \frac{K \cdot C_{lip,i}}{C_w + K \cdot C_{lip,i}} \quad (1)$$

where F_0 is the initial fluorescence of peptide alone, C_w is the concentration of water (55 M) and F_{inf} is the fluorescence at 'full' partitioning, i.e. after infinite liposome addition, which is a fitted value.

eq. 1 is reorganized to yield

$$\frac{F_i - F_0}{F_{inf} - F_0} = \frac{K \cdot C_{lip,i}}{C_w + K \cdot C_{lip,i}} \quad (2)$$

which is equal to the concentration of peptide bound in the membrane C_M divided by the total concentration of peptide C_{tot}, i.e. the fraction of peptide that is membrane-bound. eq. 2 was used for plotting (the left hand side) and fitting (the right hand side), where the fit was an iterative least-squares fit with respect to K and F_{inf} (Gnuplot).

The partition coefficient K can be converted to the standard Gibbs free energy of partitioning (ΔG°) through:

$$\Delta G^{\circ} = -R \cdot T \cdot ln(K) \quad (3)$$

where R is the gas constant (8.314 J/(K mol)) and T is the temperature (310 K). For simplicity, the absolute value of ΔG° is displayed in graphs.

The partition coefficient K is unitless, but can be converted to the more commonly used molar partition coefficient (in units M^{-1}) through dividing by the molarity of water (55 M).

Addition of liposomes to the peptide solution causes scattering of excitation and emission light, which yields artifacts in the experimental data that are accounted for by Ladokhin et al. [34]. To minimize these effects the fluorescence was measured using cross-polarized light settings, where the excitation light was horizontally polarized and the emission was measured vertically polarized. This ensures that only the emitted light is measured, as scattering does not alter the polarization, whereas fluorescence

randomizes the polarization. However, scattering still causes a decrease in measured fluorescence, which is corrected for by a correction factor Θ, measured by titrating the non-partitioning probe L-Trp with liposomes:

$$\Theta = \frac{F_{L-Trp,i}}{F_{L-Trp,0}} \quad (4)$$

where $F_{L-Trp,i}$ is the fluorescence of L-Trp after the *i'th* addition of liposome and $F_{L-Trp,0}$ is the initial fluorescence before liposome addition.

Θ was fitted to a polynomial, which was used to correct the measured peptide fluorescence during titration with liposomes.

All fluorescence measurements were normalized for peptide concentration, including the slight concentration decrease during titration.

Interaction with cells

Luciferase assay. A BHK cell line (GLP-2R BHK) was previously modified to stably express the human GLP-2 receptor, which controls the expression of firefly luciferase [26,27].

GLP-2R cells were cultured in DMEM with 10% FCS, 100 U penicillin, 100 μg/mL streptomycin, 1 mM Na-Pyruvate, 250 nM methotrexate, 1 mg/ml geneticin and 0.4 mg/ml hygromycin. The assay was performed in DMEM without phenol red, containing 10 mM HEPES, 1% glutamax and 1 mg/ml OVA.

For experiments, cells were seeded in 96-well plates at 20.000 cells/well (100 μL/well) and incubated overnight. The medium was removed and the cells were washed once and replenished with 50 μL/well assay medium. The test solution (containing peptide) was diluted in HBSS buffer (containing 10 mM HEPES and 1 mg/ml OVA, pH 7.4) and 50 μL/well was added to the cells. The cells were incubated for 3 h (at 37°C and 5% CO_2) and the test compound was removed. 100 μL/well HBSS buffer was added along with 100 μL/well luciferase substrate, the plate was sealed and incubated at room temperature for 30 minutes. The luminescence (Relative Luminescence Units, *RLU*) was measured in a topcounter (Packard Topcount) and depends on the peptide concentration as:

$$RLU = A + \frac{B-A}{1+10^{((logEC_{50}-x)\cdot C)}} \quad (5)$$

where x is log(concentration) of the peptide in M, and A, B, C and EC_{50} are fitting parameters [35].

The peptide test solutions were diluted to fall within the dynamic range of the assay (approximately 1–100 pM), and on each plate with test solutions a peptide standard row was included, which was fitted according to eq. 5 (using GraphPad Prism).

Caco-2 cells. Caco-2 cells (passage 40–65) were cultured routinely [11] in DMEM with 10% (v/v) FBS, 1% (v/v) nonessential amino acids, 100 U penicillin, 0.1 mg/mL streptomycin and 2 mM L-glutamine. The Caco-2 cells were seeded at a density of $1{\cdot}10^5$ cells/well on 12 well Transwells plates and grown for 14–16 days in DMEM with media change every second day. The cell layer was confirmed to consist of a single monolayer of cells by fixing and staining the cell layer, and visualizing by fluorescence microscopy.

Before transport experiments, DMEM medium was changed to HBSS buffer (containing 10 mM HEPES and 0.1% (w/v) OVA; 0.4 mL apical side and 1 mL basolateral) and left to equilibrate for 60 minutes. Buffer was replaced apically by 0.4 mL test solution at time zero, and the plates were incubated at 37°C and 5% CO_2 with gentle shaking. Test solutions contained 100 μM peptide and 0.8 μCi/mL [^{3}H]mannitol (a permeability marker). Basolateral samples of 200 μL were taken every 15 minutes for 1 hour, and replaced by buffer. The apical test solution and basolateral samples were diluted and analyzed for peptide content with the luciferase assay and for [^{3}H]mannitol content in a scintillation counter (Packard TopCount), after mixing 1:1 with scintillation fluid.

The integrity of cell monolayers before, during, and after experiments was verified by measuring the the translocation of radioactively labelled mannitol and the transepithelial electrical resistance (TEER), using a Milicell ERS-2 epithelial volt-ohm meter (Millipore, USA) [11]. Mannitol translocation and TEER values were not affected by addition of peptide or analogues compared to buffer.

After experiments, the cells were washed twice with buffer and replenished with medium for 24 hour recovery, or washed thrice with ice cold buffer and frozen at −80°C for cell binding and uptake analysis.

For cell binding and uptake studies, all preparations were carried out on ice, and all the buffers were ice cold. The filters were cut out of the inserts and placed in 12 well plates with the cell layer facing up. 250 μL of buffer was added and the cells were scraped off carefully with a cell scraper. The scraping was repeated, and the cell suspensions were pooled and centrifuged (13.000 rpm, 20 min, 4°C). The supernatant was analyzed for peptide content (cell uptake), and the pellet was resuspended in buffer and vortexed thoroughly. The membrane-bound peptide was recovered from the cell debris by addition of ethanol, followed by thorough vortexing and centrifugation (13.000 rpm, 20 min, 4°C). The supernatant solvent was evaporated under nitrogen-flow, and the dry peptide was dissolved in buffer and analyzed for peptide content (cell membrane binding). The cell uptake and membrane binding of peptide and analogues are displayed as the total amount of peptide in the cell layer. It was tested whether the recovery of peptide from cell debris was efficient and/or dependent on acyl chain length. Peptide or analogues were added to the cell debris pellet after the first centrifugation, taken from control cell layers with no added peptide, and after following the subsequent steps for membrane binding, the peptide recovery was measured. Essentially all added peptide was recovered, and there was no measurable difference for the different analogues.

The Caco-2 translocation of peptide or mannitol over Caco-2 layers is expressed as the apparent permeability (P_{app}), given by:

$$P_{app} = \frac{dQ}{dt} \cdot \frac{1}{A \cdot C_0} \quad (6)$$

where $\frac{dQ}{dt}$ is the steady-state flux of peptide (pmol/s), A is the surface area of the cell monolayer (1.12 cm^2), and C_0 is the initial sample concentration added to the cell layer [11].

Data analysis

Statistical analysis was carried out using GraphPad Prism, where unpaired Students t-tests were used for comparison and significant differences required $p<0.05$.

Results and Discussion

Characterization of peptide analogues

We synthesized and investigated native GLP-2 and the acylated analogues shown in fig. 2, where the acyl chain is conjugated to the $\epsilon-$amino group of a lysine via a $\beta-$alanine spacer [8,36].

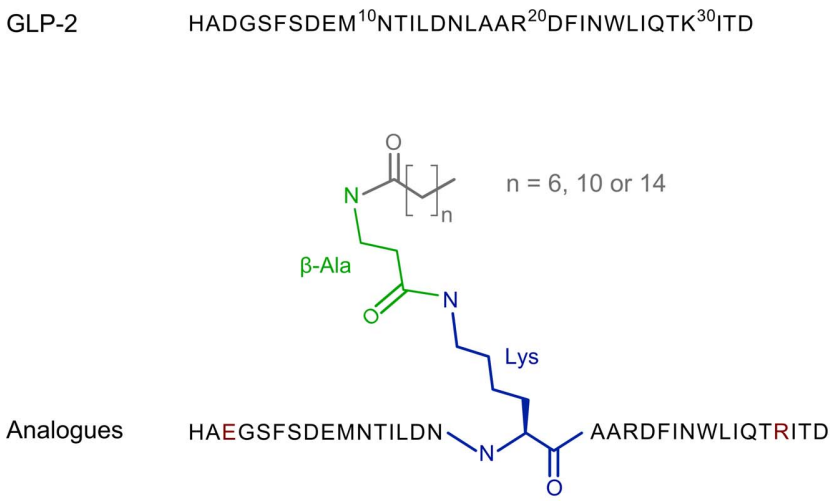

Figure 2. Schematic representation of native GLP-2 and its acylated analogues. GLP-2 is acylated with c8, c12 or c16-chains (grey) at the $\epsilon-$amino group of Lys17 (blue) via a $\beta-$alanine spacer (green). The lysine residue replaces a leucine at position 17 and the natural lysine at position 30 in GLP-2 is mutated to an arginine (red). The aspartic acid at position 3 is mutated to a glutamic acid (red) to avoid racemization during synthesis. None of these mutations caused measurable loss-of-function.
doi:10.1371/journal.pone.0109939.g002

The concentration-dependent self-association of GLP-2 and its analogues was investigated by tryptophan fluorescence (fig. 3). The acyl chains confer increased hydrophobicity, causing self-assembly at lower concentrations for the acylated analogues compared to the native peptide. Furthermore, the self-association concentration decreased with increasing acyl chain length, consistent with increasing hydrophobicity.

At physiological ionic strength, the secondary structure of the c16 acylated analogue was similar to native GLP-2 (investigated by circular dichroism (CD), see fig. S1). It is worth noting that the buffer ionic strength is crucial for self-association, as no self-association was observed with 0 or 10 mM NaCl. This is consistent with electrostatic screening of the peptides's multiple negative charges as a requirement for self-association. The peptide oligomers of native GLP-2 and its c16-analogue were characterized by static and dynamic light scattering (DLS/SLS) and transmission electron microscopy (TEM), which showed that the oligomers were spherical and well-defined in size (smaller for the native peptide than the analogue), and composed of less than 10 monomers (see fig. S2).

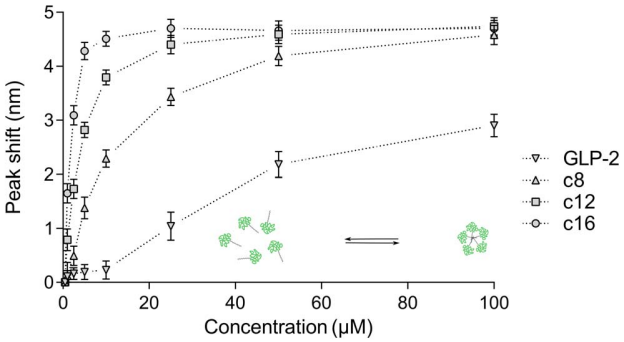

Figure 3. Concentration-dependent self-association of GLP-2 and its analogues. Increasing concentration leads to a blue-shift and increase in tryptophan maximum fluorescence, indicating self-association of the peptides. Control experiments with L-Trp, which does not self-associate, displayed no blue-shift. For the acylated analogues the self-association concentration decreases with increasing chain length, consistent with increased hydrophobicity which renders self-association more favorable. Native GLP-2 is less prone to self-association, and higher concentrations than the displayed 100 μM are required to reach full self-association. Data points are mean $\pm$ SD of 2 separate experiments, and lines are provided to guide the eye. The sketch serves as an illustration of self-association.
doi:10.1371/journal.pone.0109939.g003

Interaction with model lipid membranes

The partitioning of peptides into liposomes was quantified by tryptophan fluorescence, in order to investigate the effect of acylation on interactions with lipid membranes. The data presented in fig. 4 shows that acylation of GLP-2 causes increased partitioning into POPC membranes, where partitioning of native GLP-2 is below the measurable limit and is not included in the graphs. The standard Gibbs free energy of partitioning increases linearly with acyl chain length for the investigated c8, c12 and c16-chains, which is consistent with previous reports of acylated glycine [37]. It is worth noting that the slope of this linear relationship is lower for the GLP-2 analogues than for the acylated glycine analogues, as reported by Peitzsch et al. [37]. This indicates that the dependence of membrane affinity on acyl chain length is influenced by the peptide or amino acid backbone, and that the small glycine residue is more sensitive to chain length than the larger GLP-2 peptide.

It should be noted that the peptides are used at a very low concentration (2 μM) in order to avoid self-association, and that the peptide/lipid ratio is quite low. For subsequent cell experiments (and possible therapeutic applications) the peptides are used at higher concentrations, and the lipid concentration is not well-defined. Therefore, caution should be exerted when comparing liposome and cell results, and speculating on *in vivo* applications.

Receptor activation

The biological activity of the analogues was verified in a Luciferase assay (sketched in fig. 5), using a cell line stably expressing the GLP-2 receptor and a luciferase gene, which is transcribed upon receptor activation.

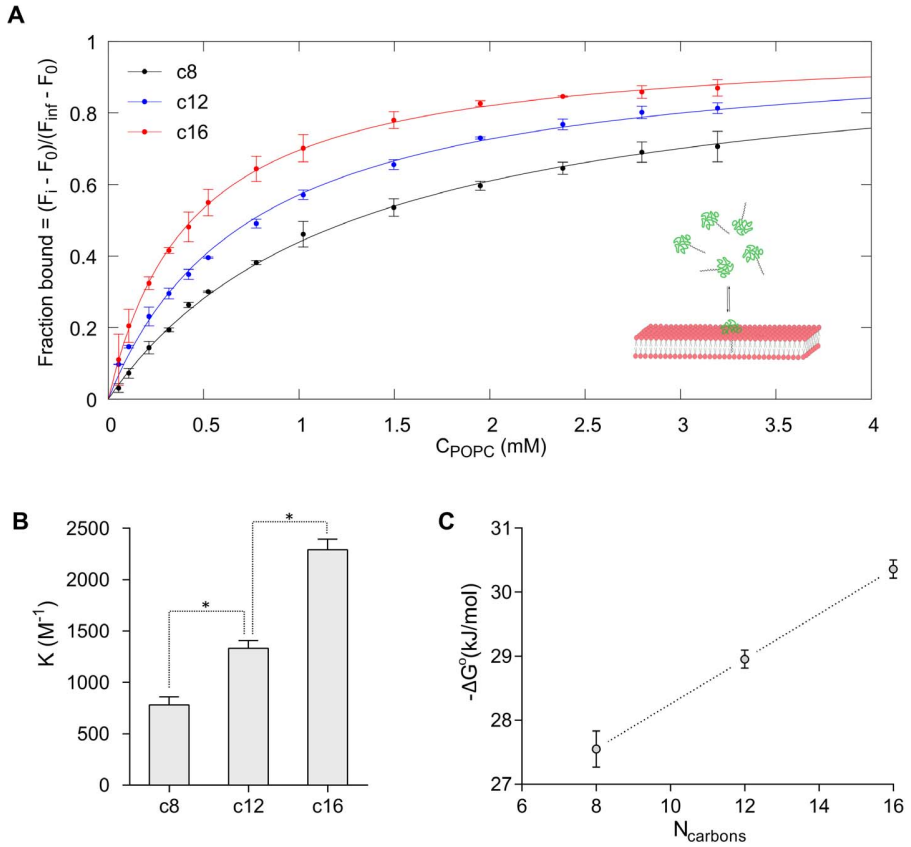

Figure 4. Binding to neutral liposomes. Addition of POPC liposomes to 2 μM peptide solutions causes an increase in tryptophan fluorescence, indicating partitioning of the peptides into the hydrophobic part of the lipid membrane. A) The peptide fluorescence during titration with POPC liposomes, fitted according to eq. 2 (solid lines), which yields the partitioning coefficients (K) shown in B). For the acylated analogues the partitioning coefficient increases with increasing chain length, and converting to the standard Gibbs free energy (ΔG°) according to eq. 3 yields a linear relationship with the chain length, C). Native GLP-2 partitions very weekly into POPC liposomes, with values below the measurable limit (K<500 M^{-1}), and GLP-2 is therefore not included in the figure. Data points represent mean $\pm$ SD of 2 separate experiments and stars in B) indicate significantly different values ($p<0.05$). The sketch serves as an illustration of membrane-partitioning.
doi:10.1371/journal.pone.0109939.g004

Alteration of therapeutic peptides is accompanied by a risk of reducing potency, and acylation is no exception. However, through a rational choice of acylation site and type and/or screening different acylations, it is often possible to limit the deleterious effects on biological activity [36]. All of of the investigated acylated GLP-2 analogues display similar function compared to native GLP-2, suggesting that these acylations did not negatively impact receptor binding and activation.

The assay is employed to measure picomolar concentrations of GLP-2 and its analogues after *in vitro* experiments with Caco-2 cells, using peptide standard curves fitted according to eq. 5. Thus, the advantage of this cell based reporter assay is its very high sensitivity.

Interaction with Caco-2 cells

The Caco-2 setup is sketched in fig. 6. The translocation of peptide over time from the apical (upper) chamber to the basolateral (lower) chamber was measured, along with the amount of peptide associated with the cells after an experiment, both in the aqueous parts of the cells (uptake) and in the lipid membranes.

Peptide translocation. The translocation of GLP-2 and its analogues is presented in fig. 7, where part A shows the accumulated amount of peptide in the basolateral compartment during the 1 hour experiment and part B shows the apparent permeability (P_{app}), calculated according to eq. 6.

The translocation depends non-trivially on the acylation chain length, as the short and medium chains (c8 and c12) increase the translocation relative to native GLP-2, but the long chain (c16) decreases it slightly. This indicates an optimum chain length where the translocation is increased by increased hydrophobicity and intermediate membrane binding, whereas the long chain causes too effective membrane insertion and strong binding, which limits translocation. For the c12 analogue, the increase in translocation through acylation is roughly a factor 1.5 compared to native GLP-2.

An alternative explanation for the decreased translocation of c16 could be increased self-association, which may limit paracellular translocation through the concomitant increase in size. The extent to which the cellular environment affects self-association is currently unknown, as is the exact degree of peptide translocation through either the paracellular or transcellular route.

The acyl chain length may have an effect on albumin binding, and thereby circulation time, which could limit the useful acyl chain lengths to medium and long chain [8,36], but this is not fully established [4] and has not been investigated in this study.

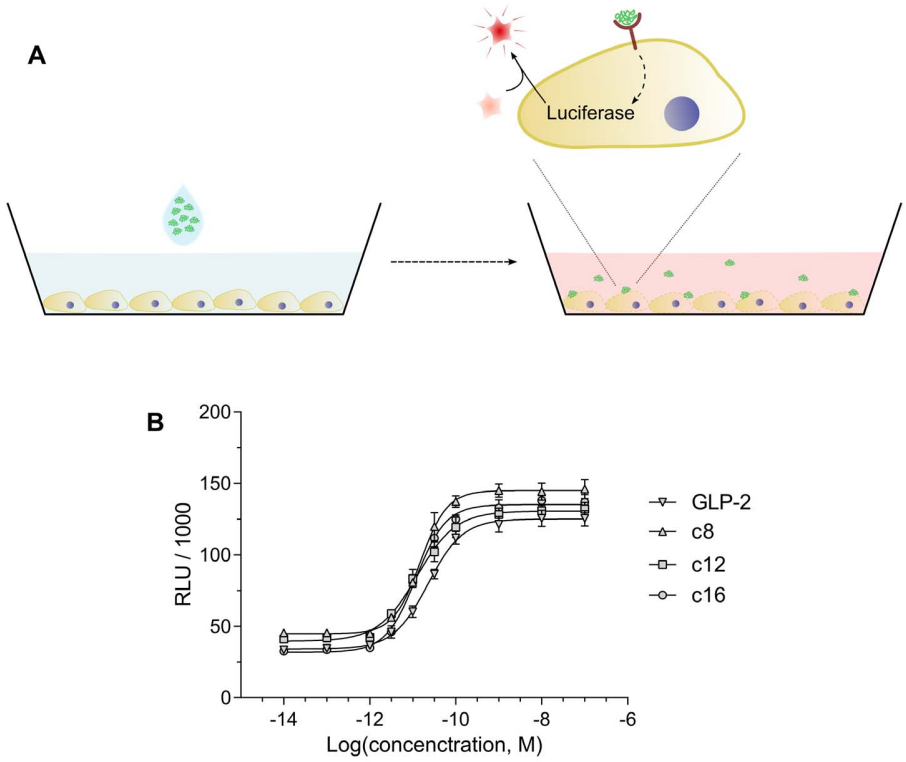

Figure 5. Schematic illustration of the Luciferase receptor activation assay and typical standard curves. A) In order to confirm biological activity of the analogues and measure picomolar concentrations of the peptides, a cell-line with the GLP-2-receptor and a luciferase reporter gene was employed. Upon receptor activation by GLP-2 or its analogues, the cells produce luciferase, which can cleave the substrate luciferin to a luminescent product. B) Representative standard curves of receptor activation (RLU) with increasing peptide concentration, for native GLP-2 and its analogues. Data points represent mean $\pm$ SD from 3 determinations, and solid lines are fitted according to eq. 5.
doi:10.1371/journal.pone.0109939.g005

Cell membrane binding and uptake. The cell membrane binding and uptake of GLP-2 and its analogues is presented in fig. 8, where it is evident that both increase with acylation and increasing chain length. The cell membrane binding qualitatively resembles the liposome membrane binding presented in fig. 4C, showing that the chain-length dependence for binding to neutral model membranes is a valid predictor for cell membrane affinity, despite the added complexity of the biological environments compared to a simplified model membrane. It should be noted that cell studies employ a higher concentration of peptide than liposome binding studies, which may cause differences in peptide self-association behavior.

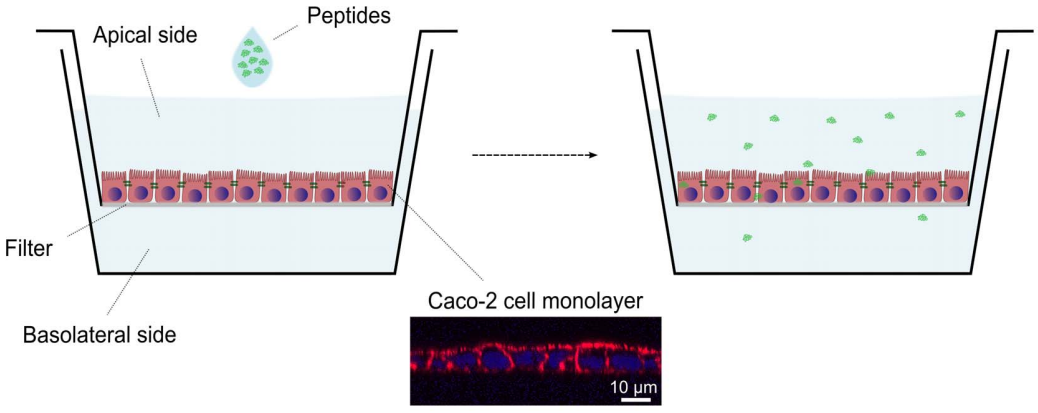

Figure 6. Schematic illustration of the Caco-2 setup. The Caco-2 intestinal model is composed of Caco-2 cells grown in a monolayer on a semipermeable filter support that separates two solution chambers. The peptide of interest is added to the top chamber (modeling the apical side of the intestine, i.e. the intestinal lumen), and the translocated peptide is sampled from the lower chamber over time (modeling the basolateral side of the intestine). Subsequently, the cells are analyzed for peptide content, both in the aqueous parts of the cells (uptake) and in the lipid membranes. The microscopy image in the insert shows a Caco-2 monolayer on the filter support, after fixing and staining for cell nucleus (blue) and actin (red).
doi:10.1371/journal.pone.0109939.g006

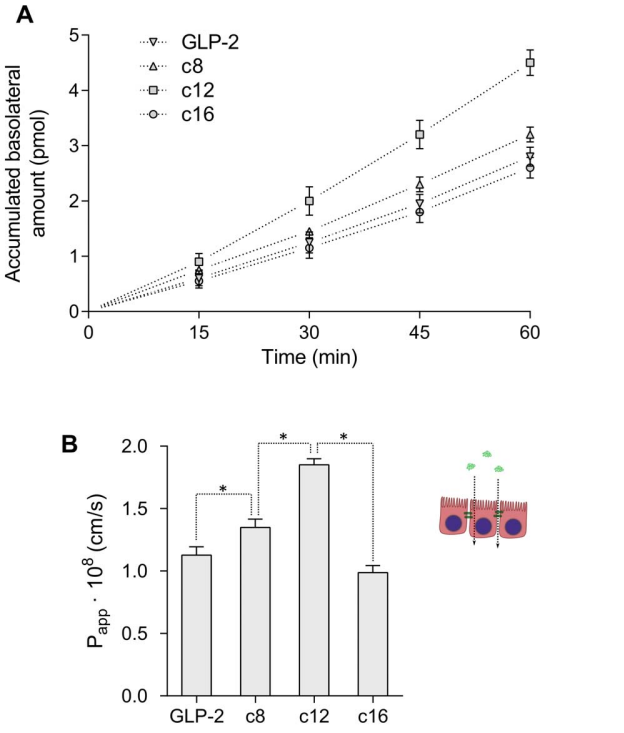

Figure 7. Translocation of GLP-2 and its analogues across Caco-2 cell monolayers. A) Accumulated amount of peptide in the basolateral chamber during the 1 hour experiment. B) Apparent permeability (P_{app}) of the peptides, calculated according to eq. 6. Data points represent mean ± SD of 3 separate experiments, each with 4 repeats, and stars indicate significant differences ($p<0.05$).
doi:10.1371/journal.pone.0109939.g007

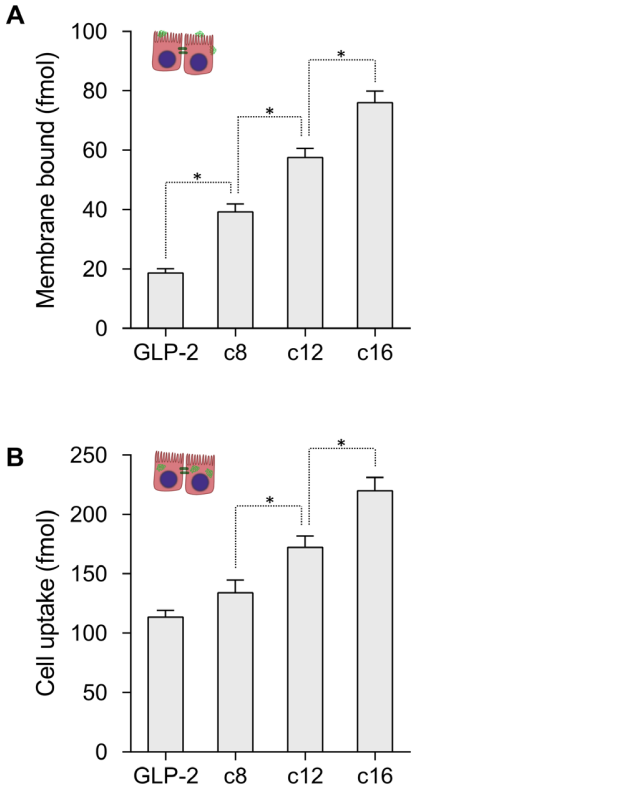

Figure 8. Cell membrane binding and uptake. The amount of peptide bound in the cell membrane A) and the amount of peptide in the aqueous parts of the cell B) increase with acylation length, indicating a larger interaction with cells. For the acylated analogues the membrane binding is roughly linear with chain length, and resembles the observed binding to model membranes shown in fig. 4C. Data points represent mean ± SD of 3 separate experiments, each with 4 repeats, and stars indicate significantly different values ($p<0.05$).
doi:10.1371/journal.pone.0109939.g008

We speculate that the increase in cell uptake with increasing acyl chain length is caused by increased cell membrane binding, where peptide bound to the cell membrane is subsequently taken up more readily.

The observed cell binding qualitatively supports the hypothesis that the decrease in cell translocation for long chain acylation is caused by their increased membrane interactions. The decrease in translocation for c16-acylation compared to c12-acylation is larger than expected from the increased membrane binding, however, this may be explained by the added effect of increased uptake that could lead to intracellular sequestration.

If the membrane binding is a powerful determinant for cell translocation, the liposome partitioning coefficient may be used as a predictor hereof, but this should be investigated in further detail, using other peptides or acylations.

Absorption enhancers. The two absorption enhancers EGTA (paracellular) and SDS (transcellular) were employed to assess the effect of different enhancement mechanisms on the acyl chain length dependence.

We hypothesize that paracellular enhancers will have little effect on the acyl chain length dependence, i.e. enhance transport of the peptide and all its analogues to a similar extent, whereas transcellular enhancers that fluidize the membrane may have an increased effect on the long-chain acylated analogue by altering the membrane affinity and/or dynamics of membrane insertion and detachment.

A previously performed dose-response experiment was used to determine the appropriate concentration of absorption enhancers, that yielded increased mannitol transport and a reversible decrease in TEER with full recovery after 24 hours, and the results using the optimal concentrations are presented in fig. 9A and B. The translocation of GLP-2 and its analogues in the presence of EGTA or SDS is presented in fig. 9C. For each peptide, the increased transport in the presence of enhancer was compared to the transport of the peptide alone as shown in fig. 9D, which emphasizes the differences between the two types of enhancer. For EGTA the increase is similar for peptide and analogues, and the dependence on acyl chain length is retained, whereas for SDS the increase is greater for the c16-acylation. These results support the hypothesis that the fluidization of cell membranes caused by SDS are beneficial for the long chain acylation, possibly due to altered membrane insertion. This could be verified by investigating liposome partitioning or cell membrane binding in the presence of SDS. However, despite the added benefit of SDS for the c16-acylation, the translocation of the c16 peptide remains lower than for the c12 peptide, suggesting that the acylation length is the primary determining factor for optimizing translocation. EGTA and SDS are employed as representatives of paracellular and transcellular enhancers, and other enhancers of these types are expected to elicit similar effects.

In conclusion, EGTA and SDS at the concentrations employed increase the translocation while retaining the acyl chain length dependence, with a medium chain length (c12) yielding the highest translocation.

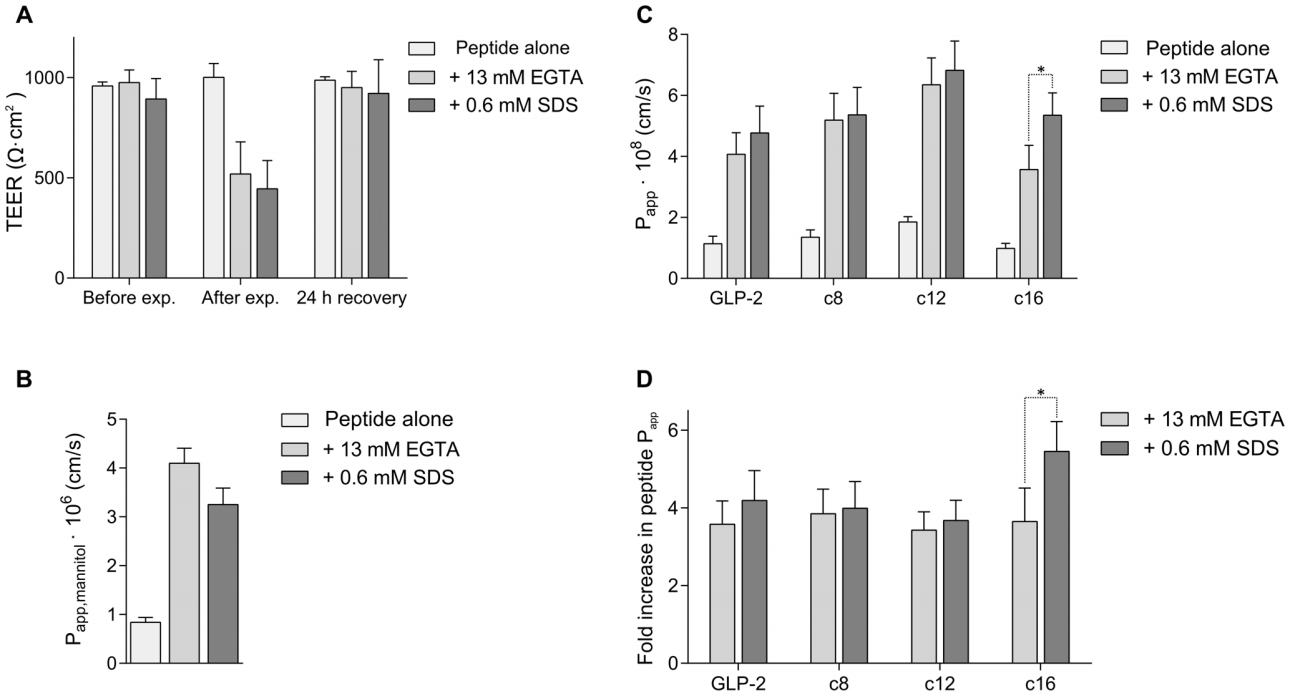

Figure 9. Effect of absorption enhancers on translocation of GLP-2 and its analogues. A) TEER values for Caco-2 cell monolayers after experiments with absorption enhancers EGTA (paracellular) or SDS (transcellular), and after 24 hour recovery in cell medium. B) Mannitol permeability in the presence of EGTA or SDS. C) Peptide permeability in the presence of EGTA or SDS. D) Fold increase in peptide permeability with enhancer, compared to each peptide alone. All data points represent mean $\pm$ SD of 2 separate experiments, each with 4 repeats, and stars indicate significant differences ($p<0.05$).
doi:10.1371/journal.pone.0109939.g009

Conclusions and Perspectivation

We have synthesized and investigated a systematic series of acylated GLP-2 analogues, in order to establish how the membrane binding correlates to *in vitro* intestinal permeability. We find that increasing acyl chain length causes increased self-association and binding to lipid and cell membranes, whereas translocation across intestinal cells displays a non-linear dependence on chain length. Short and medium chains improve translocation compared to the native peptide, but long chain acylation does not. We explain this correlation by an initial benefit for translocation for shorter chains through increased interaction with the cell membrane, which reverts to a hindrance for long chains, i.e. the analogues get stuck in the cell membrane. Measurements of liposome binding may be used to predict the optimal acylation chain length (e.g. the partitioning coefficient of approximately 1300 M^{-1} for c12-GLP-2), which can be further investigated by using other peptides or acylation types.

The translocation of peptide and analogues increases in the presence of both paracellular and transcellular absorption enhancers. The acyl chain length dependence persists for the paracellular enhancer and partially for the transcellular enhancer, with an increased benefit for the long chain acylation. This can be explained on the basis of a membrane fluidizing effect of the transcellular enhancer, which alters the dynamics and strength of membrane insertion, however, this requires further investigation. For both enhancers the medium chain acylation (c12) yields the highest translocation, approximately 1.5 times the native peptide.

The presented results suggest that rational acylation of GLP-2 increases intestinal absorption, and may benefit the oral delivery route. However, this should be verified *in vivo*, *e.g.* by investigating the intestinal absorption in an animal model following in situ administration to the intestine. Dosing directly to the rat intestine circumvents the esophagus and stomach, where the peptide would most likely require further stabilization to remain intact, *e.g.* through encapsulation and/or enteric coating.

In order to assert whether the effect of acylation on GLP-2 is general and can be used to benefit oral delivery of other therapeutic peptides, we are currently investigating other acylated peptides. GLP-2 exerts is therapeutic function locally in the intestine, which eases oral delivery and limits the challenging requirement for long circulation times in the blood stream. However, other therapeutic peptides that function systemically or at sites apart from the intestine may benefit thrice from acylation, *i.e.* on intestinal absorption, enzymatic stability, and circulation life time.

Supporting Information

Figure S1 Secondary structure of native and acylated GLP-2. Circular dichroism spectra of GLP-2 and its c16 analogue in buffers with different ionic strength (0–150 mM NaCl). The secondary structure of native GLP-2 and its acylated c16 analogue is different at low ionic strength (as previously reported in [38]), but similar at physiological ionic strength. It should be noted that self-association alters the secondary structure, and as described in the main text, the self-association behavior is affected by acylation. The employed concentration 150 μM was chosen in order to compare to [38], and at this concentration the peptides are expected to be self-associated.
(TIF)

Figure S2 Size of selected peptide oligomers. TEM (middle) and DLS (bottom) show that the native peptide and its c16-analogue forms oligomers with radius 2.4 $\pm$ 0.1 nm and 2.8 $\pm$ 0.1 nm, respectively. SLS-measurements show that the native peptide oligomers are composed of approximately 4 peptide monomers, whereas the c16 analogue oligomers are larger and composed of around 7–10 monomers. The top sketch serves as an illustration of peptide oligomers.
(TIF)

Materials S1 Materials and Methods for Cicular Dichroism (CD), Dynamic and Static Light Scattering (DLS/SLS) and Transmission Electron Microscopy (TEM).
(PDF)

References

1. Dasgupta P, Singh A, Mukherjee R (2002) N-terminal acylation of somatostatin analog with long chain fatty acids enhances its stability and anti-proliferative activity in human breast adenocarcinoma cells. Biol Pharm Bull 25: 29–36.
2. Yuan L, Wang J, Shen WC (2005) Reversible Lipidization Prolongs the Pharmacological Effect, Plasma Duration, and Liver Retention of Octreotide. Pharm Res 22: 220–227.
3. Gozes I, Bardea A, Reshef A, Zamostiano R, Zhukovsky S, et al. (1996) Neuroprotective strategy for Alzheimer disease: intranasal administration of a fatty neuropeptide. Proc Natl Acad Sci U S A 93: 427–32.
4. Kurtzhals P, Havelund S, Kiehr B, Larsen UD, Ribel U, et al. (1995) Albumin binding of insulins acylated. Biochem J 312: 725–731.
5. Havelund S, Plum A, Ribel U, Jonassen I, Vølund A, et al. (2004) The mechanism of protraction of insulin detemir, a long-acting, acylated analog of human insulin. Pharm Res 21: 1498–504.
6. Zhang L, Bulaj G (2012) Converting peptides into drug leads by lipidation. Curr Med Chem 19: 1602–18.
7. Wang J, Chow D, Heiati H, Shen WC (2003) Reversible lipidization for the oral delivery of salmon calcitonin. J Control Release 88: 369–80.
8. Knudsen LB, Nielsen PF, Huusfeldt PO, Johansen NL, Madsen K, et al. (2000) Potent derivatives of glucagon-like peptide-1 with pharmacokinetic properties suitable for once daily administration. J Med Chem 43: 1664–9.
9. Wang J, Shen WC (2000) Gastric retention and stability of lipidized BowmanBirk protease inhibitor in mice. Int J Pharm 204: 111–116.
10. Morishita M, Peppas NA (2006) Is the oral route possible for peptide and protein drug delivery? Drug discov today 11: 905–10.
11. Hubatsch I, Ragnarsson EGE, Artursson P (2007) Determination of drug permeability and prediction of drug absorption in Caco-2 monolayers. Nature protocols 2: 2111–9.
12. Artursson P, Palm K, Luthman K (2001) Caco-2 monolayers in experimental and theoretical predictions of drug transport. Adv Drug Delivery Rev 46: 27-43.
13. Uchiyama T, Kotani A, Tatsumi H (2000) Development of novel lipophilic derivatives of DADLE (leucine enkephalin analogue): Intestinal permeability characteristics of DADLE derivatives in rats. Pharm Res 17.
14. Rogers J, Wong A (1980) The temperature dependence and thermodynamics of partitioning of phenols in the n-octanol-water system. Int J Pharm 6: 339–348.
15. Balon K, Riebesehl B, Müller B (1999) Drug liposome partitioning as a tool for the prediction of human passive intestinal absorption. Pharm Res 16: 882–888.
16. Krämer S (1999) Absorption prediction from physicochemical parameters. Pharm Sci Technol To 2: 373–380.
17. Drucker DJ (1999) Glucagon-like Peptide 2. Trends in Endocrinology & Metabolism 10: 153–156.
18. Orskov C, Holst JJ, Knuhtsen S, Baldissara FGA, Poulsen SS, et al. (1986) Glucagon-Like Peptides GLP-1 and GLP-2, Predicted Products of the Glucagon Gene, Are Secreted Separately from Pig Small Intestine but Not Pancreas. Endocrinology 119: 1467–1475.
19. Wallis K, Walters JRF, Forbes A (2007) Review article: glucagon-like peptide 2-current applications and future directions. Alimentary pharmacology & therapeutics 25: 365–72.
20. Jeppesen PB (2012) Teduglutide, a novel glucagon-like peptide 2 analog, in the treatment of patients with short bowel syndrome. Therap Adv Gastroenterol 5: 159–71.
21. Hartmann B, Johnsen AH, Orskov C, Adelhorst K, Thim L, et al. (2000) Structure, measurement, and secretion of human glucagon-like peptide-2. Peptides 21: 73–80.
22. Tavares W, Drucker DJ, Brubaker PL (2000) Enzymatic- and renal-dependent catabolism of the intestinotropic hormone glucagon-like peptide-2 in rats. Am J Physiol Endocrinol Metab 278: E134–139.
23. te Welscher YM, Chinnapen DJF, Kaoutzani L, Mrsny RJ, Lencer WI (2014) Unsaturated glycoceramides as molecular carriers for mucosal drug delivery of GLP-1. J Control Release 175: 72–8.
24. Deli MA (2009) Potential use of tight junction modulators to reversibly open membranous barriers and improve drug delivery. Biochim Biophys Acta 1788: 892–910.
25. Sakai M, Imai T, Ohtake H, Otagiri M (1998) Cytotoxicity of Absorption Enhancers in Caco-2 Cell Monolayers. J Pharm Pharmacol 50: 1101–1108.
26. Thulesen J, Knudsen LB, Hartmann B, Hastrup S, Kissow H, et al. (2002) The truncated metabolite GLP-2 (3-33) interacts with the GLP-2 receptor as a partial agonist. Regul Pept 103: 9–15.
27. Sams A, Hastrup S, Andersen M, Thim L (2006) Naturally occurring glucagon-like peptide-2 (GLP-2) receptors in human intestinal cell lines. Eur J Pharmacol 532: 18–23.
28. Palasek SA, Cox ZJ, Collins JM (2007) Limiting racemization and aspartimide formation in microwave-enhanced Fmoc solid phase peptide synthesis. J Pept Sci 13: 143–8.
29. Fujinari E, Courthaudon L (1992) Nitrogen-specific liquid chromatography detector based on chemiluminescence: Application to the analysis of ammonium nitrogen in waste water. J Chromatogr 592: 209–214.
30. Jesorka A, Orwar O (2008) Liposomes: technologies and analytical applications. Annu Rev Anal Chem 1: 801–32.
31. Rouser G, Siakotos AN, Fleischer S (1966) Quantitative analysis of phospholipids by thin-layer chromatography and phosphorus analysis of spots. Lipids 1: 85–6.
32. Burstein EA, Abornev SM, Reshetnyak YK (2001) Decomposition of protein tryptophan fluorescence spectra into log-normal components. I. Decomposition algorithms. Biophys J 81: 1699–709.
33. Etzerodt T, Henriksen JR, Rasmussen P, Clausen MH, Andresen TL (2011) Selective acylation enhances membrane charge sensitivity of the antimicrobial peptide mastoparan-x. Biophys J 100: 399–409.
34. Ladokhin AS, Jayasinghe S, White SH (2000) How to measure and analyze tryptophan fluorescence in membranes properly, and why bother? Anal Biochem 285: 235–45.
35. Naylor LH (1999) Reporter gene technology: the future looks bright. Biochem Pharmacol 58: 749–757.
36. Madsen K, Knudsen LB, Agersoe H, Nielsen PF, Thø gersen H, et al. (2007) Structure-activity and protraction relationship of long-acting glucagon-like peptide-1 derivatives: importance of fatty acid length, polarity, and bulkiness. J Med Chem 50: 6126–32.
37. Peitzsch RM, McLaughlin S (1993) Binding of acylated peptides and fatty acids to phospholipid vesicles: pertinence to myristoylated proteins. Biochemistry 32: 10436–43.
38. Pinholt C, Kapp SJ, Bukrinsky JT, Hostrup S, Frokjaer S, et al. (2012) Influence of acylation on the adsorption of GLP-2 to hydrophobic surfaces. Int J Pharm: 1–9.

Acknowledgments

We thank Holger Martin Strauss for helpful discussions regarding study design and manuscript preparation; Jonas Henriksen for assistance with the liposome partitioning assay; Lars Thim for providing native GLP-2 and a modified c16-analogue; Anja Knudsen for assistance with peptide synthesis; Anette Sams for providing hGLP-2R cells; and Lisette G. Nielsen for assistance with Caco-2 and hGLP-2R cells.

Author Contributions

Conceived and designed the experiments: ST LL SB TLA ULR. Performed the experiments: ST. Analyzed the data: ST LL SB TLA ULR. Contributed reagents/materials/analysis tools: ST LL ULR. Wrote the paper: ST LL SB TLA ULR.

Supporting Information

Materials and Methods

Circular Dichroism, CD UV CD spectra were obtained on a Jasco-J-815 circular dichroism spectrophotometer (Jasco, Tokyo, Japan). 150 μM peptide samples in HEPES buffers (10 mM HEPES, 0-150 mM NaCl, pH 7.4) were scanned at room temperature in 0.1 mm cells from 200-260 nm using a bandwidth of 2 nm, a response time of 2 s, a data pitch of 0.5 nm and a scanning speed of 50 nm/min. The instrument was calibrated with camphersulfonic acid. A background spectrum of the buffer was subtracted from each peptide spectrum, and the spectra were converted to molar CD using instrument software.

Dynamic and Static Light Scattering, DLS and SLS A modified commercial Laser Light Scattering (LLS) spectrometer (ALV/DLS/SLS-5022F) equipped with a multi$-\tau$ digital time correlator (ALV5000) and a cylindrical 22 mW He-Ne laser (λ_0 632.8 nm) was used for static and dynamic light scattering (SLS and DLS). LLS was performed at angles between 20° and 150° and the DLS time correlation was analyzed by ALV Correlator 3.0 software. SLS results were analyzed manually, and the molecular weight of the peptide oligomers was obtained using the previously reported partial refractive index of 0.186 mL/g (for proteins in saline buffer with λ_0 633 nm) [1].

250 μM peptide samples in HEPES buffer were filtered through 0.22 μM PVDF filters (non-protein binding Whatman, GE healthcare), while care was taken to avoid dust in the solution and measuring container.

Transmission Electron Microscopy, TEM TEM imaging was performed on 250 μM peptide samples, as prepared for LLS measurements. 10 μL of sample was applied onto a carbon covered copper grid for 1 minute, after which excess sample was removed carefully with filter paper. The peptides were stained with 3% (w/v) phosphotungstic acid (PTA), by applying 10 μL PTA solution to the copper grid for 2 minutes, after which excess solution was removed. The copper grid was rinsed once with a droplet of MQ water and dried in air for 5 minutes. Samples were imaged at 120 kV in a Technai TEM (FEI).

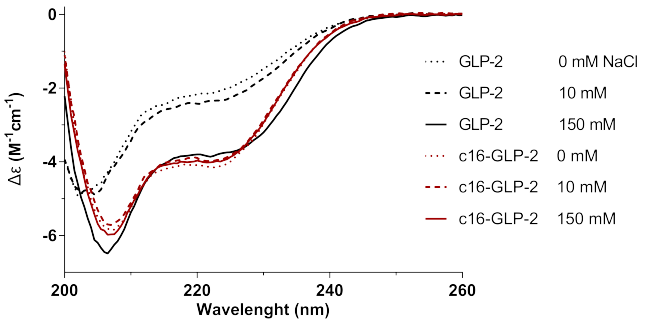

Figure 1: **(Figure S1) Secondary structure of native and acylated GLP-2.** Circular dichroism spectra of GLP-2 and its c16 analogue in buffers with different ionic strength (0-150 mM NaCl). The secondary structure of native GLP-2 and its acylated c16 analogue is different at low ionic strength (as previously reported in [2]), but similar at physiological ionic strength. It should be noted that self-association alters the secondary structure, and as described in the main text, the self-association behavior is affected by acylation. The employed concentration 150 μM was chosen in order to compare to [2], and at this concentration the peptides are expected to be self-associated.

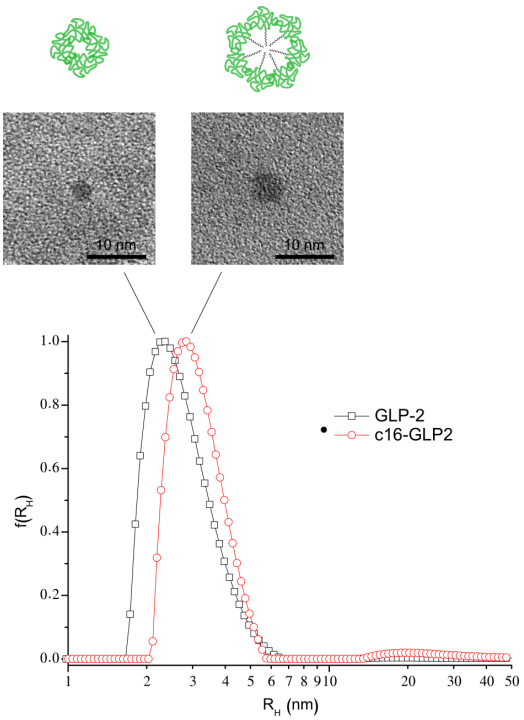

Figure 2: **(Figure S2) Size of selected peptide oligomers.** TEM (middle) and DLS (bottom) show that the native peptide and its c16-analogue forms oligomers with radius 2.4 ± 0.1 nm and 2.8 ± 0.1 nm, respectively. SLS-measurements show that the native peptide oligomers are composed of approximately 4 peptide monomers, whereas the c16 analogue oligomers are larger and composed of around 7-10 monomers. The top sketch serves as an illustration of peptide oligomers.

References

[1] J Wen, T Arakawa (2000) Refractive index of proteins in aqueous sodium chloride. Anal. Biochem. 280: 327–9.

[2] C Pinholt, SJ Kapp, JT Bukrinsky, S Hostrup, S Frokjaer, W Norde, L Jorgensen (2012) Influence of acylation on the adsorption of GLP-2 to hydrophobic surfaces. Int. J. Pharm. 1–9.

3.1.1 Notes on paper 1 and GLP-2 results

The paper presents results obtained for GLP-2 analogues, but a few additional points deserve mentioning.

Attaching a hydrophobic moiety to GLP-2 reduced its solubility and 'ease of handling', so extra care was required for verifying peptide concentration in solutions and planning experiments. Interestingly, the receptor potency did not appear to decrease significantly by acylation. In most experiments, native GLP-2 was used as reference, however, the acylated analogues contained several backbone mutations. Thus, GLP-2 with D3E and K30R could be a better reference, whereas L17K was best omitted due to the extra positive charge, which disappears upon acylation. The GLP-2 backbone (E3, R30, K17) was compared to native GLP-2 with regard to self-association and liposome partitioning, which yielded similar results, and caco-2 permeability, where permeability was slightly higher for the backbone, presumably explained by the reduced negative charge.

In the beginning of the project, several complimentary methods were used to characterize GLP-2 analogues, some of which yielded results not included in the paper. For completeness sake they are briefly mentioned here, but the methods are not described in detail. The hydrophobicity of GLP-2 analogues was measured in reverse-phase HPLC, with consistent results for increasing hydrophobicity with chain length. However, HPLC elution is a very simple model which requires organic solvents, and we deemed that the liposome partitioning method was more nuanced, well-controlled and precise (however, also more labor-intensive). Isothermal Titration Calorimetry (ITC) was briefly attempted for measuring liposome partitioning, but the quite limited membrane-affinity gave rise to very weak heat-spikes and experiments were discontinued. Regarding the self-association, NMR studies yielded similar concentration-dependent results as Trp-fluorescence and CD and were discontinued. The self-association was initially characterized for native GLP-2 and its c16-analogue using Analytical Ultra Centrifugation (AUC), which roughly supported DLS, SLS, and TEM studies, i.e. larger oligomers for the acylated analogue than the native peptide. Native GLP-2 oligomers were not very stable, but were most likely composed of 4 monomers, whereas c16-acylated GLP-2 oligomers most likely contained 7-8 monomers.

Initially, further *in vitro* experiments were planned with GLP-2 analogues, but their very limited interaction with Caco-2 cells motivated us to switch to sCT more rapidly than anticipated. We found no published reports of Caco-2/GLP-2 studies, but both translocation across and interaction with Caco-2 cells was very low compared to other peptides, e.g. sCT and insulin. This may be due to multiple negative charges in GLP-2, whereas sCT is positively charged.

And with these words we turn to the next chapter concerning sCT.

Chapter 4

Results for sCT

4.1 Paper 2

The following section contains Paper 2, as typeset by the journal, as well as the supplementary information available online.

Summary The paper investigates two systematic series of acylated sCT analogues, with c8, c12 or c16 acyl chains at the N-terminus or Lys18.

The results demonstrate an unpredicted effect of acylation which largely superseded the anticipated membrane interactions; i.e. acylated sCT acts as its own *in vitro* intestinal permeation enhancer. Acylation drastically increases peptide permeability, through reversible cell effect similar to transcellular permeation enhancers, supported by the observed permeabilization of model lipid membranes. The effect likely stems from a synergy between the positive peptide charge and membrane-active acyl moiety, supported by its pH-dependency, whereby the effect increases with decreasing pH and concomitant charge increase. The extent of permeation enhancing effect is highly dependent on acylation chain length and position, with highest peptide permeability for short chain N-terminal acylation or medium/long chain Lys18 acylation, whereas permeability and cell membrane binding appeared correlated only for some analogues.

European Journal of Pharmaceutics and Biopharmaceutics 96 (2015) 329–337

Contents lists available at ScienceDirect

European Journal of Pharmaceutics and Biopharmaceutics

journal homepage: www.elsevier.com/locate/ejpb

Research Paper

Acylation of salmon calcitonin modulates *in vitro* intestinal peptide flux through membrane permeability enhancement

Sofie Trier [a,b], Lars Linderoth [b], Simon Bjerregaard [b], Holger M. Strauss [b], Ulrik L. Rahbek [b], Thomas L. Andresen [a,*]

[a] Dept. of Micro- and Nanotechnology, Center for Nanomedicine and Theranostics, Technical University of Denmark, Building 423, Produktionstorvet, DK-2800 Kgs. Lyngby, Denmark
[b] Global Research, Novo Nordisk A/S, Novo Nordisk Park 1, DK-2760 Maaloev, Denmark

ARTICLE INFO

Article history:
Received 17 April 2015
Revised 24 August 2015
Accepted in revised form 2 September 2015
Available online 5 September 2015

Keywords:
Acylation
Peptide
Salmon calcitonin
Oral
Caco-2
Intestinal permeability
Lipid membranes

ABSTRACT

Acylation of peptide drugs with fatty acid chains has proven beneficial for prolonging systemic circulation, as well as increasing enzymatic stability and interactions with lipid cell membranes. Thus, acylation offers several potential benefits for oral delivery of therapeutic peptides, and we hypothesize that tailoring the acylation may be used to optimize intestinal translocation. This work aims to characterize acylated analogues of the therapeutic peptide salmon calcitonin (sCT), which lowers blood calcium, by systematically increasing acyl chain length at two positions, in order to elucidate its influence on intestinal cell translocation and membrane interaction.

We find that acylation drastically increases *in vitro* intestinal peptide flux and confers a transient permeability enhancing effect on the cell layer. The analogues permeabilize model lipid membranes, indicating that the effect is due to a solubilization of the cell membrane, similar to transcellular oral permeation enhancers. The effect is dependent on pH, with larger effect at lower pH, and is impacted by acylation chain length and position. Compared to the unacylated peptide backbone, N-terminal acylation with a short chain provides 6- or 9-fold increase in peptide translocation at pH 7.4 and 5.5, respectively. Prolonging the chain length appears to hamper translocation, possibly due to self-association or aggregation, although the long chain acylated analogues remain superior to the unacylated peptide. For K^{18}-acylation a short chain provides a moderate improvement, whereas medium and long chain analogues are highly efficient, with a 12-fold increase in permeability compared to the unacylated peptide backbone, on par with currently employed oral permeation enhancers. For K^{18}-acylation the medium chain acylation appears to be optimal, as elongating the chain causes greater binding to the cell membrane but similar permeability, and we speculate that increasing the chain length further may decrease the permeability.

In conclusion, acylated sCT acts as its own *in vitro* intestinal permeation enhancer, with reversible effects on Caco-2 cells, indicating that acylation of sCT may represent a promising tool to increase intestinal permeability without adding oral permeation enhancers.

1. Introduction

Acylation of therapeutic peptides with fatty acids is a widely used peptide alteration strategy in drug delivery, which has found particular use for prolonging peptide circulation in blood of otherwise rapidly cleared peptide drugs, e.g. by exploiting the affinity of serum albumin toward fatty acids [1] and for increasing enzymatic stability [2–5]. Acylation has been employed for a multitude of therapeutic peptides [1,3,6,7], including several marketed drugs (e.g. insulin and Glucagon-like peptide-1). An important drawback for alteration of therapeutic peptides is the risk of reducing potency; however, through a rational choice of acylation site and type and/or screening different acylation positions, it is often possible to limit the deleterious effects on biological activity [8,9].

The majority of reports regarding acylated peptides have focused on subcutaneous injection, whereas the potential for oral administration remains an emerging field. Acylation may benefit several of the challenges in oral delivery, e.g. the highly metabolic environment in the stomach and intestine [10], and the limited absorption of large, hydrophillic peptide drugs through the intestinal epithelial barrier [11]. A widely used method for predicting

* Corresponding author.
E-mail address: thomas.andresen@nanotech.dtu.dk (T.L. Andresen).

http://dx.doi.org/10.1016/j.ejpb.2015.09.001
0939-6411/

in vivo oral absorption is *in vitro* quantification of translocation across monolayers of the human colon cancer cell line (Caco-2), which has been shown to correlate well with oral bioavailability [12,13]. In a few cases, acylation has been shown to increase intestinal permeability of peptide drugs [6,8,14]; however, detailed investigations of systematic acyl variations are lacking. Such investigations will benefit rational design of new peptide drugs, as investigations of peptide interactions with model lipid membranes [15–17] can elucidate its influence on cellular membrane translocation potentially leading to higher oral bioavailability.

Calcitonin (CT) is a single-chain 32 amino acid peptide hormone, with an N-terminal disulphide bridge between positions 1 and 7, and a C-terminal amidated proline. It is produced in the thyroid gland and secreted in response to excess calcium in serum [18], and its primary biological function is the inhibition of osteoclast-mediated bone resorption. Calcitonin is employed in the treatment of bone-related disorders such as osteoporosis, osteoarthritis, Paget's disease, and hypercalcemia [19,20]. Whereas human calcitonin (hCT) is physically and chemically unstable [21], salmon calcitonin (sCT) is more stable, potent [22] and has a longer *in vivo* half-life [20,23]. Consequently, the therapeutic use is mainly based on sCT.

Administration of sCT is currently limited to either parenteral or intranasal routes; however, several examples of oral delivery exist in the literature and, recently, several clinical trials have been completed [20,24]. Most of these reports deal with native sCT in combination with oral permeation enhancers or enzyme inhibitors [20,23,24], which is challenging due to the requirement for sufficiently high additive concentration to allow for intact peptide permeation. Other approaches include advanced delivery systems [25–28] and a few examples of modifying the peptide itself [6,29–31]. 2K PEGylation at Lys18 was shown to increase *in vivo* efficacy but not *in vitro* permeability, so the improvement was ascribed primarily to increased enzymatic stability [31]. Dual acylation with long chains at the sulphide bridge in a reversible or permanent manner was shown to increase oral bioavailability but the *in vitro* permeability was not investigated [6,29,30].

A previous study of acylated analogues of Glucagon-like peptide-2 (GLP-2), a negatively charged peptide hormone [32], revealed a non-trivial relationship between translocation ability and acyl chain length, which correlated with the level of peptide–membrane interactions.

In the present study we wish to investigate this effect in more detail, and have, similar to the GLP-2 analogues, synthesized and characterized a series of acylated sCT analogues where the systematically increasing acyl chains have been placed at two positions on the positively charged backbone. This allows an investigation into the effects of the acyl chain length, backbone charge and acylation placement on membrane interaction and *in vitro* intestinal permeability and, when compared to acylated GLP-2, enables elucidation of potential general trends of peptide acylations on membrane translocation properties.

2. Materials and methods

2.1. Materials

Resin and natural amino acids were purchased from Novabiochem (Germany). c8, c12 and c16 carboxylic acids, Fmoc-beta-Alanine and native sCT were provided by Novo Nordisk A/S. Palmitoyloleoylglycerophosphocholine (POPC) was purchased from Avanti Polar Lipids (USA). HEPES, Ovalbumin (OVA, from chicken egg white) and other standard chemicals were purchased from Sigma–Aldrich (Denmark).

Dulbecco's Modified Eagle Medium (DMEM), L-glutamine and penicillin/streptomycin were purchased from Lonza (Switzerland). Hank's Balanced Salt Solution (HBSS), foetal bovine serum (FBS), nonessential amino acid and other standard cell culture products were purchased from Gibco (Denmark). Radioactively labelled [^{3}H]mannitol, scintillation fluid (Microscint-40), luciferase substrate (SteadyLitePlus) and 96-well plates for luciferase assay (CulturPlate, black) were purchased from PerkinElmer (USA). 12 well Transwell plates for Caco-2 cell monolayers (polycarbonate, 12 mm, pore size 0.4 μM) were purchased from Corning Costar Corp. (USA). hCT-R BHK cells (Hollex-1, ZymoGenetics, US patent 5622839) were provided by Novo Nordisk and Caco-2 cells (HTB-37) were purchased from ATCC.

2.2. Peptide synthesis

The peptides were synthesized by automated Fmoc based SPPS, using a Rink Amide AM resin in a 0.25 mmol scale on a Prelude peptide synthesizer (Protein Technologies), using standard protocols (coupling with 6 eq. amino acid or fatty acid, diisopropylcarbodiimide (DIC) and ethyl 2-cyano-2-(hydroxyimino)acetate (Trade name Oxyma Pure) in N-Methyl-2-pyrrolidone (NMP) for 60 min at r.t.; deprotection with 20% piperidine in NMP for 2 × 10 min). Acetamidomethyl (Acm) was used as protecting groups for Cys. Formation of the disulphide bridge was performed by dissolving the peptides in H_2O (1 mg/1 ml), adjusting pH to 5.5 with acetic acid (AcOH) and oxidizing with a solution of 5% I_2/AcOH at room temperature for approximately 2 h. For N-ε-lysine acylated peptides the 4-Methyltrityl (Mtt) protecting group was used. Mtt was removed with neat hexafluoro-2-propanol (HFIP, 3 × 15 min) followed by washings with dichloromethane (DCM) and the acylation performed on a Prelude peptide synthesizer, using the same conditions as described above. The peptides were cleaved from the resin and deprotected using Trifluoroacetic acid (TFA)/H_2O/Thioanisole (TIS) 92.5:2.5:5 v/v for 3 h, followed by precipitation with diethylether. The peptide was dissolved in a suitable solvent (e.g. 95:5 H_2O:MeCN) and purified by preparative RP-HPLC on an XBridge c18 column (Waters) using MeCN/H_2O/TFA. The fractions were analyzed by UPLC, LCMS, and chemiluminescent nitrogen detection [33], and the appropriate fractions were pooled and portioned for lyophilization.

2.3. hCT receptor activation

The receptor potency of modified sCT analogues was assessed using a hCT-R transfected BHK cell line, similar to previously described for GLP-2 [32].

Briefly, hCT-R cells were cultured in DMEM with 10% FBS and 1% penicillin/streptomycin, and the assay was performed in DMEM without phenol red, containing 10 mM HEPES, 1% glutamax, 0.1% OVA and 1% penicillin/streptomycin. Prior to experiments, cells were plated in 384-well plates (CulturPlate) at 1 × 10^5 cells/ml, centrifuged for 20 s at 1500 rpm, and incubated overnight (at 37 °C and 5% CO_2). After wash with assay medium, cells were incubated with peptide analogues for 3 h, prepared by 7-fold dilutions in the concentration range 0.1 pM–10 nM (and pure buffer as 10 fM point). Cells were then incubated with luciferase substrate for 30 min at room temperature while protected from light, and after a brief shake the luminescence was measured in a topcounter (Packard Topcount). Relative Luminescence Units (RLU) depend on peptide concentration as shown in Eq. (1):

$$\mathrm{RLU} = A + \frac{B - A}{1 + 10^{((\log \mathrm{EC}_{50} - x)\cdot C)}} \quad (1)$$

where x is log(concentration) of the peptide in M, and A, B, C and EC_{50} are fitting parameters [35]. Curves were fitted in GraphPad Prism.

2.4. Caco-2 cells and translocation experiments

Caco-2 cells (passage 40–65) were cultured routinely [12] in DMEM with 10% (v/v) FBS, 1% (v/v) nonessential amino acids, 100 U penicillin, 0.1 mg/mL streptomycin and 2 mM L-glutamine. The Caco-2 cells were seeded at a density of 10^5 cells/well on 12 well Transwell plates (polycarbonate, 12 mm, pore size 0.4 μM) and grown for 14–16 days in DMEM with media change every second day. The cell layer was previously confirmed to consist of a single monolayer of cells by immunohistochemistry and fluorescence microscopy (data in [32]). Per standard nomenclature [12] the upper compartment above the cell layer is designated the apical side, and the lower compartment below the cell layer is designated the basolateral side.

The barrier property and integrity of cell monolayers during growth and before/after experiments was verified by the transepithelial electrical resistance (TEER), measured using a Millicell ERS-2 epithelial volt-ohm meter (Millipore, USA). The widely used translocation marker mannitol (radioactively labelled) was included in all test solutions as another control of the cell layer tightness and integrity [12]. Test solutions were prepared freshly in either HBSS/HEPES buffer (pH 7.4) or HBSS/MES buffer (pH 5.5) (buffers containing 0.1% (w/v) OVA and 20 mM HEPES or MES), and were treated very gently to avoid physical instability. Although more stable than hCT, native sCT can form amyloid fibrils in solution [34], and preliminary tests indicated that the acylated analogues were less stable in HBSS buffer than in sCT. The stability in HBSS buffer increased with decreasing pH, presumably through increased charge and inter-peptide repulsion. Investigating the peptide at lower pH is furthermore interesting from an oral drug delivery perspective, as the pH is slightly acidic in the upper gastrointestinal tract, i.e. the duodenum and proximal jejunum [35,36].

Before transport experiments, DMEM medium was changed to HBSS/HEPES buffer (0.4 mL apical side and 1 mL basolateral) and left to equilibrate for 60 min. Buffer was replaced apically by 0.4 mL test solution at time zero, and the plates were incubated at 37 °C and 5% CO_2 with gentle shaking. Test solutions contained 100 μM peptide and 0.8 μCi/mL [^{3}H]mannitol. Basolateral samples of 200 μL were taken every 15 min for 1 h, and replaced by buffer. The apical test solutions and basolateral samples were analyzed for peptide content with commercial ELISA kits (see next paragraph) and for [^{3}H]mannitol content in a scintillation counter (Packard TopCount), after mixing 1:1 with scintillation fluid.

After experiments, the cells were washed twice with buffer and replenished with medium for 24 h recovery, or washed thrice with ice cold buffer and frozen at −80 °C for cell membrane binding and uptake analysis. Membrane binding and uptake were performed as previously described [32]. Briefly, the frozen cells were scraped off filter inserts, resuspended in cold buffer and centrifuged. The supernatant was analyzed for peptide content (cell uptake), and the pellet was resuspended in buffer, vortexed thoroughly, and centrifuged after addition of ethanol and thorough vortexing. The supernatant solvent was evaporated under nitrogen-flow, and the dry peptide was dissolved in buffer and analyzed for peptide content (cell membrane binding). The cell uptake and membrane binding of peptide and analogues are displayed as the total amount of peptide in the cell layer as percentage of apically added amount (40.000 pmol).

The Caco-2 translocation of peptide or [^{3}H]mannitol over Caco-2 layers is expressed as the apparent permeability (P_{app}), given by

$$P_{app} = \frac{dQ}{dt}\frac{1}{A \cdot C_0} \quad (2)$$

where dQ/dt is the steady-state flux across the cell layer (pmol/s), A is the surface area (1.12 cm^2), and C_0 is the initial sample concentration [12].

2.5. sCT concentration measurements

Apical and basolateral samples from Caco-2 experiments were analyzed using commercial sCT EIA kits, as recommended by the manufacturer. sCT samples and standards were diluted in HBSS buffer as used for Caco-2 experiments, and for each analogue standards were included on the same plate as samples. Standards were prepared for each analogue from sCT test solutions by 10-fold dilutions in the concentration range 1 nM–10 μM, and were fitted to Eq. (3) using GraphPad Prism:

$$\text{Abs (450 nm)} = A + \frac{B - A}{1 + 10^{((\log EC_{50} - x)\cdot C)}} \quad (3)$$

where x is log(concentration) of peptide in M, and A, B, C and EC_{50} are fitting parameters [35].

2.6. Liposome calcein release

A possible membrane-permeabilizing effect of the acylated peptide analogues was studied using POPC liposomes encapsulating the water-soluble fluorophore calcein. POPC lipid films were prepared by evaporation from chloroform:methanol (9:1 v/v) using a gentle nitrogen flow. The residual organic solvent was evaporated in vacuum overnight and the lipid films were rehydrated to 25 mM in HEPES/calcein buffer (20 mM HEPES, 75 mM calcein, pH 7.4) at room temperature with frequent vigorous agitation for 1 h. The multilamellar lipid suspensions were subjected to 10 cycles of freeze–thawing (isopropanol/dry-ice and 40 °C water bath) and extruded to 100 nm liposomes by passing it 21 times through a 100 nm polycarbonate filter in a manual extruder (Avanti Polar Lipids) [37]. The liposome hydrodynamic size after extrusion was measured in a ZetaPALS Zeta Potential Analyzer (Brookhaven Instruments Corporation), after dilution to 50 μM in sterile filtered HEPES buffer. In all experiments the liposome diameter was 130 ± 5 nm with PDI 0.1.

Liposomes were separated from unencapsulated calcein by size-exclusion chromatography on a Sepharose CL-4B column (GE Healthcare, Sweden), with HEPES buffer as eluent (20 mM HEPES, 150 mM NaCl, pH 7.4). The liposomes eluted first, and were collected by an automatic fraction collector. The lipid concentration after extrusion and column purification were measured in triplicate with ICP-MS, as the amount of atomic phosphor compared to phosphor standard curves, and with Ga as internal standard. Roughly 80% lipid is lost during extrusion and column purification, so the expected concentration is around 5 mM, and a typical measured concentration was 6.7 ± 0.3 mM.

The peptide-induced leakage of encapsulated calcein from POPC liposomes was measured in a Victor plate reader (PerkinElmer) with black 96-well microplates, where peptide was mixed with the appropriate buffer to a total volume of 90 μL, and at time zero 10 μL liposome suspension was added to all wells. The plate was incubated at 37 °C while the calcein fluorescence (I_t) was measured regularly (Ex/Em at 485/535 nm), and after 1 h 10 μL 1% Triton X-100 was added to each well to cause total leakage (I_∞). Buffer was used as a negative control and initial fluorescence (I_0), and the calcein release was calculated according to

$$\text{Release (\%)} = \frac{I_t - I_0}{I_\infty - I_0} \cdot 100\% \quad (4)$$

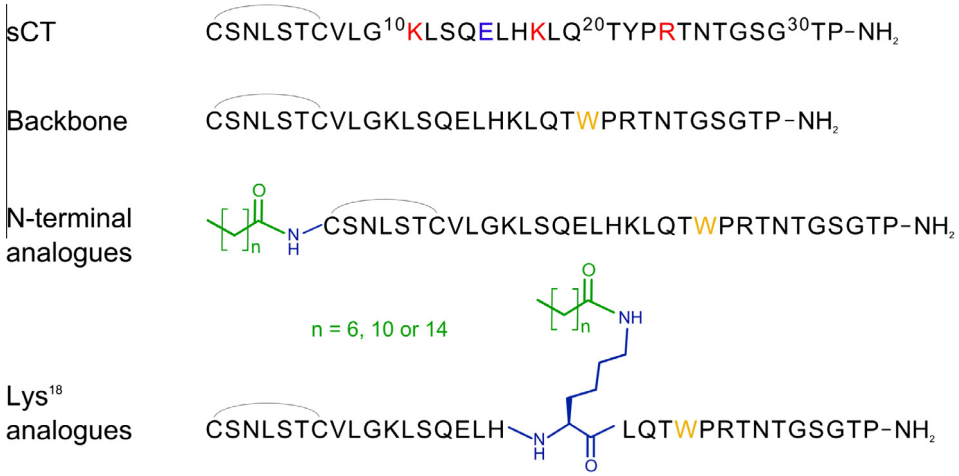

Fig. 1. Schematic representation of the analogues. sCT (with positive and negative amino acids highlighted) is acylated with c8, c12 or c16-chains (green) at either the N-terminus or Lys18 (blue). Tyr22 is changed to Trp (yellow) to allow for fluorescence measurements, and the unacylated peptide backbone (BB) with W22 is used for comparison.

2.7. Data analysis

Statistical analysis was carried out using Prism-6 (GraphPad, USA). Results are presented as the mean ± standard deviation of the mean (SDOM). Unpaired Student's *t*-tests were used for comparison, and a significant difference was considered if $p < 0.05$.

3. Results and discussion

3.1. Peptide analogues

sCT and its acylated analogues are shown in Fig. 1, where the acyl chain is conjugated to a primary amine at either the N-terminus or the lysine in position 18. The peptide backbone (BB) differs from native sCT in the Y^{22}→W mutation, introduced to allow for fluorescence measurements. The potency of sCT is highly dependent on the C-terminus [19], whereas the role of the N-terminal cysteine bridge and the central α-helix motif is somewhat unclear [38]. Since reports have described biological activity of sCT di-acylated at the cysteines or PEGylated at K^{18} [6,31], we placed the acylation at the N-terminus or K^{18}, and deemed that the Y^{22}→W mutation would have limited effect due to the conservative character of the alteration and proximity to K^{18}.

3.2. Receptor activation

The biological activity of the analogues was verified via Luciferase expression in an hCT receptor transfected cell line, and the relative potency values are shown in Fig. 1 (examples of response curves are shown in supplementary information, Fig. S1).

All analogues were active toward the hCT receptor, although the receptor activation was affected by the Y^{22}→W mutation and by acylation. The effect of acylation depends on its position, as the K^{18}-analogues were more potent than the N-terminal analogues, and especially for K^{18}-analogues the potency appeared to increase with acylation chain length.

The potency reduction observed for the peptide backbone and peptide analogues may be due to an altered peptide secondary structure, which preliminary structure investigations suggests for BB and c8-N (see supplementary information, Fig. S2).

3.3. Effect of acylation on interaction with Caco-2 cells

Addition of the acylated analogues to Caco-2 cell monolayers elicited a somewhat unexpected response, as the cell layer integrity was transiently affected, and the analogue permeability was drastically increased compared to the peptide backbone (see Fig. 2) and native sCT (similar to BB, data not shown). The permeability of the widely used transport marker mannitol [12] was increased for the c8-analogue in a similar manner as the peptide itself, which together with the reversible TEER-decrease and a moderate release of LDH from the cells (data not shown) appears suggestive of an intestinal permeation enhancer effect [39,40].

The enhancer-like effect was even more pronounced at lower pH, indicating a synergy between the acylation and positive charge of the peptide, which increases at lower pH. The theoretical charges of c8-N at pH 5.5 and 7.4 are roughly +3 and +2, respectively, calculated based on the amino acid sequence. Initial studies showed an even higher effect at pH 4.5 (data not shown), but at this pH the TEER was not completely reversible after 24 h in fresh medium.

The pH-effect could also be due to pH-dependent structural changes of the acylated peptide, in particular when interacting with the membrane, as both pH- and charge-dependent interactions with lipid membranes are widely reported for antimicrobial peptides [41,42] and fusogenic peptides [43].

The accumulated amount of peptide in the basolateral compartment throughout the experiment is calculated as % of amount added apically (see supplementary information, Fig. S3), and after a 1 h experiment the values are roughly 0.05% and 0.5% for BB and c8-N, respectively, at pH 5.5. The dependence on acylation and pH is very similar to the permeability data shown in Fig. 3B, thus displaying an acylation-induced improvement in peptide translocation on par with currently employed oral translocation enhancers [44].

To further investigate the effect of acylation and pH, the amount of peptide bound in the Caco-2 cell membrane or aqueous lumen was measured after the permeation experiment (see Fig. 4).

The cell membrane binding was increased drastically by acylation, whereas the cell uptake was increased moderately. Interestingly, the pH-effect was reversed by acylation, as the peptide backbone displays largest membrane binding and uptake at low pH where the positive charge is largest, whereas the c8-analogue displayed less binding and uptake at low pH. Thus, at lower pH

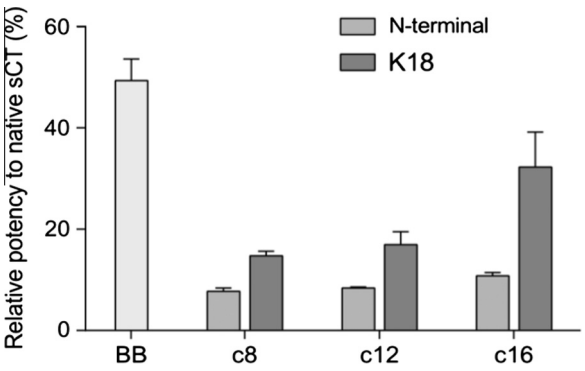

Fig. 2. *In vitro* receptor activation of hCT receptor by sCT analogues. IC50 potency relative to native sCT, presented as mean ± SDOM of ⩾2 separate experiments, each in duplicate. All analogues activate the receptor, although the potency is reduced relative to native sCT. The potency is lowest for N-terminal acylated analogues, whereas K18-acylation has less effect.

the acylated peptide translocates more efficiently across Caco-2 cell monolayers and less is retained in the cell layer.

3.4. Effect of acylation on interaction with model lipid membranes

To further investigate the effect of acylated sCT on Caco-2 cells and resemblance to permeation enhancers, we utilized model lipid membranes in the form of liposomes, encapsulating the water-soluble fluorophore calcein. If the effect that the acylated analogue exerts on Caco-2 cell monolayers is a detergent-like permeabilization of the membrane, it is expected to cause fluorophore leakage from liposomes. The results are shown in Fig. 5, where it is evident that the acylation induces a strong membrane-permeabilization, in a pH- and concentration dependent manner. The pH-dependency correlates well with Caco-2 permeability (Fig. 3), indicating that the enhancer-like effect on Caco-2 cells is due to permeabilization of the cell membrane.

The peptide backbone and native sCT (data not shown) caused only negligible leakage within the 1 h experiment, although there are reports in the literature of native sCT forming pores in model membranes [45]. However, this was only observed for very specific lipid mixtures, and not for PC liposomes around neutral pH [45]. For c8-N the leakage was measured in a range of concentrations, in order to investigate the effect of different peptide/lipid ratios (as lipid concentration was kept constant). The leakage after 15 min increased with concentration of c8-N, ranging from very limited leakage at 5 or 10 μM, to very rapid leakage at 100 μM. The pH-dependency was retained at all concentrations, and subsequent experiments were performed at 50 and 100 μM. In calcein release experiments the peptide/lipid ratio is approximately 0.15 for 100 μM peptide, as used in Caco-2 experiments, but for cell experiments the lipid concentrations are less well-defined. Thus, it may also be interesting to vary the lipid concentration, while keeping peptide concentration constant at 100 μM.

Triton X-100 was used to cause total leakage, and two previously investigated permeation enhancers [32] with different enhancing mechanism were included for validation purposes.

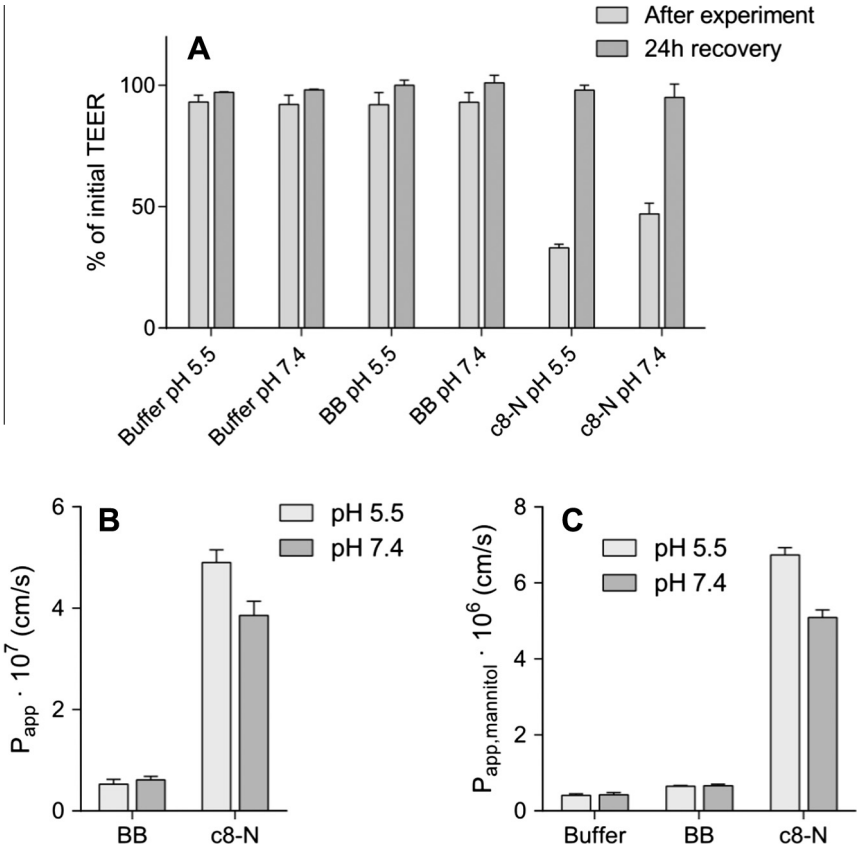

Fig. 3. Effect of acylation on sCT permeation across Caco-2 monolayers, investigated for sCT backbone (BB) and c8-N analogue at pH 5.5 or 7.4. (A) TEER values for Caco-2 cell monolayers after experiments and after 24 h recovery in cell medium. (B) Peptide and (C) mannitol permeability during the experiment. The acylation causes a reversible TEER-decrease and large increase in peptide and mannitol permeability. The effect is enhanced at lower pH, where the peptide is more positively charged, indicating a synergistic effect of acylation and charge. For the peptide backbone, native sCT (data not shown) or buffer alone there is no pH-dependence, and the permeability is consistent with previously reported values for native sCT [23,31]. All data points represent mean ± SDOM of ⩾2 separate experiments, each with 4 repeats.

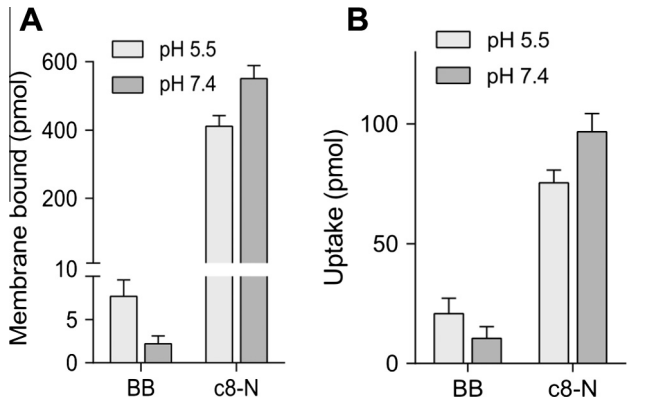

Fig. 4. Effect of acylation on sCT interaction with Caco-2 monolayers, investigated for sCT backbone and c8-N analogue at pH 5.5 or 7.4. (A) Peptide amount bound in the Caco-2 cell membranes and (B) inside the cells after 1 h permeation experiment, presented as a percentage of apically added peptide. Acylation increased both cell membrane binding and uptake, and the effect of pH appears to be reversed by acylation, where the peptide backbone displayed increased binding and uptake at low pH, where the peptide has the largest positive charge. All data points represent mean ± SDOM of 2 separate experiments, each with 4 repeats.

Ethylene glycol-bis(β-aminoethyl ether)-N, N, N, N-tetraacetic acid (EGTA) is a paracellular enhancer which increases transport between the cells by opening of the tight junctions [46], and sodium dodecyl sulphate (SDS) is a transcellular enhancer which increases transport through the cells at low concentrations, predominantly by fluidizing the cell membrane [47]. Thus, EGTA is not expected to cause leakage, whereas SDS is. The two enhancers were tested at the concentrations used in previous Caco-2 experiments (13 mM and 0.6 mM, respectively), which caused a reversible TEER-decrease and approximately 4-fold increased permeability of mannitol and GLP-2 [32]. EGTA caused no liposome leakage, whereas SDS caused moderate leakage (slow compared to c8-N), with approximately 30% after 15 min (see supplementary, Fig. S4). These results indicate that the liposome system is a useful tool for understanding interactions with Caco-2 cell monolayers, despite its simplicity.

From the leakage of encapsulated calcein, it is difficult to say whether the liposomes are still intact, i.e. whether or not the peptides create a form of pores in the membrane or if they destroy the liposomes in a detergent-like micellization. Liposomes incubated with either 100 μM BB or c8-N for 15 min appeared intact as no change was observed by DLS measurements (data not shown) suggestive of the former, whereas the positive control Triton X-100 caused disappearance of liposomes, suggestive of the latter.

3.5. Dependence of Caco-2 permeability on acylation position and chain length

The different combinations of acylation chain length and placement on the sCT backbone were compared at pH 5.5, and as shown in Fig. 6, all acylated analogues affected Caco-2 cells in a similar fashion to the N-terminal c8-analogue, where some even displayed larger increases in peptide translocation. The large, transient TEER-effect of the acylated analogues correlated well with the permeability of peptide and mannitol, and was highly dependent on acy-

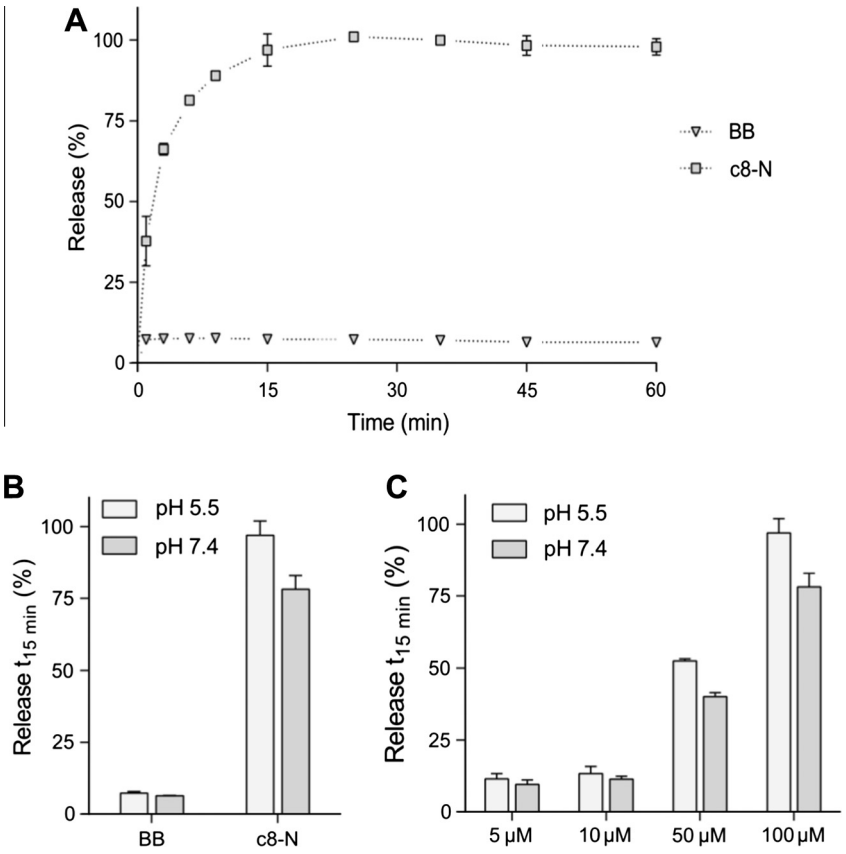

Fig. 5. Permeabilization of model lipid membranes for the acylated c8-analogue, as evidenced by release of encapsulated calcein from POPC liposomes. (A) Example of release curves for 100 μM sCT backbone and its N-terminal acylated c8 analogue at pH 5.5, (B) release after 15 min at pH 5.5 and 7.4 (for 100 μM) and (C) concentration-dependence for c8-N. Acylation of sCT backbone confers a strong membrane interaction, causing rapid permeabilization of liposomes. For c8-N the effect is pH- and concentration-dependent, with larger (or more rapid) release at lower pH and/or higher concentration (although 5 and 10 μM are similar). All data points represent mean ± SD of 2 separate experiments, each with 2 repeats.

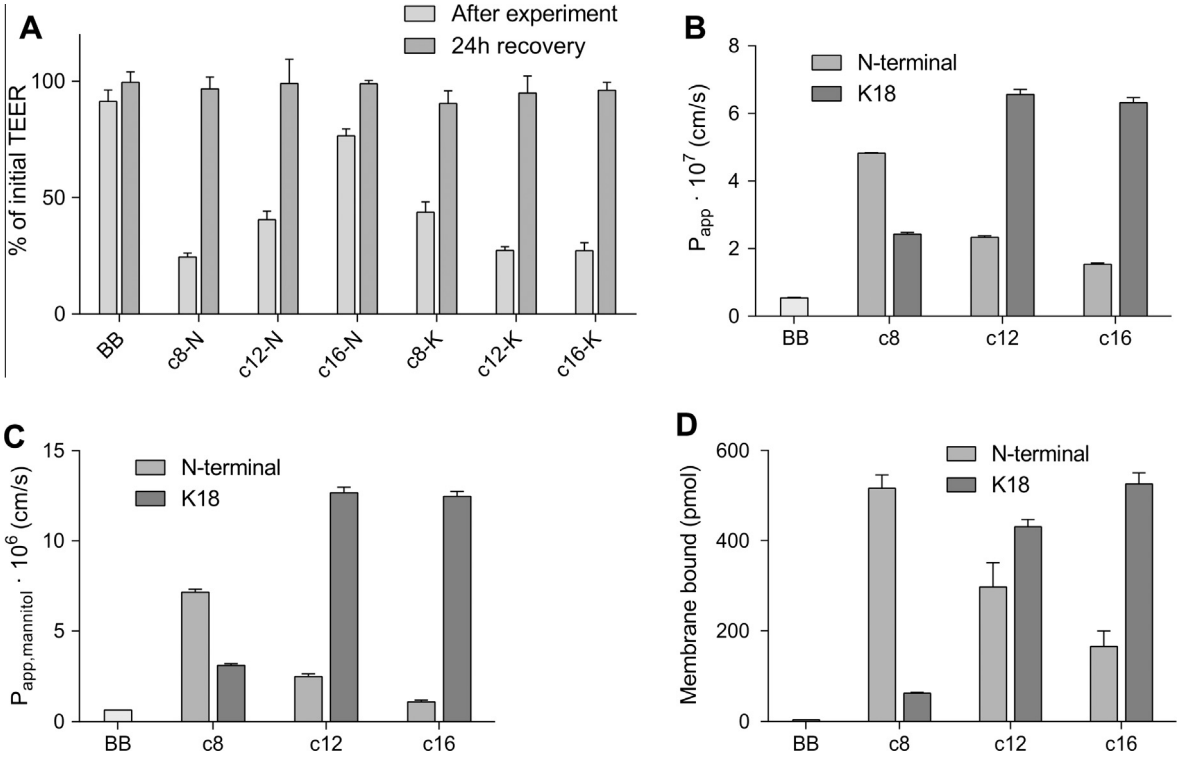

Fig. 6. Interaction of sCT backbone and acylated analogues with Caco-2 monolayers, investigated for c8-, c12- or c16-acylations at the N-terminal or Lys18. (A) TEER values for Caco-2 cell monolayers after experiments and after 24 h recovery in cell medium. (B) Peptide and (C) mannitol permeability during the experiment. (D) Cell membrane bound peptide after the experiment. All acylated analogues caused a reversible decrease in TEER, increased permeability of peptide and mannitol, as well as increased cell membrane binding (and uptake, data not shown). TEER-decrease and permeability are quite well correlated, and show a marked dependence on both acylation chain length and position. For N-terminal acylation, the longer chains display lower permeability, whereas for K^{18}-analogues the dependence is reversed, with c12- and c16-K showing comparable permeability. The amount of peptide bound in the cell membrane shows a similar trend, although with a higher value for c16-K than c12-K. All data points represent mean ± SDOM of ⩾2 separate experiments, each with 4 repeats.

lation chain length and position. For N-terminal acylation, the shorter chain(s) gave rise to the highest permeability, whereas moving the acylation to K^{18} reversed this, although with comparable permeability for c12- and c16-K. Compared to the unacylated peptide backbone, all acylation chain lengths at both positions gave rise to an increased peptide translocation, particularly for c8-N (roughly 9-fold increase at pH 5.5) and c12-K/c16-K (roughly 12-fold). This acylation-induced improvement is on the same scale as currently employed oral permeation enhancers [44], suggesting that acylation of sCT could reduce or eliminate the need for these in oral formulations.

For the K^{18}-acylated analogues the amount of peptide bound in the cell membrane increased with increasing chain length, which is similar to what has been observed previously for GLP-2 analogues [32]. Surprisingly, for the N-terminal acylated analogues the chain-length dependence was reversed, indicative of a competitive self-association or aggregation. Preliminary studies suggest that N-terminal acylation increases peptide self-association at conditions similar to Caco-2 experiments, as evidenced by altered Trp-fluorescence (method described in [32], data not shown). However, the decreased cell-membrane binding for longer chain acylations indicates that the self-association may not be entirely reversible, and could limit the interaction with and permeation across Caco-2 monolayers. For K^{18}-acylated analogues, increasing the acyl chain length from c8 to c12 increased permeability. However, increasing chain length further to c16 did not increase the permeability in comparison with c12, which in combination with the increased cell-membrane binding, could indicate that an acylation chain length around c12 is optimal for K^{18}-acylation, whereas N-terminal acylation is optimal with a chain length around c8.

For sCT, acylation drastically increases Caco-2 interaction and translocation, in particular for short and medium chains, but for longer chains the cell membrane binding (and possibly self-association) becomes somewhat limiting for translocation. We have previously observed an optimum for c12-acylation of GLP-2, where increased chain length caused decreased permeability [32]. However, the GLP-2 analogues did not exhibit an effect on Caco-2 cell layers as observed for sCT in the present study, and the benefit of GLP-2 acylation was quite modest compared to the current results.

3.6. Dependence of membrane interaction on acylation position and chain length

We further investigated the liposome permeabilization, and found that the acylated analogues caused leakage of calcein (Fig. 7), consistent with cell membrane permeabilization as a cause of enhanced Caco-2 translocation. The permeabilization potency of the different analogues qualitatively correlated reasonably well with their Caco-2 permeability, and the subtle differences may be ascribed to the simplicity of the model system, e.g. different affinities of the analogues to the POPC membrane compared to the cell membrane with its complex mixture of lipids and membrane proteins.

For selected analogues, the liposomes were investigated by DLS after incubation, and for 100 μM c16-K the liposomes appeared intact right after mixing, but absent after 15 min. For c16-K the leakage was very rapid (almost instantaneous), which correlates well with a micellization of the liposomes as opposed to leakage

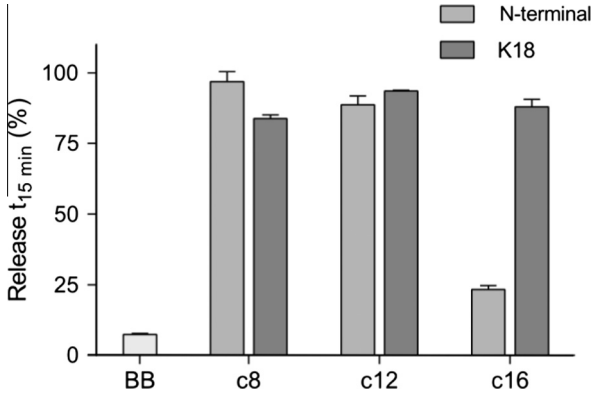

Fig. 7. Permeabilization of model lipid membranes for the acylated analogues, as evidenced by release of encapsulated calcein from POPC liposomes after 15 min. Acylation confers rapid membrane-permeabilizing behavior to all analogues, although for c16-N only very modestly. All data points represent mean ± SD of 2 separate experiments, each with 2 repeats.

through pores. As described previously, leakage caused by c8-N was not accompanied by destruction of liposomes after 15 min.

4. Conclusions

In the present work a series of systematically acylated sCT analogues were investigated, in order to establish how *in vitro* intestinal permeability is affected by acylation of different lengths in different positions. We find that peptide acylation results in a permeation enhancing effect in an *in vitro* intestinal model and that acylated sCT exhibits a cell penetrating peptide like effect on cellular membranes. The acylation-induced permeability enhancing effect on the cell layer was found to be transient, as the cellular barrier fully recovered after peptide exposure. The analogues permeabilized model lipid membranes, indicating that the effect is due to a detergent-like solubilization of the cell membrane, similar to certain oral permeation enhancers.

The permeability enhancing effect of the peptides was highest at reduced pH, and was further dependent on acylation chain length and position. For N-terminal acylation the short c8-acylation provided the most pronounced effect, whereas the longer chain acylations may be hampered by self-association or aggregation. For K^{18}-acylation the short chain provided a moderate improvement, whereas the c12 and c16 analogues were highly efficient, with a 12-fold increase in cell translocation compared to the unacylated peptide backbone. For K^{18}-acylation an optimum acylation length appears to exist around c12, as the c16 chain caused greater binding to the cell membrane but similar permeability, and we speculate that increasing the chain length further may decrease the permeability as previously observed for GLP-2 analogues [32].

Acylated sCT acts as its own permeation enhancer, with effects on Caco-2 cells that are rapid, reversible and on par with currently employed oral permeation enhancers; thus, acylation of sCT could represent a promising tool to increase its intestinal permeability without simultaneous administration of absorption enhancers. Although the receptor activation potency is moderately reduced, acylation is expected to confer increased enzymatic stability and prolonged blood circulation, and the presented results suggest that acylation of sCT increases intestinal absorption, which might improve delivery by the oral route.

Acknowledgments

We thank Lauge Schäffer for synthesis of BB, Tinna Berg Larsen for hCT-R luciferase measurements and Lisette G. Nielsen for assistance with Caco-2 cells. This work was supported by The Technical University of Denmark, The Danish Agency for Science, Technology and Innovation, and Novo Nordisk A/S. The funders did not have any role in the study design, data collection and analysis, decision to publish, or preparation of the manuscript. Disclosure: LL, SB, HMS and ULR are shareholders in Novo Nordisk A/S.

Appendix A. Supplementary material

Supplementary data associated with this article can be found, in the online version, at http://dx.doi.org/10.1016/j.ejpb.2015.09.001.

References

[1] P. Kurtzhals, S. Havelund, B. Kiehr, U.D. Larsen, U. Ribel, J. Markussen, Albumin binding of insulins acylated, Biochem. J. 312 (1995) 725–731.
[2] P. Dasgupta, A. Singh, R. Mukherjee, N-terminal acylation of somatostatin analog with long chain fatty acids enhances its stability and anti-proliferative activity in human breast adenocarcinoma cells, Biol. Pharm. Bull. 25 (2002) 29–36.
[3] L. Yuan, J. Wang, W.-C. Shen, Reversible lipidization prolongs the pharmacological effect, plasma duration, and liver retention of octreotide, Pharm. Res. 22 (2005) 220–227, http://dx.doi.org/10.1007/s11095-004-1189-z.
[4] I. Gozes, A. Bardea, A. Reshef, R. Zamostiano, S. Zhukovsky, S. Rubinraut, et al., Neuroprotective strategy for Alzheimer disease: intranasal administration of a fatty neuropeptide, Proc. Natl. Acad. Sci. USA 93 (1996) 427–432.
[5] L.S. Dalbøge, S.L. Pedersen, S.B. van Witteloostuijn, J.E. Rasmussen, K.T.G. Rigbolt, K.J. Jensen, et al., Synthesis and evaluation of novel lipidated neuromedin U analogs with increased stability and effects on food intake, J. Pept. Sci. (2014), http://dx.doi.org/10.1002/psc.2727.
[6] J. Wang, D. Chow, H. Heiati, W.-C. Shen, Reversible lipidization for the oral delivery of salmon calcitonin, J. Control. Release 88 (2003) 369–380.
[7] L.B. Knudsen, P.F. Nielsen, P.O. Huusfeldt, N.L. Johansen, K. Madsen, F.Z. Pedersen, et al., Potent derivatives of glucagon-like peptide-1 with pharmacokinetic properties suitable for once daily administration, J. Med. Chem. 43 (2000) 1664–1669.
[8] L. Zhang, G. Bulaj, Converting peptides into drug leads by lipidation, Curr. Med. Chem. 19 (2012) 1602–1618.
[9] K. Madsen, L.B. Knudsen, H. Agersoe, P.F. Nielsen, H. Thøgersen, M. Wilken, et al., Structure-activity and protraction relationship of long-acting glucagon-like peptide-1 derivatives: importance of fatty acid length, polarity, and bulkiness, J. Med. Chem. 50 (2007) 6126–6132, http://dx.doi.org/10.1021/jm070861j.
[10] J. Wang, W.-C. Shen, Gastric retention and stability of lipidized Bowman–Birk protease inhibitor in mice, Int. J. Pharm. 204 (2000) 111–116, http://dx.doi.org/10.1016/S0378-5173(00)00489-0.
[11] M. Morishita, N.A. Peppas, Is the oral route possible for peptide and protein drug delivery?, Drug Discov Today 11 (2006) 905–910, http://dx.doi.org/10.1016/j.drudis.2006.08.005.
[12] I. Hubatsch, E.G.E. Ragnarsson, P. Artursson, Determination of drug permeability and prediction of drug absorption in Caco-2 monolayers, Nat. Protoc. 2 (2007) 2111–2119, http://dx.doi.org/10.1038/nprot.2007.303.
[13] P. Artursson, K. Palm, K. Luthman, Caco-2 monolayers in experimental and theoretical predictions of drug transport, Adv. Drug Deliv. Rev. 46 (2001) 27–43, http://dx.doi.org/10.1016/j.addr.2012.09.005.
[14] T. Uchiyama, A. Kotani, H. Tatsumi, Development of novel lipophilic derivatives of DADLE (leucine enkephalin analogue): intestinal permeability characteristics of DADLE derivatives in rats, Pharm. Res. 17 (2000).
[15] J.A. Rogers, A. Wong, The temperature dependence and thermodynamics of partitioning of phenols in the n-octanol-water system, Int. J. Pharm. 6 (1980) 339–348, http://dx.doi.org/10.1016/0378-5173(80)90117-9.
[16] K. Balon, B. Riebesehl, B. Müller, Drug liposome partitioning as a tool for the prediction of human passive intestinal absorption, Pharm. Res. 16 (1999) 882–888.
[17] S. Krämer, Absorption prediction from physicochemical parameters, Pharm. Sci. Technol. Today 2 (1999) 373–380.
[18] D. Copp, B. Cheney, Calcitonin-a hormone from the parathyroid which lowers the calcium-level of the blood, Nature 193 (1962).
[19] B.W. Purdue, N. Tilakaratne, P.M. Sexton, Molecular pharmacology of the calcitonin receptor, Recept. Channels 8 (2002) 243–255.
[20] M.A. Karsdal, K. Henriksen, A.C. Bay-Jensen, B. Molloy, M. Arnold, M.R. John, et al., Lessons learned from the development of oral calcitonin: the first tablet formulation of a protein in phase III clinical trials, J. Clin. Pharmacol. 51 (2011) 460–471, http://dx.doi.org/10.1177/0091270010372625.
[21] T. Arvinte, A. Cudd, A.F. Drake, The structure and mechanism of formation of human calcitonin fibrils, J. Biol. Chem. 268 (1993) 6415–6422.
[22] A. Cudd, T. Arvinte, R.E.G. Das, C. Chinni, I. Macintyre, Enhanced potency of human calcitonin when fibrillation is avoided, J. Pharm. Sci. 84 (1995) 717–719, http://dx.doi.org/10.1002/jps.2600840610.
[23] S.B. Petersen, L.G. Nielsen, U.L. Rahbek, M. Guldbrandt, D.J. Brayden, Colonic absorption of salmon calcitonin using tetradecyl maltoside (TDM) as a

permeation enhancer, Eur. J. Pharm. Sci. 48 (2013) 726–734, http://dx.doi.org/10.1016/j.ejps.2013.01.009.
[24] N. Binkley, M. Bolognese, A. Sidorowicz-Bialynicka, T. Vally, R. Trout, C. Miller, et al., A phase 3 trial of the efficacy and safety of oral recombinant calcitonin: the Oral Calcitonin in Postmenopausal Osteoporosis (ORACAL) trial, J. Bone Miner. Res. 27 (2012) 1821–1829, http://dx.doi.org/10.1002/jbmr.1602.
[25] V. Gupta, B.H. Hwang, J. Lee, A.C. Anselmo, N. Doshi, S. Mitragotri, Mucoadhesive intestinal devices for oral delivery of salmon calcitonin, J. Control. Release 172 (2013) 753–762, http://dx.doi.org/10.1016/j.jconrel.2013.09.004.
[26] H. Sang Yoo, T. Gwan Park, Biodegradable nanoparticles containing protein-fatty acid complexes for oral delivery of salmon calcitonin, J. Pharm. Sci. 93 (2004) 488–495, http://dx.doi.org/10.1002/jps.10573.
[27] K.-H. Song, S.-J. Chung, C.-K. Shim, Enhanced intestinal absorption of salmon calcitonin (sCT) from proliposomes containing bile salts, J. Control. Release 106 (2005) 298–308, http://dx.doi.org/10.1016/j.jconrel.2005.05.016.
[28] M. Werle, H. Takeuchi, Chitosan–aprotinin coated liposomes for oral peptide delivery: development, characterisation and in vivo evaluation, Int. J. Pharm. 370 (2009) 26–32, http://dx.doi.org/10.1016/j.ijpharm.2008.11.013.
[29] W. Cheng, S. Satyanarayanajois, L.-Y. Lim, Aqueous-soluble, non-reversible lipid conjugate of salmon calcitonin: synthesis, characterization and in vivo activity, Pharm. Res. 24 (2007) 99–110, http://dx.doi.org/10.1007/s11095-006-9128-9.
[30] W. Cheng, L. Lim, Comparison of reversible and nonreversible aqueous-soluble lipidized conjugates of salmon calcitonin, Mol. Pharm. 88 (2008).
[31] Y.S. Youn, J.Y. Jung, S.H. Oh, S.D. Yoo, K.C. Lee, Improved intestinal delivery of salmon calcitonin by Lys18-amine specific PEGylation: stability, permeability, pharmacokinetic behavior and in vivo hypocalcemic efficacy, J. Control. Release 114 (2006) 334–342, http://dx.doi.org/10.1016/j.jconrel.2006.06.007.
[32] S. Trier, L. Linderoth, S. Bjerregaard, T.L. Andresen, U.L. Rahbek, Acylation of Glucagon-like peptide-2: interaction with lipid membranes and in vitro intestinal permeability, PLoS ONE 9 (2014) e109939, http://dx.doi.org/10.1371/journal.pone.0109939.
[33] E. Fujinari, L. Courthaudon, Nitrogen-specific liquid chromatography detector based on chemiluminescence: application to the analysis of ammonium nitrogen in waste water, J. Chromatogr. 592 (1992) 209–214.
[34] M. Diociaiuti, M.C. Gaudiano, F. Malchiodi-Albedi, The slowly aggregating salmon Calcitonin: a useful tool for the study of the amyloid oligomers structure and activity, Int. J. Mol. Sci. 12 (2011) 9277–9295, http://dx.doi.org/10.3390/ijms12129277.
[35] J. Fallingborg, Intraluminal pH of the human gastrointestinal tract, Dan. Med. Bull. 46 (1999) 183–196. <http://www.ncbi.nlm.nih.gov/pubmed/10421978> (accessed 15.12.14).
[36] G. Borchard, The absorption barrier, in: A. Bernkop-Schnürch (Ed.), Oral Deliv. Macromol. Drugs, Springer, US, New York, 2009, pp. 49–64, http://dx.doi.org/10.1007/978-1-4419-0200-9.
[37] A. Jesorka, O. Orwar, Liposomes: technologies and analytical applications, Annu. Rev. Anal. Chem. 1 (2008) 801–832, http://dx.doi.org/10.1146/annurev.anchem.1.031207.112747.
[38] G. Andreotti, B.L. Méndez, P. Amodeo, M.A.C. Morelli, H. Nakamuta, A. Motta, Structural determinants of salmon calcitonin bioactivity: the role of the Leu-based amphipathic alpha-helix, J. Biol. Chem. 281 (2006) 24193–24203, http://dx.doi.org/10.1074/jbc.M603528200.
[39] B. Aungst, Intestinal permeation enhancers, J. Pharm. Sci. 89 (2000).
[40] K. Whitehead, N. Karr, S. Mitragotri, Safe and effective permeation enhancers for oral drug delivery, Pharm. Res. 25 (2008) 1782–1788, http://dx.doi.org/10.1007/s11095-007-9488-9.
[41] T. Etzerodt, J.R. Henriksen, P. Rasmussen, M.H. Clausen, T.L. Andresen, Selective acylation enhances membrane charge sensitivity of the antimicrobial peptide mastoparan-x, Biophys. J. 100 (2011) 399–409, http://dx.doi.org/10.1016/j.bpj.2010.11.040.
[42] J.R. Henriksen, T.L. Andresen, Thermodynamic profiling of peptide membrane interactions by isothermal titration calorimetry: a search for pores and micelles, Biophys. J. 101 (2011) 100–109, http://dx.doi.org/10.1016/j.bpj.2011.05.047.
[43] T.P. Etzerodt, S. Trier, J.R. Henriksen, T.L. Andresen, A GALA lipopeptide mediates pH- and membrane charge dependent fusion with stable giant unilamellar vesicles, Soft Matter 8 (2012) 5933, http://dx.doi.org/10.1039/c2sm25075f.
[44] S. Maher, T.W. Leonard, J. Jacobsen, D.J. Brayden, Safety and efficacy of sodium caprate in promoting oral drug absorption: from in vitro to the clinic, Adv. Drug Deliv. Rev. 61 (2009) 1427–1449, http://dx.doi.org/10.1016/j.addr.2009.09.006.
[45] M. Diociaiuti, L.Z. Polzi, L. Valvo, F. Malchiodi-Albedi, C. Bombelli, M.C. Gaudiano, Calcitonin forms oligomeric pore-like structures in lipid membranes, Biophys. J. 91 (2006) 2275–2281, http://dx.doi.org/10.1529/biophysj.105.079475.
[46] M.A. Deli, Potential use of tight junction modulators to reversibly open membranous barriers and improve drug delivery, Biochim. Biophys. Acta 1788 (2009) 892–910, http://dx.doi.org/10.1016/j.bbamem.2008.09.016.
[47] M. Sakai, T. Imai, H. Ohtake, M. Otagiri, Cytotoxicity of absorption enhancers in Caco-2 cell monolayers, J. Pharm. Pharmacol. 50 (1998) 1101–1108, http://dx.doi.org/10.1111/j.2042-7158.1998.tb03319.x.

Supplementary Information

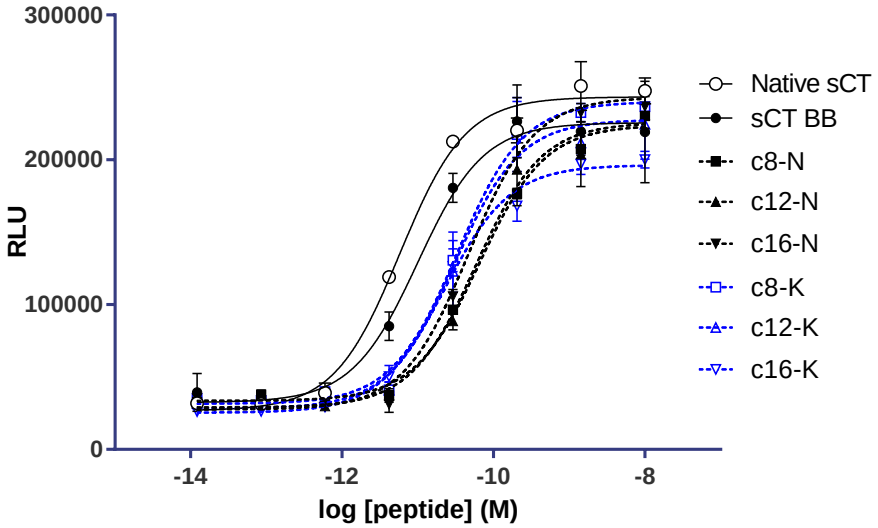

Figure S1. *In vitro* receptor activation of human calcitonin receptor (hCT-R) by salmon calcitonin (sCT) analogues, presented as mean ± SDOM of duplicates, with sigmoidal fitted curves.

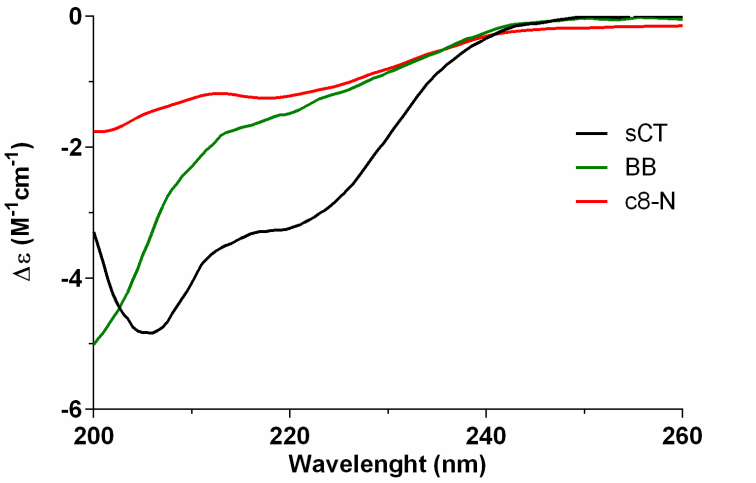

Figure S2. Circular dichroism spectra of 100 μM native sCT, peptide backbone (BB) and c8-N analogue in the physiological HBSS/HEPES buffer (pH 7.4) used for cell studies (although without OVA). The Y^{22}->W mutation and/or acylation appears to alter the secondary structure, e.g. by decreasing the α-helix content, which may explain the receptor potency reduction observed in fig. S1. Preliminary measurements further suggests a buffer- and pH-dependency of c8-N structure, with a CD-response resembling BB in either a more simple HEPES/NaCl buffer (pH 7.4, 150 mM NaCl) or in HBSS buffer at pH 5.5 (data not shown).

Interaction with Caco-2 cells

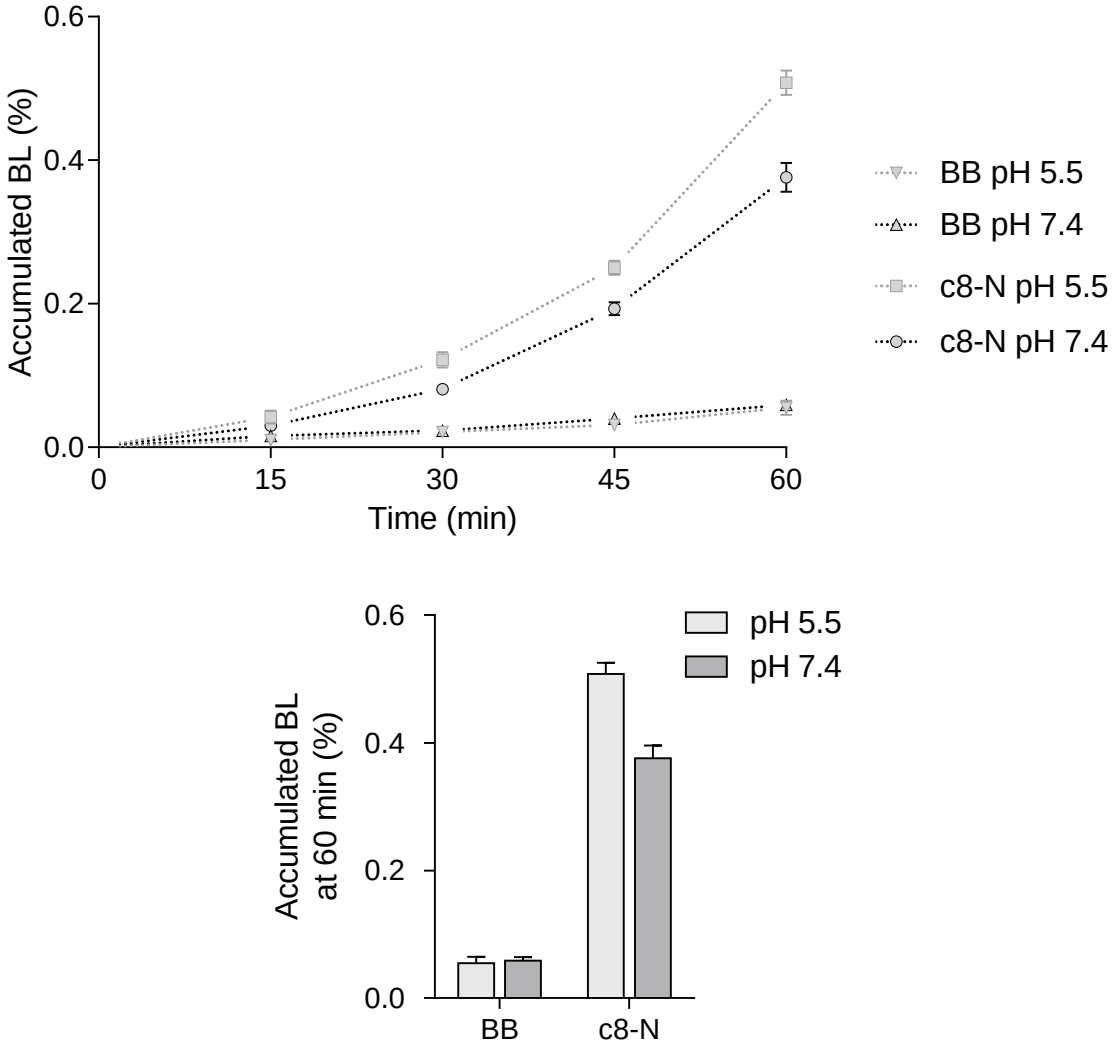

Figure S3. Accumulated amounts of peptide during Caco-2 permeability experiment, presented as % in basolateral (BL) compartment of added apical (AP) amount. All data points represent mean ± SDOM of 2 or 3 separate experiments, each with 4 repeats.

The time-resolved accumulation is not completely linear for c8-N, and the calculation of P_{app} (eq. (2) in Materials and Methods) assumes linearity between 2 consecutive time points, but the error is minimal (and would diminish with closer sampling time points). The increasing rate of accumulation throughout the experiment indicates that the effect exerted by c8-N on the cell layer continues and increases through the experiment, which is reasonable considering that the majority of peptide remains above the cell layer.

Calcein release

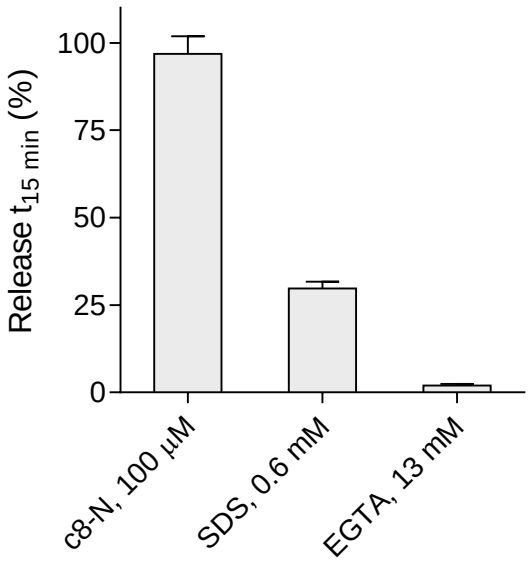

Figure S4. Permeabilization of model lipid membranes as evidenced by release of encapsulated calcein from POPC liposomes. The acylated c8-analogue is compared to a transcellular enhancer (SDS) and paracellular enhancer (EGTA), at the concentrations where they transiently decrease TEER and increase Caco-2 permeability approximately 4-fold [1]. The transcellular detergent-like enhancer SDS causes moderate leakage after 15 minutes, whereas the paracellular enhancer EGTA does not cause leakage, consistent with their respective mechanism of action.

All data points represent mean ± SDOM of 2 separate experiments, each with 2 repeats.

[1] S. Trier, L. Linderoth, S. Bjerregaard, T.L. Andresen, U.L. Rahbek, Acylation of Glucagon-like peptide-2: interaction with lipid membranes and in vitro intestinal permeability., PLoS One. 9 (2014) e109939.

4.1.1 Notes on paper 2

The figure caption of fig. 4 contains a small error, as the cell bound peptide is expressed as pmol instead of as % of AP amount as stated.

Caco-2 experiments also featured measurements of Lactate Dehydrogenase (LDH) release after experiments with sCT analogues, which is indicative of cell stress or damage. These measurements were very consistent with liposome permeabilization and reversible TEER decreases, and were not included in the paper.

Peptide modifications and potency Conjugating the acylation to a primary amine reduces the peptides positive charge (most pronounced for K-analogues and at higher pH), which may in itself alter the peptide. This could be compensated by adding a cationic amino acid in the peptide backbone, however, it was not attempted due to the risk of perturbing the peptide structure and/or function in an unpredictable manner.

As described in paper 1, GLP-2 contains a tryptophan in position 25, which was used in fluorescence spectroscopy studies of peptide self-association and membrane partitioning. sCT does not contain a tryptophan, so we altered the tyrosine at pos. 22, but the combination of a point mutation and acylation appeared to affect the peptide in a synergistic manner (particularly the physical stability, as described later), and furthermore the fluorescence studies turned out not to be entirely feasible (described in the next section).

The receptor potency of all analogues (fig. 2 in paper 2) was affected to a surprising degree, particularly BB, where the Y22W point mutation reduced potency by 50 %. Acylation decreased it further, particularly N-terminal acylation, somewhat in contrast to reported sCT analogues with dual long-chain acylations at both cysteines (pos 1 and 7) and reasonable potency [96]. Interestingly, the potency appeared to increase slightly with increasing chain length for both acylation positions. For this group of analogues the separate effect of acylation can not be distinguished, but in section 4.3.1 we describe a group of acylated analogues without the backbone mutation.

The receptor potency was measured quite late in the project, and as sCT was partially used as a model peptide it was not a 'show-stopper', but there were other issues with the analogues.

Failed fluorescence spectroscopy As briefly mentioned in paper 1, peptide self-assocation and liposome partitioning elicit similar changes in Trp fluorescence, and therefore liposome partitioning measuremens require peptide concentrations below the self-association threshold. Unacylated GLP-2 or sCT do not readily self-associate, whereas acylation increases self-association, and although employing low peptide concentrations did not pose problems for GLP-2 analogues, it caused difficulties for sCT analogues. Trp measurements for pure peptide solutions in quartz cuvettes showed a gradual and substantial decrease in fluorescence when stirring was initiated, plateauing after roughly 30 minutes. We later found a very similar fluorescence profile reported in [75], explained by adsorption of cationic peptide to the walls of the quartz cuvette and to the stirring bar. The adsorption may be aggravated by acylation [78], but was not observed for acylated GLP-2 analogues in the current setup. Adsorption may possibly be avoided by using higher peptide concentrations, using containers designed to limit binding (e.g. Protein LoBind tubes) or coating the inner surfaces with inert polymers or proteins [53]. However, fluorescence experiments are very restrictive regarding peptide concentration, and to our knowledge there is no LoBind alternative to the quartz cuvette. Surface coating with an inert protein is in fact employed in all other experiments, as OVA is included in buffers, but here it would interfere with Trp fluorescence. Polymer coating (e.g. PEI as in [75]) is labor-intensive and requires validation in the present experimental setup. For the record, liposome partitioning experiment are already quite time-consuming.

Furthermore, since Caco-2 studies indicated a more profound effect on membranes than simple partitioning, we focused instead on investigating the membrane-destabilization effect described in paper 2 (calcein release), where it was possible to use higher peptide concentrations and include OVA.

Liposome partitioning was initially an important part of the thesis scope, and as mentioned in paper 1, we aimed at using the partitioning coefficient as a predictor of Caco-2 permeability. However, the enhancer-effect on Caco-2 cells might render this idea moot.

The concentration dependent self-association of sCT analogues was intended to be estimated using Trp fluorescence (as for GLP-2 analogues in paper 1), mostly as a prerequisite for liposome partitioning studies. However, apart from peptide surface adsorption at low concentrations, measurements at high concentrations were marred by the physical instability described in the next section. Although, an interesting result was obtained for BB and c8-N. As briefly introduced in paper 1, the fluorescence spectrum for Trp is red-shifted in a polar environment, e.g. for free L-Trp in solution, and blue-shifts in a more hydrophobic environment, e.g. in oligomers of acylated GLP-2 analogues. However, c8-N exhibited the opposite behavior, with red-shifted signal (similar to BB) at high concentration and blue-shifted at lower concentration. This may be explained if the Trp residue is situated in a hydrophobic environment ('protected' by the acyl chain?) in the monomeric peptide. If one then assumes self-association in a micelle-like oligomer centered around the acylated N-termini, then the Trp residue, which is situated at pos. 22, in a somewhat hydrophilic region of the peptide, may be pushed out towards water. This is extremely speculative, and based on quite preliminary results, but it illustrates the potential use of Trp fluorescence for more advanced purposes, as it has been used to follow conformational changes in larger proteins [83].

Solution stability 'Traditional' sample preparation for Caco-2 experiments or Trp fluorescence studies did not play well with some sCT analogues, specifically, prolonged heating to 37 °C and shaking or magnet stirring in the physiological HBSS buffer caused solutions to become turbid and/or gel-like. This behavior may be indicative of peptide fibrillation, which is investigated in paper 3. Initial attempts with different buffers indicated that the issue persisted in other physiological buffers, such as PBS and FASSIF (simulated intestinal fluid), also when preparing stock solutions in DMSO. Non-physiological buffers with e.g. low salt concentration or very low pH were highly beneficial, but can not be used in caco-2 experiments. Instead, moderate improvements were achieved by very careful handling of samples (i.e. no shaking!), preparing stock solutions in MQ and diluting in the relevant buffer immediately before experiments. This enabled the experiments presented in paper 2, but further improvements were attempted, as presented in paper 3.

(Incidently, lowering pH to 5.5, which was tolerated by caco-2 cells, revealed the interesting pH dependency presented in paper 2.)

4.2 Paper 3 (draft)

The following section contains a manuscript draft for Paper 3, which concerns the acylated sCT analogues introduced in paper 2. The investigation is not a part of the thesis scope, and as such was a bit of a detour project, but it is included here as it represents an interesting perspective on acylation.

Summary The manuscript draft investigates sCT analogues with c8, c12 or c16 acyl chains at the N-terminus or Lys18.

The results demonstrate that prolonged heating and/or solution storage of certain acylated sCT analogues cause aggregation in physiological buffer solutions, potentially forming fibril-like structures. Lys18 acylation appears superior to N-terminal acylation, most clearly exemplified by the short chain c8-analogues, however, no systematic dependence on acylation chain length is apparent. For all analogues, self-association is efficiently inhibited by addition of DM-β-CD, however, the separate permeability enhancing effects of acylated analogues and DM-β-CD are reduced in the mixtures. Thus, acylation of sCT for oral delivery purposes may not be indiscriminately applicable, and requires rational choices of acylation details and/or additives.

Acylated salmon calcitonin and dimethyl-β-cyclodextrin – self-association and *in vitro* intestinal permeability

Sofie Trier[1,2], Lars Linderoth[2], Simon Bjerregaard[2], Holger M. Strauss[2], Thomas L. Andresen[1], Ulrik L. Rahbek[2]*

[1]Dept. of Micro- and Nanotechnology, Center for Nanomedicine and Theranostics, Technical University of Denmark, DK- 2800 Kgs. Lyngby, Denmark, [2]Global Research, Novo Nordisk A/S, DK-2760 Maaloev, Denmark

Abstract

Acylation of the therapeutic peptide salmon calcitonin (sCT) increases its enzymatic stability, and was recently shown to confer intestinal permeability enhancement to the peptide when acylated with various chain lengths at the N-terminus or K^{18}. However, certain acylations appeared to cause aggregation of sCT, and this work aims to characterize this solution behavior. Furthermore, the effect of adding dimethyl-β-cyclodextrin (DM-β-CD) to monomerize peptide analogues is investigated, in terms of solution behavior and *in vitro* permeability in Caco-2 cell monolayers.

We find that N-terminally acylated analogues aggregate into fibril-like structures upon prolonged heating in physiological buffers, whereas moving the acylation to Lys^{18} decreases or delays aggregation. Short c8-chain analogues display time-dependent binding profiles to Thioflavin T, where the lag-time is extended roughly 2-fold for Lys^{18} vs. N-terminal acylation, whereas longer chain analogues display less well-defined profiles. Addition of DM-β-CD strongly inhibits aggregation for all analogues, however, the intestinal permeability enhancing effect of both acylated analogues and DM-β-CD appears hampered in the mixture. The permeability is efficiently increased by addition of DM-β-CD to the unacylated peptide backbone, whereas it is only slightly increased for c8-K and reduced for N-terminal analogues. In conclusion, acylation of sCT can increase its intestinal permeability, but also its propensity to fibrillate in physiological buffers, with a marked dependence on acylation chain length and position. Addition of DM-β-CD abolishes aggregation, however, this combination may not be optimal for intestinal translocation. Thus, acylation of sCT for oral delivery purposes is not indiscriminately applicable, and requires rational choices of acylation details and/or additives.

Introduction

The 32 amino acid peptide hormone calcitonin, which lowers blood calcium and is employed in the treatment of bone-related disorders such as osteoporosis and hypercalcemia, has been described extensively elsewhere [1–4]. Whereas human calcitonin (hCT) is physically and chemically unstable[5], salmon calcitonin is more

stable, potent [6] and has a longer *in vivo* half-life [4,7]. Consequently, the therapeutic use is mainly based on sCT, through either parenteral or intranasal routes. Literature reports and clinical trials attempting oral delivery of sCT has mostly employed native sCT in combination with oral permeation enhancers [4,7,8], although there are a few examples of advanced delivery systems [9–11] and modifying the peptide itself [2,12–16]. Acylation of therapeutic peptides with fatty acids is beneficial for prolonging circulation [17], increasing enzymatic stability [18–21], and may moderately increase oral bioavailability of peptide drugs [12,22,23]. Intestinal absorption is often assessed *in vitro* in the caco-2 model [24,25], and we recently described how acylation of sCT elicited a drastic increase in caco-2 monolayer translocation, due to an oral enhancer-like permeabilization of the cell membranes [2].

However, although sCT is more stable than hCT, fibrillation occurs upon ageing or otherwise challenging solutions [26], and acylation appeared to affect the solution behavior. Some acylated analogues showed signs of gel-formation upon ageing, agitation or prolonged incubation at 37°C in the physiological HBSS buffer used for Caco-2 experiments, although they were quite stable in MQ and low salt buffers. This prompted a more detailed study of the solution behavior of sCT analogues. We further attempt to limit self-association by addition of DM-β-CD to peptide solutions, as similar β-cyclodextrins have been reported to monomerize peptides [27–29], likely through binding of hydrophobic peptide side chains in the hydrophobic core of β-CD. Furthermore, cyclodextrins have been employed as absorption enhancers for nasal [30] or oral peptide delivery [31,32], acting through binding of the peptides or depletion of cholesterol from epithelial cell membranes [29,30,33,34], thus lowering their barrier function. We investigate the effect of combining acylated sCT analogues with DM-β-CD on *in vitro* intestinal peptide permeability.

Materials and Methods

Peptide synthesis

The peptide synthesis has been described previously [2]. Briefly, peptides were synthesized by automated Fmoc based SPPS, using Rink Amide AM resin on a Prelude peptide synthesizer (Protein Technologies), employing standard protocols (coupling with 6 eq. amino acid or fatty acid, DIC and Oxyma Pure in NMP for 60 min at r.t.; deprotection with 20% piperidine in NMP for 2 x 10 min). Cys was protected with acetamidomethyl (Acm), and the disulfide bridge was formed by dissolving peptides in MQ, adjusting pH to 5.5 with acetic acid and oxidizing with a solution of 5% I_2/AcOH at room temperature for approximately 2h. Primary amines were protected with 4-methyltrityl, and deprotected in neat HFIP, followed by washings with DCM. Peptides were cleaved from the resin and deprotected using TFA/H_2O/TIS for 3 hours, followed by precipitation with diethylether. Peptides were

dissolved in H_2O/MeCN and purified by preparative RP-HPLC. The fractions were analyzed by UPLC, LCMS, and chemiluminescent nitrogen detection [35] and the appropriate fractions were pooled and portioned for lyophilization. The peptide concentration of each analogue stock solution in MQ was verified with chemiluminescent nitrogen detection [35]. The cysteine bridge was verified by measuring peptide mass in LCMS following reduction with DTT.

Thioflavin T (ThT) assay

100 μM peptide samples were mixed with 1 μM ThT in 96 well microtiter plate (Packard OptiPlate-96, white) and incubated at 37 °C, while ThT fluorescence was measured (Ex 444 nm/ Em 485 nm) in a Fluoroskan Ascent FL fluorescence plate reader (Thermo Labsystems).

Transmission Electron Microscopy (TEM)

100 μM peptide samples were placed on Formvar-coated copper grids (1 min residence time, then removed with filter paper) and stained with a 2 % (w/v) uranyl acetate solution (1 min, then removed). Samples were examined with a FEI Morgagni 268 electron microscope operating at 80 kV. Samples were prepared in HBSS/MES buffer, similar to Caco-2 experiments (see below), apart from the absence of ovalbumin (OVA), which was verified in ThT assay to be inconsequential for self-association.

Caco-2 cells

The growth of and experimental setup for Caco-2 cell monolayers has been described previously [2,16]. Briefly, Caco-2 cells (HTB-37, ATCC, passage 40–65) were cultured routinely [24], seeded at 10^5 cells/well on 12 well Transwell plates and grown for 14–16 days in DMEM with media change every second day. The barrier property and integrity of cell monolayers during growth and before/after experiments was verified by the transepithelial electrical resistance (TEER), measured using a Milicell ERS-2 epithelial volt-ohm meter (Millipore, USA), and 0.8 μCi/mL [^{3}H]mannitol was included in all test solutions as a translocation marker [24]. Test solutions were prepared freshly with 0-100mM DM-β-CD in HBSS/HEPES buffer (0.1% OVA (w/v) and 20 mM HEPES, pH 7.4), and were treated very gently.

Transport experiments were performed in HBSS/HEPES buffer, with test solutions added apically after 60 min. equilibration with buffer, while incubated with gentle shaking. Basolateral samples were collected every 15 minutes for 1 hour and analyzed along with apical test solutions, for peptide content using commercial ELISA kits (see next paragraph) and for [^{3}H]mannitol content in a scintillation counter (Packard TopCount), after mixing with scintillation fluid (Microscint-40).

After experiments, cells were washed twice with buffer and replenished with medium for 24 hour recovery. The Caco-2 translocation of peptide or [^{3}H]mannitol over Caco-2 layers is expressed as the apparent permeability (P_{app}), given by:

Eq. (1): $$P_{app} = \frac{dQ}{dt}\,\frac{1}{A \cdot C_0}$$

where dQ/dt is the steady-state flux across the cell layer (pmol/s), A is the surface area (1.12 cm^2), and C_0 is the initial sample concentration [24].

sCT concentration measurements

Apical and basolateral samples from Caco-2 experiments were analyzed using commercial sCT EIA kits, as recommended by the manufacturer (Phoenix Pharmaceuticals). sCT standards were prepared for each analogue from sCT test solutions, and were fitted to eq. 2 using GraphPad Prism.

Eq. (2): $$Abs(450nm) = A + \frac{B-A}{1+10^{((logEC_{50}-x)\cdot C)}}$$

where x is log(concentration), and A, B, C and EC_{50} are fitting parameters [36].

Data analysis

Statistical analysis was carried out using GraphPad Prism, where unpaired Students t-tests were used for comparison, and a significant difference was considered if $p < 0.05$.

Results and Discussion

Peptide analogues

Acyl chains were conjugated to a primary amine in sCT at either the N-terminus or at K^{18}, and the peptide backbone (BB) differs from native sCT in a $Y^{22}W$ mutation, initally introduced to allow for fluorescence measurements. Despite the mutation's conservative character and its vicinity to previously described major alterations not causing loss-of-function [12,15], the potency of BB towards the hCT receptor was found to be reduced roughly 50% compared to native sCT [2]. Acylation caused further reduction, particularly for N-terminal acylations, although all analogues displayed activity towards the receptor.

Solution behaviour of sCT analogues in physiological buffer

The fluorophore ThT is widely used to probe fibrillation due to its propensity to bind cross-β structures in (amyloid) fibrils [37], where the resulting excitation and emission shifts enables fast and sensitive screening for fibril formation. Freshly prepared peptide solutions gave rise to quite varied time profiles (fig. 1).

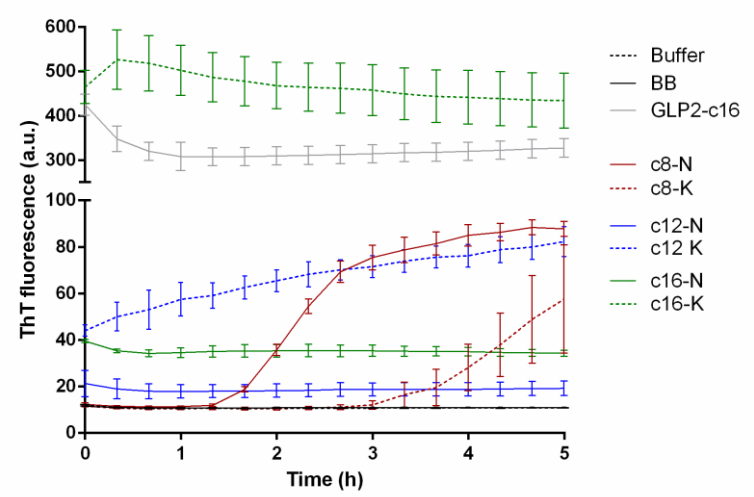

Figure 1 ThT fluorescence intensity measured over time, for incubation of sCT analogues and a control peptide at 37 °C. A gradual increase in fluorescence intensity as observed for c8-analogues indicates fibrillation, whereas the constantly low value for BB (similar to buffer) indicates no fibrillation during the time course of the experiment. Data points represent mean ± SDOM of 3 separate experiments.

During the time course of the experiment, BB (and native sCT, data not shown) displayed a constant low ThT signal similar to buffer, indicating no fibrillation. For c8-analogues the gradual increase in fluorescence indicates fibrillation during the experiment, with a longer lag-phase for c8-K than for c8-N. For the longer chain acylations the data is less clear, with a low and constant signal (c12- and c16-N), high and constant (c16-K) or a slight increase over time (c12-K). False-negative signals for fibrils and ThT fluorescence have been reported, as well as similar profiles to those observed for c16-analogues [27,38], which was ascribed to fibril subtypes which did not bind ThT and conformational changes in fibrils causing changes in ThT fluorescence, respectively. However, the signals could also be due to non-fibril self-association, so the previously investigated peptide analogue GLP2-c16 [16] was included as a control (fig. 1). The c16-acylated analogue of Glucagon-like peptide-2 (GLP-2) was previously observed to form well-defined oligomers in saline buffers at physiological pH [16], and fibrillation was not observed on intermediate time scales. As evident from fig. 1, the ThT fluorescence profile of the peptide control is similar to the c16-sCT analogues, although with a higher signal than for c16-N. This indicates that the ThT-signals observed for the long chain acylations could be caused by self-association or other modes of aggregation than fibrillation.

In order to investigate the self-assemblies in more detail, peptide solutions were visualized using TEM, where an initial positive control using an aged c8-N solution (several days old) showed widespread elongated structures. TEM images for selected samples are presented in fig. 2.

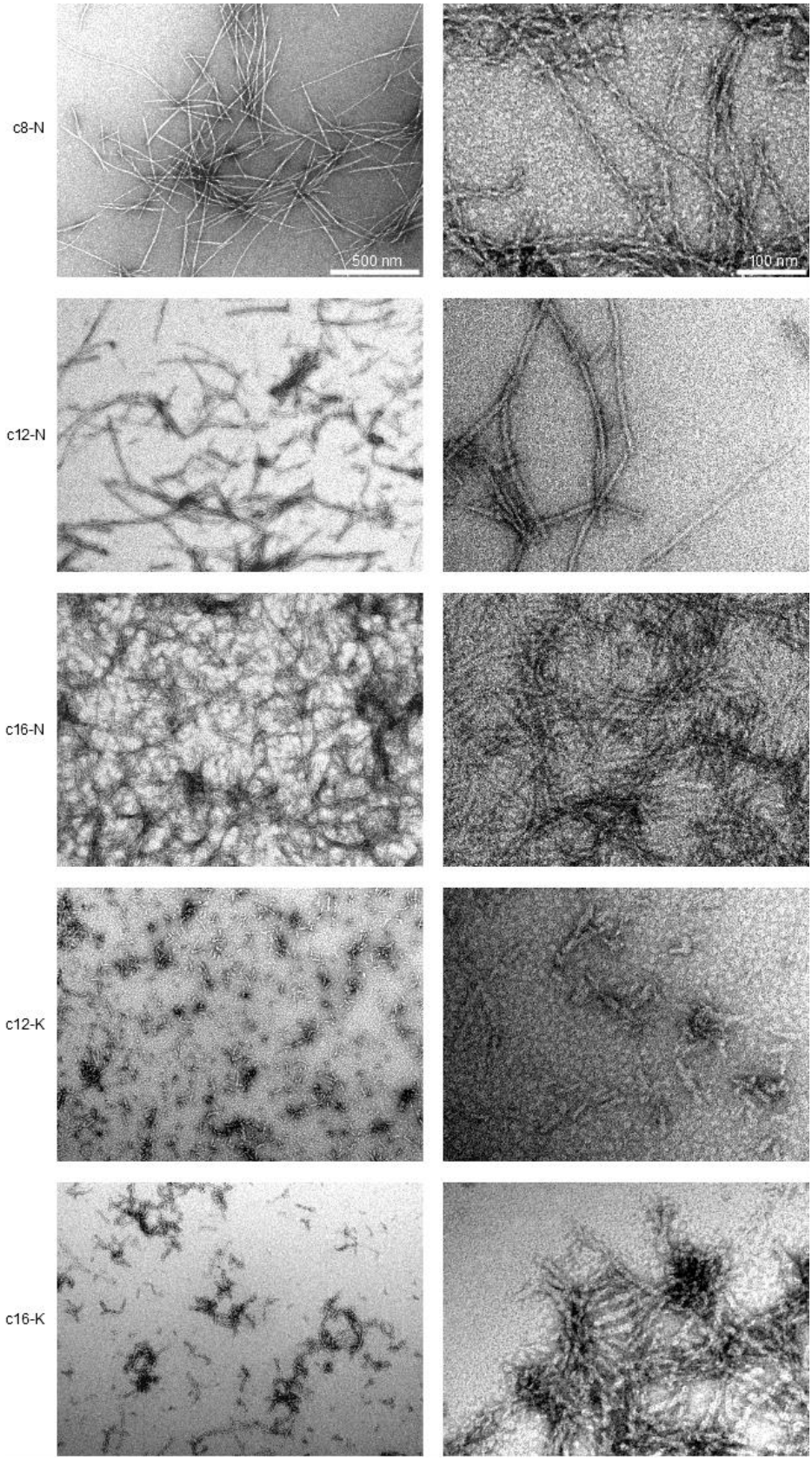

Figure 2 TEM images of peptide analogues, with 44kx (left) or 180kx magnification (right). TEM visualization was repeated 2-3 times with similar results.

In fig. 2, c8-N displayed elongated structures, slightly entangled networks, and longitudinal twisting at high magnification. c12-N and c16-N appeared as untwisted, shorter fibers, whereas c12-K and c16-K displayed very short rods. For BB and c8-K, no structures were visible in TEM, however, room temperature incubation of the c8-K solution for 3 hours caused development of some visible structures.

The acylation was initially placed at the N-terminus, but the analogues' aggregation propensity spurred an alternative placement at K^{18}. Peptide fibrils have been reported to consist of parallel or anti-parallel alignment of peptides, perpendicular to the fiber axis [39], and the N-terminal acylation might increase parallel alignment of sCT analogues. Acylation at K^{18} may alleviate this, and ThT and TEM results show some reduction in aggregation through moving the acylation, in particular for c8-analogues. However, previously reported results [2] show a non-trivial relationship between acylation chain length or position and intestinal permeability, where the short c8 chain is optimal for N-terminal acylation and the medium or long chain is optimal for K^{18}-acylation (superior to c8-N).

Addition of DM-β-CD

For c8-analogues mixed with DM-β-CD, the ThT fluorescence intensity increase was delayed or abolished altogether (fig. 3), indicating inhibition of self-association at the employed concentrations. For c12- and c16-analogues DM-β-CD caused a lowering of ThT fluorescence signals to time-independent values, and for c12-K thus abolished the slight signal-increase over time, however, the values remained higher than buffer. In preliminary experiments DM-β-CD was employed at 10, 50 or 100 mM with similar impact on ThT fluorescence intensity, but the lowest concentration was chosen for further experiments based on a preliminary Caco-2 screening of cyclodextrin toxicity (see next section). The lower concentration limit for inhibition of aggregation was not investigated.

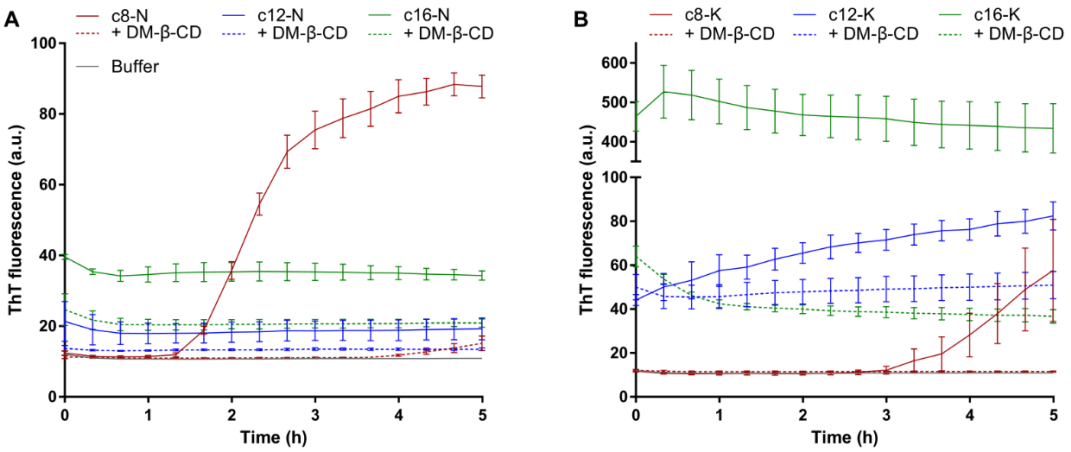

Figure 3 ThT fluorescence intensity measured over time, for incubation of sCT analogues +/- DM-β-cyclodextrin at 37 °C. Data points represent mean ± SDOM of 2-3 separate experiments.

The effect of cyclodextrin was investigated with TEM, where self-association was drastically reduced for all analogues, and essentially no structures were visible in the presence of DM-β-CD. Furthermore, preliminary DLS investigations confirmed the presence of large structures in the solutions of acylated analogues (not for BB), which in most cases disappeared in the presence of cyclodextrin, consistent with TEM images.

Interaction with Caco-2 cells

The translocation of sCT analogues through Caco-2 monolayers was previously found to cause enhanced translocation through permeation enhancer-like effects on the cells, which depended non-trivially on acylation chain length and position [2]. The peptide samples were treated gently to avoid fibrillation, and for c8-analogues the lag time preceding an increase in ThT fluorescence did not indicate significant fibrillation during the 1 h Caco-2 experiment. For c8-N the use of aged solutions (positive control for fibrillation) reduced the translocation and enhancer-effect on the cells, indicating a detrimental effect of aggregation into larger structures. Translocation of the large peptide structures is presumably negligible, and dissociation may be either irreversible or slower than the time-scale of the 1 h cell experiment, thus limiting the amount of peptide monomer free to interact with the cells. For longer chain acylations, K^{18} analogues displayed far superior translocation, enhancer-effect and binding to the cell membrane compared to N-terminal analogues [2]. This may indicate that K^{18} analogues aggregate less or in a more reversible manner, which is partially supported by TEM visualization (fig. 2).

If the Caco-2 interaction of longer chain N-terminal analogues is in fact impaired by aggregation, then monomerization by DM-β-CD should improve Caco-2 interaction, and ease the handling of samples for future applications.

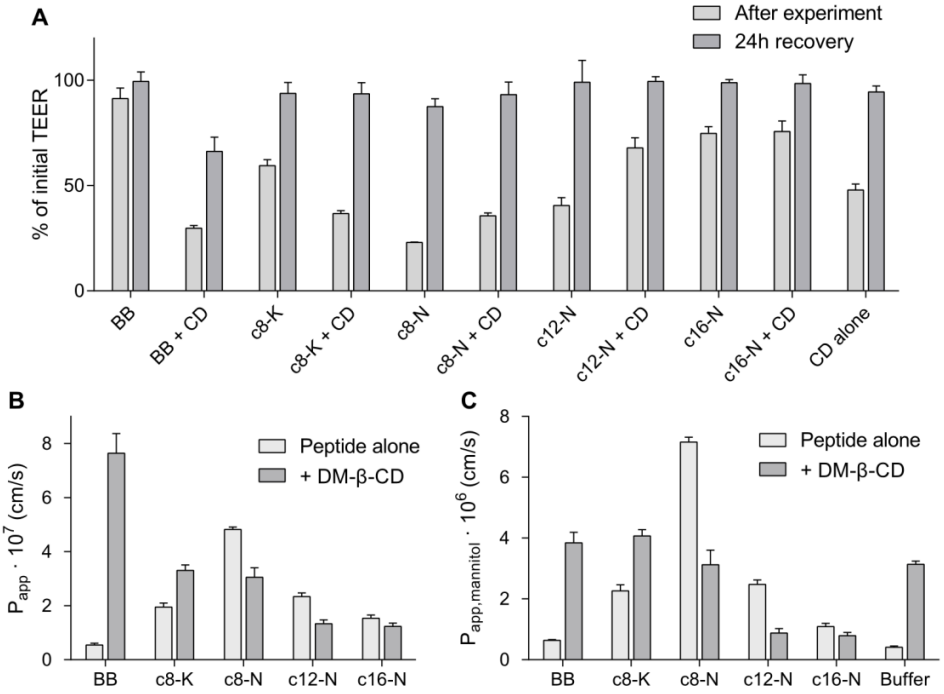

Figure 4. Effect of DM-β-CD on the interaction of sCT analogues with Caco-2 monolayers, investigated for BB and N-terminal or K^{18}-acylated analogues. A) TEER values for Caco-2 cell monolayers after experiments and after 24-hour recovery in cell medium. B) Peptide and C) mannitol permeability during the experiment. All data points represent mean ± SD of 2 separate experiments, each with 4 repeats.

However, Caco-2 translocation in the presence of DM-β-CD (fig. 4) indicates an interesting effect. Cyclodextrin addition to BB provides an efficient permeability enhancement, which is not observed for the acylated analogues, and for N-terminal analogues the acylation-induced enhancement is in fact less efficient in the presence of DM-β-CD. For c8-K, cyclodextrin addition appears to be slightly beneficial, but the enhancement is very limited compared to the effect for BB, or the acylation-induced enhancement.

Cylodextrin alone enhances mannitol permeability enhancement and decreases TEER, which indicates an unspecific effect on the cell layer, e.g. through cholesterol depletion. For the BB/DM-β-CD-mixture, TEER values do not recover entirely after 24 h in fresh medium, and preliminary experiments with higher DM-β-CD concentrations (50 and 100 mM), either alone or in combination with c8-N, showed very large decreases in TEER with no recovery after 24 h. Full recovery after exposure to the BB/ DM-β-CD-combination could presumably be obtained by lowering the

cyclodextrin concentration, however, the unacylated peptide was not the focus of this work.

The ability of DM-β-CD to limit aggregation of acylated sCT analogues may explain the somewhat detrimental effects on caco-2 translocation. The ability of acylated sCT analogues to act as their own permeability enhancer are speculated to be due to a synergy between the hydrophobic acyl chain and the positively charged peptide backbone, causing efficient insertion into the caco-2 cell membrane and a disruptive effect similar to transcellular oral permeation enhancers [2]. However, if the acyl chain binds in the hydrophobic core of DM-β-CD with a high affinity, then the insertion into caco-2 cells may be hindered. Furthermore, if the permeation enhancer effect previously observed for similar β-CDs [31,34] is partially due to extraction of cholesterol from cell membranes, this could be hampered by too tight binding to acylated sCT analogues. However, the high molar excess of DM-β-CD to peptide (100:1) should lower the possible importance of 'scavenging' by sCT analogues.

In fig. 4, addition of cyclodextrin affects the caco-2 permeability of the two c8-analogues differently, as it is decreased for c8-N (particularly mannitol permeability) and it is slightly increased for c8-K. This difference may be caused by different binding affinity of the two analogues to DM-β-CD. Cyclodextrin addition to c12-N and c16-N caused very limited effects on the cell layer tightness and mannitol translocation, which could be due to even tighter binding, and the expected improvement due to cyclodextrin-mediated inhibition of aggregation is not observed.

Conclusions

Depending on acylation chain length and position, certain acylated sCT analogues aggregate in physiological buffer solutions, potentially forming fibril-like structures. Placement of the acylation at Lys^{18} appears to cause less aggregation compared to the N-terminal, most clearly exemplified by the short chain c8-analogues. These analogues display well-defined fibrillation time profiles during heating, with a lag-time for c8-K roughly twice as long as for c8-N. All N-terminal analogues appear as elongated structures in TEM, with c8-N displaying longitudinal twisting. K^{18} analogues are less well-defined, with c8-K initially displaying no visible structures (similar to the unacylated peptide backbone), whereas c12-K and c16-K display short rods that are not well-defined. For all analogues, self-association is efficiently inhibited by addition of DM-β-CD, likely through monomerization of peptides via binding in the hydrophobic cavity. However, binding may hamper the interaction of both acylated analogues and DM-β-CD with Caco-2 cells, as their respective permeability enhancing effects are reduced in the mixtures. Whereas DM-β-CD is an efficient enhancer for the unacylated peptide backbone, it confers only a slight

improvement to c8-K, and all N-terminal analogues display reduced permeability when combined with DM-β-CD. The impairment of permeability enhancing may be reduced by varying peptide to cyclodextrin ratio, or using different cyclodextrins with lower affinity for the acylated peptides, but we speculate that this will also diminish the self-association inhibition.

Acylation of sCT can increase its intestinal permeability, however, the risk of reduced solution stability demands rational choices or optimization of acylation details for oral delivery purposes.

Acknowledgements

This work was supported by The Technical University of Denmark, The Danish Agency for Science, Technology and Innovation, and Novo Nordisk A/S. The funders did not have any role in the study design, data collection and analysis, decision to publish, or preparation of the manuscript. Financial disclosure: LL, SB, HMS and ULR are shareholders in Novo Nordisk A/S.

References

1. Copp D, Cheney B. Calcitonin-a hormone from the parathyroid which lowers the calcium-level of the blood. Nature. 1962;193.
2. Trier S, Linderoth L, Bjerregaard S, Strauss HM, Rahbek UL, Andresen TL. Acylation of salmon calcitonin modulates in vitro intestinal peptide flux through membrane permeability enhancement. Eur J Pharm Biopharm. 2015;96: 329–37. doi:10.1016/j.ejpb.2015.09.001
3. Purdue BW, Tilakaratne N, Sexton PM. Molecular Pharmacology of the Calcitonin Receptor. Recept Channels. Informa UK Ltd UK; 2002;8: 243–255.
4. Karsdal MA, Henriksen K, Bay-Jensen AC, Molloy B, Arnold M, John MR, et al. Lessons learned from the development of oral calcitonin: the first tablet formulation of a protein in phase III clinical trials. J Clin Pharmacol. 2011;51: 460–71. doi:10.1177/0091270010372625
5. Arvinte T, Cudd A, Drake AF. The structure and mechanism of formation of human calcitonin fibrils. J Biol Chem. 1993;268: 6415–22.
6. Cudd A, Arvinte T, Das REG, Chinni C, Macintyre I. Enhanced potency of human calcitonin when fibrillation is avoided. J Pharm Sci. 1995;84: 717–719. doi:10.1002/jps.2600840610
7. Petersen SB, Nielsen LG, Rahbek UL, Guldbrandt M, Brayden DJ. Colonic absorption of salmon calcitonin using tetradecyl maltoside (TDM) as a permeation enhancer. Eur J Pharm Sci. 2013;48: 726–34. doi:10.1016/j.ejps.2013.01.009
8. Binkley N, Bolognese M, Sidorowicz-Bialynicka A, Vally T, Trout R, Miller C, et al. A phase 3 trial of the efficacy and safety of oral recombinant calcitonin: the Oral Calcitonin in Postmenopausal Osteoporosis (ORACAL) trial. J Bone Miner Res. 2012;27: 1821–9. doi:10.1002/jbmr.1602
9. Werle M, Takeuchi H. Chitosan-aprotinin coated liposomes for oral peptide delivery:

Development, characterisation and in vivo evaluation. Int J Pharm. 2009;370: 26–32. doi:10.1016/j.ijpharm.2008.11.013

10. Sang Yoo H, Gwan Park T. Biodegradable nanoparticles containing protein-fatty acid complexes for oral delivery of salmon calcitonin. J Pharm Sci. 2004;93: 488–95. doi:10.1002/jps.10573

11. Song K-H, Chung S-J, Shim C-K. Enhanced intestinal absorption of salmon calcitonin (sCT) from proliposomes containing bile salts. J Control Release. 2005;106: 298–308. doi:10.1016/j.jconrel.2005.05.016

12. Wang J, Chow D, Heiati H, Shen W-C. Reversible lipidization for the oral delivery of salmon calcitonin. J Control Release. 2003;88: 369–80.

13. Cheng W, Satyanarayanajois S, Lim L-Y. Aqueous-soluble, non-reversible lipid conjugate of salmon calcitonin: synthesis, characterization and in vivo activity. Pharm Res. 2007;24: 99–110. doi:10.1007/s11095-006-9128-9

14. Cheng W, Lim L. Comparison of reversible and nonreversible aqueous-soluble lipidized conjugates of salmon calcitonin. Mol pharm. 2008;88.

15. Youn YS, Jung JY, Oh SH, Yoo SD, Lee KC. Improved intestinal delivery of salmon calcitonin by Lys18-amine specific PEGylation: stability, permeability, pharmacokinetic behavior and in vivo hypocalcemic efficacy. J Control Release. 2006;114: 334–42. doi:10.1016/j.jconrel.2006.06.007

16. Trier S, Linderoth L, Bjerregaard S, Andresen TL, Rahbek UL. Acylation of Glucagon-like peptide-2: interaction with lipid membranes and in vitro intestinal permeability. PLoS One. 2014;9: e109939. doi:10.1371/journal.pone.0109939

17. Kurtzhals P, Havelund S, Kiehr B, Larsen UD, Ribel U, Markussen J. Albumin binding of insulins acylated. Biochem J. 1995;312: 725–731.

18. Dasgupta P, Singh A, Mukherjee R. N-terminal acylation of somatostatin analog with long chain fatty acids enhances its stability and anti-proliferative activity in human breast adenocarcinoma cells. Biol Pharm Bull. 2002;25: 29–36.

19. Yuan L, Wang J, Shen W-C. Reversible Lipidization Prolongs the Pharmacological Effect, Plasma Duration, and Liver Retention of Octreotide. Pharm Res. 2005;22: 220–227. doi:10.1007/s11095-004-1189-z

20. Gozes I, Bardea A, Reshef A, Zamostiano R, Zhukovsky S, Rubinraut S, et al. Neuroprotective strategy for Alzheimer disease: intranasal administration of a fatty neuropeptide. Proc Natl Acad Sci U S A. 1996;93: 427–32.

21. Dalbøge LS, Pedersen SL, van Witteloostuijn SB, Rasmussen JE, Rigbolt KTG, Jensen KJ, et al. Synthesis and evaluation of novel lipidated neuromedin U analogs with increased stability and effects on food intake. J Pept Sci. 2014; doi:10.1002/psc.2727

22. Zhang L, Bulaj G. Converting peptides into drug leads by lipidation. Curr Med Chem. 2012;19: 1602–18.

23. Uchiyama T, Kotani A, Tatsumi H. Development of novel lipophilic derivatives of DADLE (leucine enkephalin analogue): Intestinal permeability characteristics of DADLE derivatives in rats. Pharm Res. 2000;17.

24. Hubatsch I, Ragnarsson EGE, Artursson P. Determination of drug permeability and prediction of drug absorption in Caco-2 monolayers. Nat Protoc. 2007;2: 2111–9. doi:10.1038/nprot.2007.303

25. Artursson P, Palm K, Luthman K. Caco-2 monolayers in experimental and theoretical predictions of drug transport. Adv Drug Deliv Rev. Elsevier B.V.; 2001;46: 27–43. doi:10.1016/j.addr.2012.09.005

26. Diociaiuti M, Gaudiano MC, Malchiodi-Albedi F. The slowly aggregating salmon Calcitonin: a useful tool for the study of the amyloid oligomers structure and activity. Int J Mol Sci. 2011;12: 9277–95. doi:10.3390/ijms12129277

27. Pedersen JS. The Nature of Amyloid-like Glucagon Fibrils. J Diabetes Sci Technol. 2010;4: 1357–1367. doi:10.1177/193229681000400609

28. Fridbjörg Sigurjónsdóttir J, Loftsson T, Másson M. Influence of cyclodextrins on the stability of the peptide salmon calcitonin in aqueous solution. Int J Pharm. 1999;186: 205–213. doi:10.1016/S0378-5173(99)00183-0

29. Irie T, Uekama K. Cyclodextrins in peptide and protein delivery. Adv Drug Deliv Rev. 1999;36: 101–123.

30. Schipper NGM, Verhoef JC, Romeijn SG, Merkus FWHM. Methylated β-cyclodextrins are able to improve the nasal absorption of salmon calcitonin. Calcif Tissue Int. 1995;56: 280–282. doi:10.1007/BF00318047

31. Zhang L, Song L, Zhang C, Ren Y. Improving intestinal insulin absorption efficiency through coadministration of cell-penetrating peptide and hydroxypropyl-β-cyclodextrin. Carbohydr Polym. Elsevier Ltd.; 2012;87: 1822–1827. doi:10.1016/j.carbpol.2011.10.002

32. Shao, Zezhi; Li, Yuping; Chermak, Todd; Mitra AK. Cyclodextrin as Mucosal Absorption Promoters of Insulin. Pharm Res. 1994;11: 1174–1179.

33. Lommerse PHM, Spaink HP, Schmidt T. In vivo plasma membrane organization: results of biophysical approaches. Biochim Biophys Acta. 2004;1664: 119–31. doi:10.1016/j.bbamem.2004.05.005

34. Tötterman AM, Schipper NG, Thompson DO, Mannermaa JP. Intestinal safety of water-soluble beta-cyclodextrins in paediatric oral solutions of spironolactone: effects on human intestinal epithelial Caco-2 cells. J Pharm Pharmacol. 1997;49: 43–48.

35. Fujinari E, Courthaudon L. Nitrogen-specific liquid chromatography detector based on chemiluminescence: Application to the analysis of ammonium nitrogen in waste water. J Chromatogr. 1992;592: 209–214.

36. Borchard G. The Absorption Barrier. In: Bernkop-Schnürch A, editor. Oral Delivery of Macromolecular Drugs. New York: Springer US; 2009. pp. 49–64. doi:10.1007/978-1-4419-0200-9

37. Biancalana M, Koide S. Molecular mechanism of Thioflavin-T binding to amyloid fibrils. Biochim Biophys Acta. 2010;1804: 1405–12. doi:10.1016/j.bbapap.2010.04.001

38. Nilsson MR. Techniques to study amyloid fibril formation in vitro. Methods. 2004;34: 151–160. doi:10.1016/j.ymeth.2004.03.012

39. Andreotti G, Motta A. Modulating calcitonin fibrillogenesis: An antiparallel α-helical dimer inhibits fibrillation of salmon calcitonin. J Biol Chem. 2004;279: 6364–6370. doi:10.1074/jbc.M310882200

4.2.1 Notes on paper 3

As mentioned earlier, the Trp backbone mutation in sCT reduced its potency, whereas the solution stability of BB appears quite similar to sCT. No aggregation/fibrillation was observed for BB in the performed experiments (similar to sCT), including ThT measurements with prolonged incubation (20 h, data not shown).

As a brief addition, preliminary experiment showed that the pH-dependency of c8-N discussed in paper 2 was retained in the mixture with DM-β-CD, with higher permeability at pH 5.5 than 7.4. The enhancer-effect of DM-β-CD alone was pH-independent in this pH range, so the effect may be due to unbound peptide, or possibly pH-dependent binding affinity of cyclodextrin and c8-N.

The solution stability of sCT analogues was tentatively investigated in FaSSIF buffer, with no apparent improvement.

4.3 Additional results

The following results have not yet been published, however, we intend to collate parts of it in a manuscript.

4.3.1 A new family of sCT analogues

The surprisingly profound impact of the Trp backbone mutation and the failed fluorescence experiments motivated us to investigate acylated sCT analogues with the native backbone. Initially, the c8-K Y22 analogue showed very promising results, and motivated synthesis and investigation of the longer chain analogues. However, the synthesis was delayed substantially, and the longer chain analogues were not characterized as thoroughly as intended. Furthermore, several experiments were postponed to include these analogues, but they did not fulfill our expectations. In the following section the results will not be presented in chronological order, but as a comparison of the various analogues, and include both old and new results for the previously described analogues.

Receptor potency of K^{18}-acylated analogues The *in vitro* receptor activation of sCT analogues with the native Tyr22 is shown in fig. 4.1, along with previously described Trp22 analogues for comparison. The c8-analogue appears to benefit somewhat from removing the backbone mutation, whereas the longer chain analogues appear independent of the mutation.

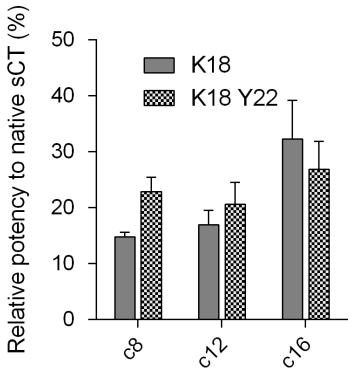

Figure 4.1: *In vitro* receptor activation. IC50 potency of K^{18}-acylated sCT analogues relative to native sCT, with native Tyr22 (labeled Y22) or with Trp22 point mutation. Values are presented as mean ±SDOM of 3 separate experiments, each in duplicate.

Solution stability of K^{18}-acylated analogues The solution stability of the new K^{18}-acylated sCT analogues with native Tyr22 is presented in fig. 4.2, along with older analogues for comparison. For c8-analogues, ThT-fluorescence increase is substantially delayed for c8-K Y22 compared to c8-K (and c8-N), indicating delayed fibrillation by reverting to the native Tyr22. However, the results are less clear for longer chain acylations, as c12- and c16-K Y22 display similar profiles but higher values than their W22-mutated counterparts. All long chain analogues were previously observed to display unclear ThT fluorescence profiles, possibly due to self-association.

Caco-2 interaction of K^{18}-acylated analogues The permeability through caco-2 monolayers and cell binding of the K^{18}-acylated sCT analogues with native Tyr22 is presented in fig. 4.3, along with old analogues for comparison. As previously alluded to, c8-K Y22 displays a very high permeability, whereas for c12- and c16-K Y22 it is surprisingly low. For c16-K Y22, the increased

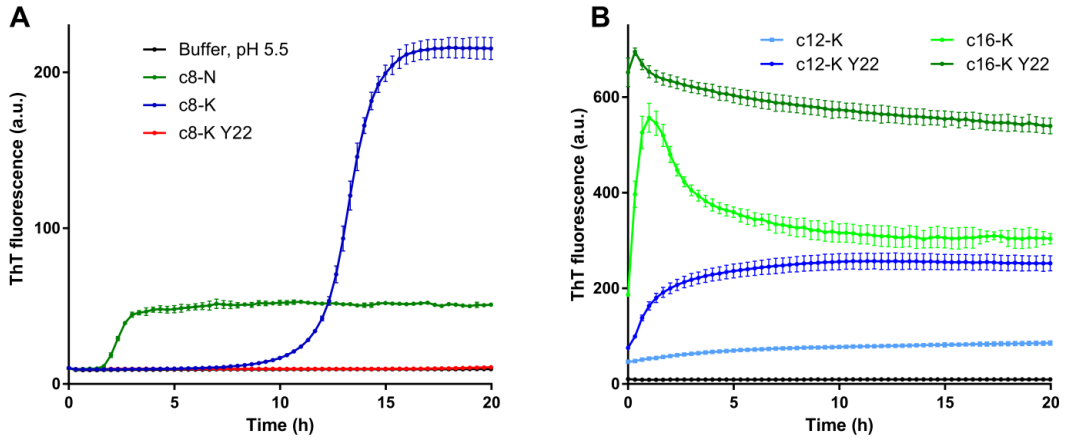

Figure 4.2: Solution stability of sCT analogues. ThT fluorescence intensity measured over time at 37 °C. sCT analogues with Trp backbone mutation or native Tyr (Y22), and short chain acylation (A) or longer chains (B) at N-terminus or K^{18}.

cell membrane binding, uptake and mannitol permeability could indicate a too great membrane affinity of the peptide, where the permeabilizing effect allows translocation of mannitol but the peptide itself is stuck. However, for c12-K Y22 all values are very low, and the long chain analogues with W^{22} display both higher permeability and higher cell-association.

For K^{18}-analogues, long chain analogues appear optimal for translocation only in combination with the W^{22} mutation, whereas a short chain acylation is far superior when using the native backbone. Apart from the differences in solution stability, we currently have no explanation for these profound effects of the backbone mutation, which limits any conclusion on the systematic effects of acylation chain length, as observed for GLP-2 analogues.

Specifically for c8-K Y22, the high peptide permeability is not accompanied by a substantial increase in mannitol permeability, indicating a more peptide-specific enhancer effect for this peptide analogue. This is supported by a limited liposome permeabilization and TEER-decrease, in contrast to previous observations for other acylated analogues.

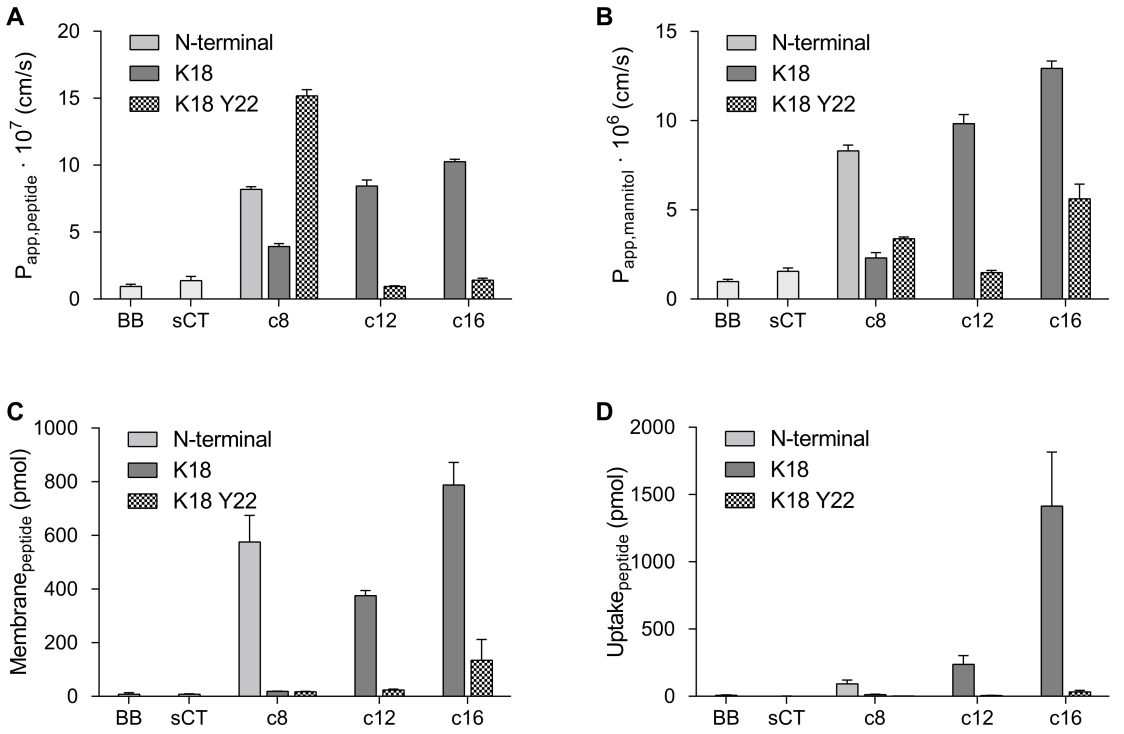

Figure 4.3: Caco-2 interaction of sCT analogues. Permeability of peptide (A) and mannitol (B), along with cell membrane binding (C) and uptake (D), investigated for native sCT, backbone (BB) with Y->W^{22} mutation and selected N-terminal or K^{18}-acylated analogues. All data points represent mean ± SD of at least 2 separate experiments, each with 4 repeats. TEER-values were transiently reduced for acylated analogues (as previously shown), to varying degrees very consistent with their respective enhancing effect, and therefore values are not included here.

4.3.2 *A closer look at cell interactions and enhancing effects*

To further investigate the enhancing effect of selected sCT analogues, we employed fluorescence microscopy, either through immunocytochemistry for caco-2 monolayers used in experiments or live-cell imaging for caco-2 cell monolayers grown on microscope slides. We originally planned to attach a fluorophore to selected peptide analogues, but this carries a risk of altering the peptide properties due to the charge/hydrophobicity/size of most fluorophore moities, particularly for small peptides as sCT. We opted instead for antibody-mediated fluorescence staining of peptide analogues and/or addition of FITC Dextran 4 kDa (FD4), which is similar to sCT in size and widely used as a model compound in caco-2 enhancer studies.

For FD4, we initially investigated the permeability and cell association in combination with peptide analogues (see fig. 4.4).

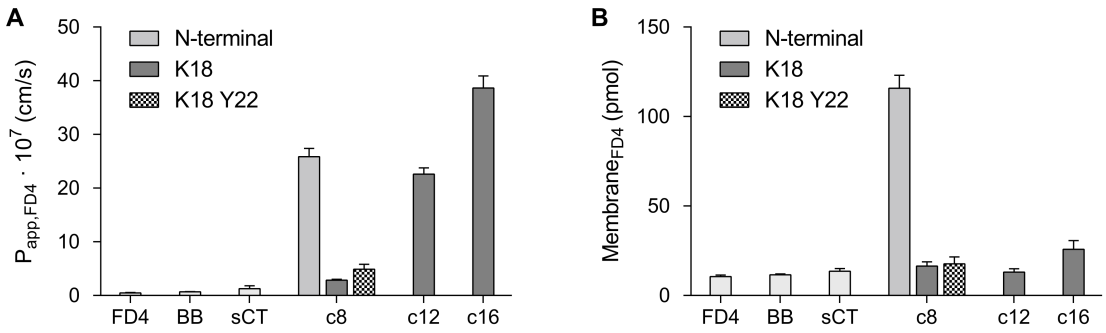

Figure 4.4: Enhancer effect of sCT analogues. Permeability (A) and membrane binding (B) of FD4 in combination with selected sCT analogues. The cell uptake for FD4 is very similar to membrane binding results, and therefore not shown here. All data points represent mean ± SD of 2 separate experiments, each with 4 repeats.

FD4-permeability is enhanced by c8-N, c12-K and c16-K, consistent with a non-specific membrane permeabilization effect as previously discussed. For c8-K Y22 the very limited enhancement is similar to mannitol-results and consistent with a more peptide-specific enhancement. The cell membrane binding and uptake of FD4 is almost unaltered by K^{18}-analogues, and independent of acylation chain length (in contrast to the peptide itself). Interestingly, FD4 cell association is greatly enhanced by c8-N, possibly indicating an interaction between c8-N and FD4 causing peptide-mediated cell anchoring.

Immunocytochemistry (See description of staining procedure in experimental section 4.3.4.)

Confocal laser scanning microscopes (CLSM) allow imaging thin section of the fixed cell layer in side-view or cross-section, as shown for an untreated caco-2 monolayer in fig. 4.5.

After permeability experiments, the distribution of sCT analogues within the caco-2 monolayer can be visualized, along with possible morphological changes to the cell layer. As shown in 4.6, the unacylated backbone displays insignificant cell-association, and the cell morphology is very similar or identical to control, whereas acylated analogues c8-N and c16-K are present in the cell layer, which also appears slightly altered. Both analogues appear to have 'stunted' the cells somewhat, and caused slight alterations in the actin structure. However, these effects are far more subtle than other permeation enhancers, which feature disruption of tight junction protein complexes causing paracellular channel opening and/or profound actin reorganization [5, 18, 63, 98, 104] (or actual holes in the cell layer), see fig. B.1 in appendix B.

c8-N appears to be bound to the apical part of the cells as large assemblies, possibly on both sides of the actin wall (it is not entirely clear in images, but videos scanning the entire cell layer are more informative). The cell distribution of c16-K is somewhat different, as it appears more

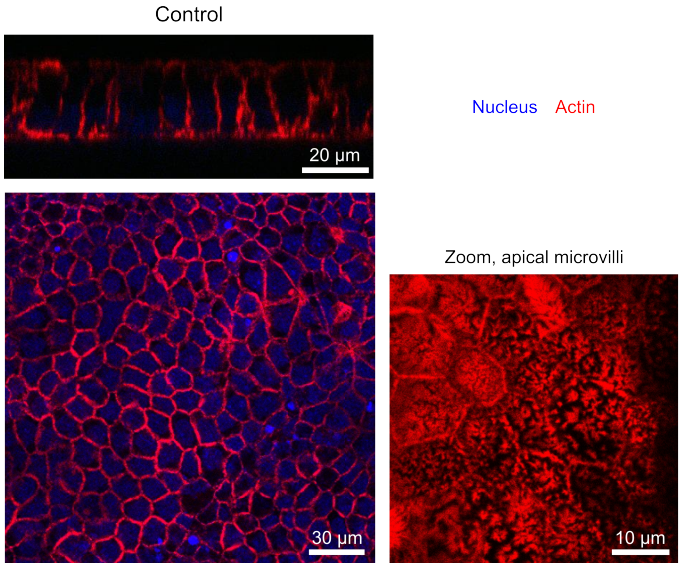

Figure 4.5: Appearence of untreated caco-2 monolayers. Fluorescence microscopy images of a caco-2 monolayers following permeability experiments with control (buffer), fixed in formalin and stained for filamentous actin (red) and nucleus (blue). A cross-section in the middle of the cell monolayer (bottom left) and side-view (top) show the tightly adhering and columnar endothelial cell morphology, and a cross-section zoom (right) at the top of the cell-layer shows the actin-rich protruding microvilli.

evenly distributed, mostly in the cell cytosol and the cytosolic side of the cell membrane. These observations are fairly consistent with the quantification of cell association in fig. 4.3, where cell membrane binding is similar for c8-N and c16-K, but cell uptake (in the aqueous cell lumen) is much greater for c16-K. However, it should be noted that 'membrane bound' comprises all membrane components in the cell (following lysis), i.e. also various cytosolic compartments. Generally, these quantifications of cell association are far less well-defined than the liposome membrane partitioning measured for GLP-2 analogues, and interpretation should be performed with caution.

Regarding microscopy images, it should be noted that the fluorescence staining is performed with a primary antibody for sCT, which binds less efficiently to the altered analogues, similarly to the previously described issues for ELISA quantification. Thus, the acylated analogues (particularly long-chain) did not stain too well. Generally, fluorophore signals are merely qualitative (not quantitative!) and images have been optimized for presentation purposes. The poor staining for acylated analogues could possibly be compensated by increasing antibody concentration based on ELISA binding efficiency, but due to lack of time this was not attempted.

Fig. 4.7 shows caco-2 monolayers exposed to native sCT and its short- or long-chain K^{18}-acylated analogues. sCT displays some cell association, almost entirely at the apical microvilli. The acylated analogues appear in the cytosol of some cells only, and not as widespread as c16-K, consistent with the measured cell association in fig. 4.3.

In a somewhat experimental attempt, FD4 distribution in cell layers was visualized directly, which simplifies the staining procedure substantially. In most cases the fluorescence signal was quite weak, but the three examples shown in fig. 4.8 appear consistent with the peptide distribution. For c8-N, the FD4-signal is in fact more clear than the peptide staining, and the quite distinct cell association is nicely visualized. The relative FD4-signals for the three acylated analogues (which is not marred by differences in antibody affinity) are very consistent with the measured cell-association presented in fig. 4.4.

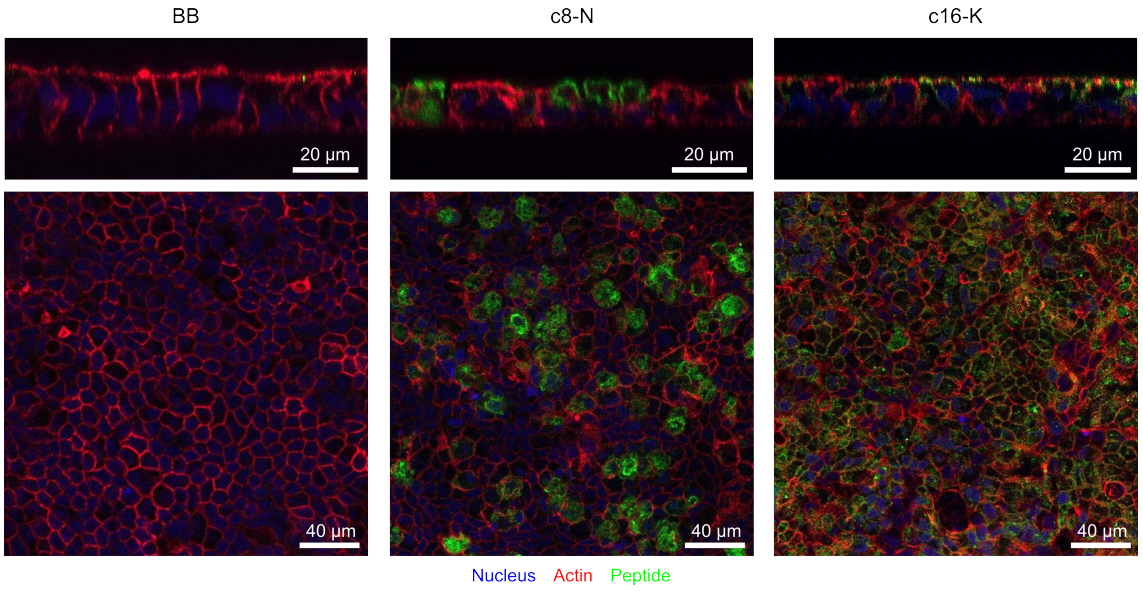

Figure 4.6: Caco-2 cell interaction of W^{22} sCT analogues. Microscopy images of caco-2 cell monolayers following permeability experiments with selected sCT analogues, in side-view (top) or cross-section in the middle of the cell layer (bottom). Cells are fixed and stained for nucleus (blue), filamentous actin (red) and sCT (green).

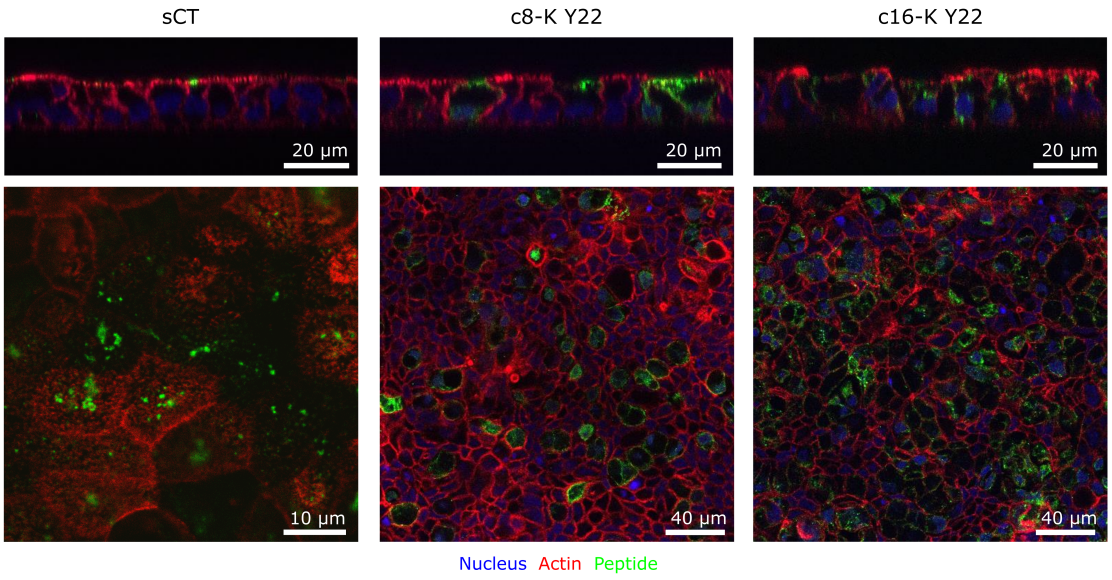

Figure 4.7: Caco-2 cell interaction of Y^{22} sCT analogues. Microscopy images of caco-2 cell monolayers following permeability experiments with selected sCT analogues, in side-view (top) or cross-section (bottom). Cells are fixed and stained for nucleus (blue), filamentous actin (red) and sCT (green).

Following caco-2 experiments, TEER was routinely measured after 24h recovery in medium, where the pronounced TEER-decreases caused by acylated sCT analogues were shown to be reversible. Imaging of the cell layers after 24h recovery was very consistent with this. For most

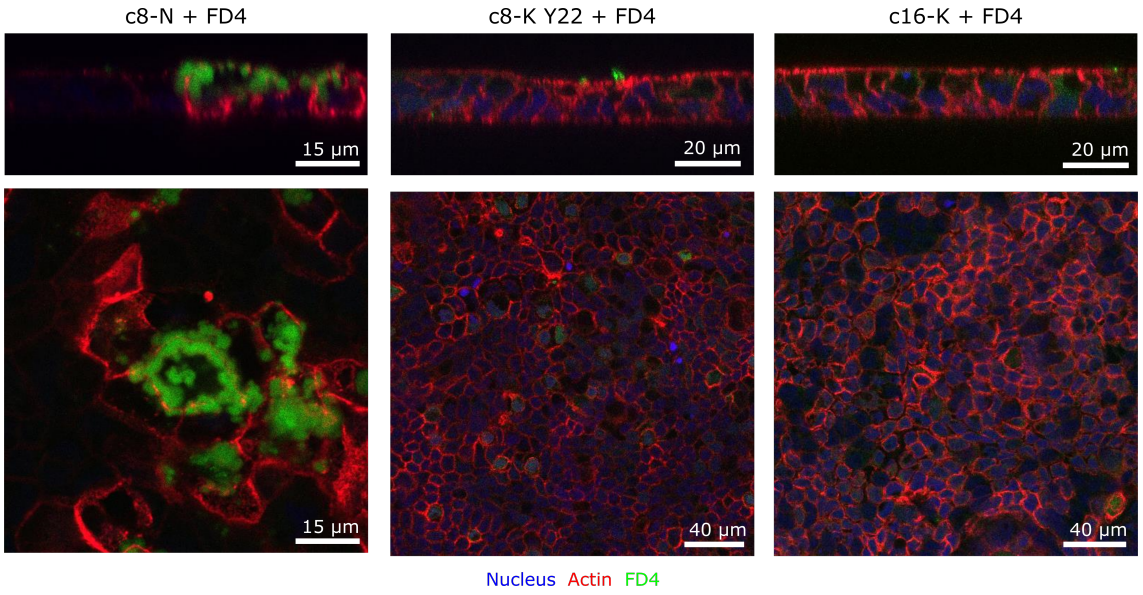

Figure 4.8: Caco-2 cell interaction of FD4 and sCT analogues. Microscopy images of caco-2 cell monolayers following permeability experiments with FD4 and selected sCT analogues, in side-view (top) or cross-section (bottom). Cells are fixed and stained for nucleus (blue) and filamentous actin (red), and FD4 fluorescence is depicted in green.

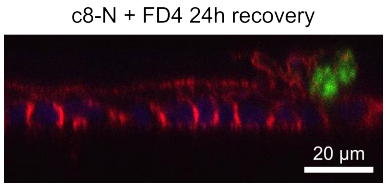

Figure 4.9: Prolonged effects of c8-N and FD4. Microscopy image (side-view) of a caco-2 cell monolayer exposed to FD4 and c8-N, after 24h recovery in medium. Cells are fixed and stained for nucleus (blue) and filamentous actin (red), and FD4 fluorescence is depicted in green.

of the investigated analogues cell layers were identical to controls, with no FD4 present (not attempted with peptide-staining). However, for c8-N an interesting feature is shown in fig. 4.9. The cell layer appeared normal and devoid of FD4, but many small lumps of cell debris and FD4 were 'clinging' to the apical side of the cell layer, again indicating a specific c8-N/FD4 association not observed for the other analogues.

Live-cell imaging (See description of experimental setup in section 4.3.4.)

Immunocytochemistry imaging is somewhat limited by its 'snapshot' character, yielding little dynamic information, and besides being time consuming it features numerous washing steps with a risk of losing cell-bound peptides or fluorophores. Therefore we attempted live-cell imaging for the two most 'cell-active' analogues, c8-N and c16-K, which previously has yielded interesting results for absorption enhancers (see e.g. fig. B.2 in appendix B).

Fig. 4.10 shows caco-2 cell monolayers after 15 minute exposure to FD4 (control) or together with c16-K. In the control, no FD4 enters the cell layer for (at least) 1h, whereas inclusion of c16-K causes a rapid decrease in cell barrier integrity.

After 15 minutes, FD4 appears visible both inside some cells and between the nuclei of adjacent cells which could indicate both paracellular and transcellular translocation. However, due to the

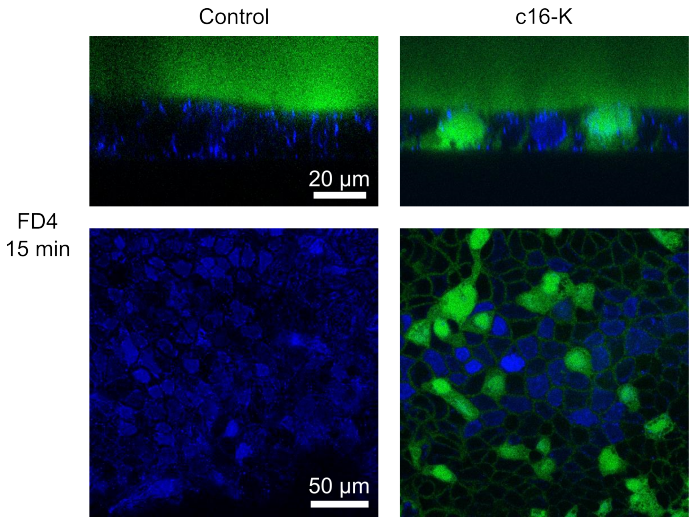

Figure 4.10: Live-cell imaging with FD4 ±c16-K. Microscopy images of caco-2 cell monolayers following exposure to FD4 and c16-K, in side-view (top) or cross-section (bottom). Cells are stained for nucleus (blue) and FD4 fluorescence is depicted in green.

lack of actin staining, the cell boundaries are not easily distinguishable. Interestingly, FD4 also appears to enter some cell nuclei, which is not widely observed in fixed cells. It should be noted that the cell monolayer may grow slightly differently on glass slides compared to Transwell filters, and when adding peptides and fluorophores apically they cannot 'escape' into the BL chamber and may accumulate to a higher degree in the cell layer.

Furthermore, the staining procedure is different, and it is worth noting that the nuclear stain appear quite different from previous immunocytochemistry images, which is due to differences in the two stains. The ToPro-3 stain for fixed cells (cell-impermeant, requires permeabilization before staining) binds dsDNA, thus has a high selectively for nuclear over cytoplasmic staining, whereas the live-cell stain SYTO 61 (cell-permeant) stains all nucleic acids.

Experiments with the small fluorophore carboxyfluorescein yield similar results for control and c16-K, possibly with more accumulation in cells and nuclei for c16-K.

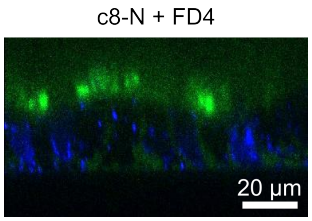

Figure 4.11: Live-cell imaging with FD4 and c8-N. Microscopy image of a caco-2 cell monolayer following exposure to FD4 and c8-N, in side-view. Cells are stained for nucleus (blue) and FD4 fluorescence is depicted in green.

Fig. 4.11 shows a caco-2 cell monolayer exposed to FD4 and c8-N, and although not the most clear image, FD4 appears to attach to the apical (top) part of the cell layer and is only weakly visible in the cell cytosol / at the cell junctions. The apical association appears reminiscent of c8-N- and FD4-behavior in figs. 4.6 and 4.8.

4.3.3 Preliminary conclusions on enhancing effects

As mentioned in section 4.3.1 and shown in fig. 4.3, the caco-2 permeability of different analogues families does not appear entirely systematic, and may involve very specific features for each analogue. If we look at the three most permeable analogues, c8-N, c8-K Y22 and c16-K, the cell-interaction and enhancing effects are profoundly different.

c16-K displays high membrane binding (consistent with its chain length) and very high uptake, and it facilitates very high permeability of mannitol and FD4 (the highest of all analogues). However, c16-K does not cause FD4 binding to cells, indicating a non-specific enhancing effect (i.e. c16-K 'opens the door' but does not interact with FD4). In liposome permeabilization studies c16-K has the greatest effect on liposomes, possibly destroying them altogether, which is consistent with a strong membrane binding and fluidizing effect, allowing translocation of other compounds. Microscopy results for c16-K indicate a mix of transcellular and paracellular translocation, both for the peptide itself and FD4. Although mannitol and FD4 permeability is often used as an indicator for paracellular translocation, this distinction is not entirely clear and several permeability enhancers may involve a mix of both pathways [11, 76]. Extensive membrane permeabilization as observed for c16-K will likely also open paracellular junctions, e.g. through dislodging membrane-bound junction proteins or actin reorganization.

c8-N displays high membrane binding (higher than expected for its chain length) and low cell uptake, and it facilitates high permeability of mannitol and FD4. Uniquely for this analogue, c8-N also increases membrane binding of FD4, as clearly evident from both measured values and microscopy images. Both the peptide and FD4 appear to adhere to the apical side of the cell layer in big clusters, possibly on both sides of the cell membrane. However, this complex behavior is not easily translated to a translocation mechanism. The membrane-permeabilization observed in liposomes indicate a transcellular component, although not as pronounced as for c16-K. The stability of peptide and FD4 clusters on the outside of cells through repeated washing steps (before fixing cells) and 24h recovery in medium, indicates either very slow dissociation kinetics or irreversible assemblies. One may speculate if the fibrillation tendencies of c8-N has a role to play in this behavior.

c8-K Y22 displays the highest caco-2 permeability, but very limited cell membrane binding and uptake. Furthermore, it leaves mannitol/FD4 permeability almost unaffected, and causes limited TEER decrease and liposome permeabilization (similar to c8-K). This indicates a quite peptide-specific translocation enhancement which is unabated by cell binding and/or peptide aggregation. The 'selfish' enhancement characteristics may be quite advantageous in a crowded gut environment.

4.3.4 Experimental details for additional methods

Caco-2 permeability studies with FD4 were carried out similar to peptide experiments, using 540 μM FD4. Samples were analyzed for FD4 content in a fluorescence plate reader (MD Spectramax Gemini) with Ex/Em 490/525 nm, based on standard curves prepared from test solutions.

Immunocytochemistry The cell layer was fixed in formaldehyde and stained for nucleus, actin and sCT analogues.

After transport experiments, filter inserts were washed twice with PBS buffer for 5 minutes, and the cells were fixed with 4 % formalin in PBS buffer for 10 minutes (1 mL basolateral and 0.5 mL apical). The filters were washed twice with PBS buffer, cut from the filter inserts and placed in a 48-well plate with 0.3 mL block buffer pr. well (PBS w. 3 % Goat serum, 1 % BSA and 0.05 % Tween20).

The filters were protected from light and incubated sequentially with 0.3 mL of the relevant antibody or stain (primary monoclonal mouse anti-sCT antibody overnight at 4 °C (2 μg/mL in block buffer); secondary goat anti-mouse antibody labeled with Alexa Flour 488 for 60 minutes (10 μg/mL in block buffer); Texas Red-X phalloidin for 30 minutes (66 nM in PBS w. 1 % (w/v) BSA); ToPro-3 for 5 minutes (200 nM in PBS buffer) or block buffer for negative controls), separated

by washing with PBS buffer (twice with 0.5 mL for 5 minutes). The filters were mounted on microscope slides (objective glass) with the cell layer facing up and covered by a cover slide, using fast drying fluorescence mounting medium (Dako). The cell layers were visualized in a confocal fluorescence microscope (CLSM, Leica SP5), using a fluid immersion objective (water: 63x magnification or oil: 100x magnification).

Live-cell imaging Caco-2 cells were seeded on 8-well chambered cover slips (Ibidi) at a density of $6.25 \cdot 10^3$ cells/well (250 μL of $2.5 \cdot 10^4$ cells/mL) and grown for 14 days in DMEM with media change every second day (every day in the last few days). The cell morphology was verified before experiments by staining the nucleus with SYTO 61 (Molecular Probes, ThermoFisher) (500 nM in HBBS buffer for 60 minutes), adding a water-soluble fluorophore (Carboxyfluorescein or FD4) above the cell layer, and visualizing the cells by CLSM. For fluorophore permeation experiments, a fluorophore/peptide mixture was added (50 μL fluorophore + 150 μL fluorophore/peptide, final concentrations 540 μM and 100 μM), and the cell layer was visualized over time. The microscope stage is encased in a box with 5 % CO_2 and 37 °C to allow prolonged live-cell imaging, and laser power was limited to avoid cell damage.

Chapter 5

Microfluidic Caco-2 setup (collaboration)

Hsih-Yin Tan, who is currently a Post.Doc at DTU Nanotech, developed a microfluidic setup for growth and permeability studies of caco-2 cells in her PhD project, and in the final phase I aided in evaluating the setup for permeability studies compared to the standard Transwell setup. We tested the permeability of mannitol and FD4 (as otherwise described in this thesis) and human insulin (similar to GLP-2 and sCT studies), alone or with addition of the permeability enhancer Tetradecyl maltoside (TDM). We showed comparable permeability values in the two setups, with increased permeability of all three compounds upon TDM addition, although the microfluidic setup displayed a large variability within the 8 chambers on each chip. The results are described in the paper draft in appendix C, along with the development of the microfluidic device and characterization of cells layers.

Chapter 6

Conclusions and future perspectives

6.1 Conclusions

Partial conclusions were presented at the end of papers 1, 2 and 3 (draft), and at the end of chapter 4. However, for completeness' sake, the following sections will briefly summarize the main conclusions of this thesis.

6.1.1 GLP-2

For GLP-2, we found that increasing acyl chain length caused increased self-association and binding to lipid and cell membranes, whereas translocation across intestinal cells displayed a non-linear dependence on chain length. Short and medium chains improved translocation compared to the native peptide, whereas long chain acylation displayed no improvement in translocation. This indicates an initial translocation benefit for shorter chains through increased interaction with the cell membrane, which reverts to a hindrance for long chains, i.e. the analogues get stuck in the cell membrane. This interpretation is supported by the effects of co-administered para- and transcellular enhancers, which increased translocation irrespective of acyl chain length for the former, whereas the latter displayed increased synergy with the long chain acylation, however, with the c12-acylation remaining optimal.

The results demonstrate that rational acylation of GLP-2 can increase its intestinal absorption, alone or in combination with permeation enhancers, and are consistent with the initial project hypothesis. We speculate that the absolute quantification of liposome binding (partitioning coefficient 1300 M^{-1} for c12-GLP-2) may be used to predict the optimal acylation chain length for other acylation types or peptides.

6.1.2 sCT

For sCT, we discovered an unpredicted effect of acylation which largely superseded the anticipated membrane interactions; i.e. acylated sCT acted as its own *in vitro* intestinal permeation enhancer. Acylation drastically increased peptide permeability, through reversible cell effect similar to transcellular permeation enhancers, supported by the observed permeabilization of model lipid membranes. The effect likely stems from a synergy between the positive peptide charge and membrane-active acyl moiety, supported by its pH-dependency, whereby the effect increased with decreasing pH and concomitant charge increase. The extent of permeation enhancing effect was highly dependent on acylation chain length and position, with highest peptide permeability for short chain N-terminal acylation or medium/long chain Lys18 acylation. Permeability and cell membrane binding did not immediately appear correlated for the N-terminal analogues, whereas increasing membrane binding with increasing chain length for Lys18 analogues may have hindered translocation slightly for the longest chain (and we speculate that further prolonging the

chain may prove problematic).

The experiments were complicated by another unforeseen effect of sCT acylation, i.e. decreased solution stability. Prolonged heating and/or solution storage of certain acylated sCT analogues caused aggregation in physiological buffer solutions, potentially forming fibril-like structures. Lys18 acylation appeared superior to N-terminal acylation, most clearly exemplified by the short chain c8-analogues, however, no systematic dependence on acylation chain length was apparent. For all analogues, self-association was efficiently inhibited by addition of DM-β-CD, however, the separate permeability enhancing effects of acylated analogues and DM-β-CD were reduced in the mixtures, and the additive was not investigated further. Thus, acylation of sCT for oral delivery purposes may not be indiscriminately applicable, and requires rational choices of acylation details and/or additives.

The surprisingly profound impact of the Trp backbone mutation motivated a new family of Lys18 sCT analogues with the native backbone, however, only the short chain analogue was superior regarding receptor potency, solution stability and cell permeation.

The most cell-permeable analogues were investigated further, which unveiled quite distinct permeation enhancer effects. c16-K exhibited high membrane binding and permeabilization, and non-specific enhancing effect on model compounds, likely through a mix of para- and transcellular pathways. c8-N exhibited high membrane binding, apparently through a clustering at the outer cell membrane, and uniquely it could anchor the model compound FD4 quite stably, although also facilitating efficient translocation of FD4. c8-K Y22 exhibited the highest peptide permeability with very limited membrane binding, and in fact showed very limited unspecific permeation enhancer effects, i.e. c8-K Y22 translocated quite efficiently and selectively.

6.1.3 Overall

The enhancer-effects observed for sCT analogues was a game-changer, which altered the scope considerably, and the initial aim of using two model peptides to distinguish subtle effects of the backbone and the acyl chains, became somewhat complicated. Whereas membrane-binding appeared to affect acylated GLP-2 cell permeability as hypothesized, the effects for sCT were not merely controlled by membrane-binding, although it may remain important for the enhancer effect. For K18 sCT analogues, the very pronounced membrane binding and cell uptake for the long chain acylation may in fact hinder translocation.

The liposome partitioning coefficient, which may be a useful metric for predicting *in vitro* permeability of acylated analogues, could not be determined for sCT analogues due to experimental difficulties, but the membrane permeabilizing effect would likely have complicated measurements (although the peptide concentration is far lower in partitioning studies than in cell studies).

As a brief note, the peptide receptor potency following acylation was quite different for the two peptides, with GLP-2 analogues retaining their potency, whereas sCT analogues displayed markedly reduced potency, depending on acylation position and length.

Lessons learned For GLP-2, the study setup worked quite well, but for sCT the number of analogues got a little out of hand, and in the end we did not entirely understand the differences. Thus, one lesson is that modifications should be more well-founded, with fewer analogues at a time, i.e. an even more circular setup.

6.2 Future perspectives

The interesting results obtained prompt a multitude of questions, and many future studies can be envisioned.

The enzyme stability and albumin binding of acylated analogues would be interesting to investigate, as both are expected to increase compared to the native peptides.

The mechanism of membrane insertion for both peptide groups would be very interesting to investigate further, e.g. through differential scanning calorimetry (DSC), circular dichroism

or other structural techniques, although the membrane permeabilizing effect for sCT analogues could cause problems. Molecular dynamics simulations might also provide additional insight into the interaction between peptides and membranes, but would have to be correlated to experimental results, e.g. partitioning coefficients for GLP-2 analogues.

The employed POPC liposomes are a very simple model system, and could be optimized to better mimic the cell membranes by addition of negatively charged lipids or cholesterol. Furthermore, the calcein-release study might be adjusted to employ FD4, in order to better model the cell membrane permeability studies.

For *in vitro* studies, numerous studies could provide interesting insight, e.g. the effect of mucus on the cell membrane binding and permeability, which may be different for the two oppositely charged peptides and their analogues. The translocation in both directions across the cell layer (AP->BL or BL->AP) should be similar for passive permeation, as expected for the studied compounds. Including FaSSIF/FeSSIF buffer could be interesting to study the effects of bile salts and lipids, that would likely interfere with the membrane binding of acylated analogues.

It would be interesting to study a few of the analogues (primarily sCT analogues) *ex vivo* in Ussing chambers, to investigate whether the effects persist in permeation across tissue. Furthermore, an *in vivo* investigation of the pharmacokinetics and therapeutic effect of native sCT compared to one or two of the most potent analogues would be highly valuable to validate the results obtained in these model systems.

Lastly, several new acylated analogues could provide interesting results, e.g. more medium-chain analogues with smaller increments in chain length. For GLP-2, c12-acylation was superior to c8- and c16-acylation, and thus c9-, c10-, c11-, c13-, c14-, and c15-acylation might improve permeability further. Similarly for sCT, smaller chain length variations 'in the vicinity' of the most potent analogues would be interesting (e.g. c13-, c14-, c15-, and c17-acylations for K18 W22-analogues, c7-, c9-, c10-acylations for N-terminal and K18 Y22-analogues). Furthermore, the reduced receptor potency of sCT analogues prompts an investigation into a more optimal acylation position, with the most ambitious version being a full scan of acylations at all backbone positions.

Bibliography

[1] T A S Aguirre et al. "Current status of selected oral peptide technologies in advanced preclinical development and in clinical trials." In: *Adv. Drug Delivery Rev.* (Feb. 2016). ISSN: 1872-8294. DOI: 10.1016/j.addr.2016.02.004.

[2] Tanira A S Aguirre et al. "In vitro and in vivo preclinical evaluation of a minisphere emulsion-based formulation (SmPillő) of salmon calcitonin." In: *Eur. J. Pharm. Sci.* 79 (Nov. 2015), pp. 102–11. ISSN: 1879-0720. DOI: 10.1016/j.ejps.2015.09.001.

[3] Fernando Albericio and Hendrik G Kruger. "Therapeutic peptides." In: *Future Med. Chem.* 4.12 (Aug. 2012), pp. 1527–31. ISSN: 1756-8927. DOI: 10.4155/fmc.12.94.

[4] Damian G Allis, Timothy J Fairchild, and Robert P Doyle. "The binding of vitamin B12 to transcobalamin(II); structural considerations for bioconjugate design–a molecular dynamics study." In: *Mol Biosyst* 6.9 (Sept. 2010), pp. 1611–8. ISSN: 1742-2051. DOI: 10.1039/c003476b.

[5] EK Anderberg, T Lindmark, and P Artursson. "Sodium caprate elicits dilatations in human intestinal tight junctions and enhances drug absorption by the paracellular route". In: *Pharm. Res.* 10 (1993), pp. 857–864.

[6] Giuseppina Andreotti et al. "Structural determinants of salmon calcitonin bioactivity: the role of the Leu-based amphipathic alpha-helix." In: *J. Biol. Chem.* 281.34 (Aug. 2006), pp. 24193–203. ISSN: 0021-9258. DOI: 10.1074/jbc.M603528200.

[7] Francisca Araújo and Bruno Sarmento. "Towards the characterization of an in vitro triple co-culture intestine cell model for permeability studies." In: *Int. J. Pharm.* 458.1 (Dec. 2013), pp. 128–34. ISSN: 1873-3476. DOI: 10.1016/j.ijpharm.2013.10.003.

[8] Michel Arnold and Moise Azria. "Oral calcitonin compositions and applications thereof". 20150283212. Oct. 2015.

[9] Per Artursson, Katrin Palm, and Kristina Luthman. "Caco-2 monolayers in experimental and theoretical predictions of drug transport." In: *Adv. Drug Delivery Rev.* 46.1-3 (Sept. 2001), pp. 27–43. ISSN: 1872-8294. DOI: 10.1016/j.addr.2012.09.005.

[10] T Arvinte, A Cudd, and A F Drake. "The structure and mechanism of formation of human calcitonin fibrils." In: *J. Biol. Chem.* 268.9 (Mar. 1993), pp. 6415–22. ISSN: 0021-9258.

[11] BJ Aungst. "Intestinal permeation enhancers". In: *J. Pharm. Sci.* 89.4 (2000).

[12] Dorit Avrahami and Yechiel Shai. "Conjugation of a magainin analogue with lipophilic acids controls hydrophobicity, solution assembly, and cell selectivity." In: *Biochemistry* 41.7 (Feb. 2002), pp. 2254–63. ISSN: 0006-2960.

[13] K Balon, BU Riebesehl, and BW Müller. "Drug liposome partitioning as a tool for the prediction of human passive intestinal absorption". In: *Pharm. Res.* 16.6 (1999), pp. 882–888.

[14] Leonardo Bandeira, E Michael Lewiecki, and John P Bilezikian. "Pharmacodynamics and pharmacokinetics of oral salmon calcitonin in the treatment of osteoporosis." en. In: *Expert Opin Drug Metab Toxicol* (Apr. 2016), pp. 1–9. ISSN: 1744-7607. DOI: 10.1080/17425255.2016.1175436.

[15] A Bernkop-Schnürch. "Low Molecular Mass Permeation Enhancers in Oral Delivery of Macromolecular Drugs". In: *Oral Delivery of Macromolecular Drugs*. 2009. ISBN: 9781441902009. DOI: 10.1007/978-1-4419-0200-9.

[16] Neil Binkley et al. "A phase 3 trial of the efficacy and safety of oral recombinant calcitonin: the Oral Calcitonin in Postmenopausal Osteoporosis (ORACAL) trial." In: *J. Bone Miner. Res.* 27.8 (Aug. 2012), pp. 1821–9. ISSN: 1523-4681. DOI: 10.1002/jbmr.1602.

[17] Gerrit Borchard. "The Absorption Barrier". In: *Oral Delivery of Macromolecular Drugs*. Ed. by Andreas Bernkop-Schnürch. New York: Springer US, 2009, pp. 49–64. ISBN: 9781441902009. DOI: 10.1007/978-1-4419-0200-9.

[18] David J Brayden, John Gleeson, and Edwin G Walsh. "A head-to-head multi-parametric high content analysis of a series of medium chain fatty acid intestinal permeation enhancers in Caco-2 cells." In: *Eur. J. Pharm. Biopharm.* 88.3 (Nov. 2014), pp. 830–39. ISSN: 1873-3441. DOI: 10.1016/j.ejpb.2014.10.008.

[19] Stephen T. Buckley, František Hubálek, and Ulrik Lytt Rahbek. "Chemically Modified Peptides and Proteins - Critical Considerations for Oral Delivery". en. In: *Tissue Barriers* (Mar. 2016), pp. 00–00. ISSN: 2168-8370. DOI: 10.1080/21688370.2016.1156805.

[20] Weiqiang Cheng and LY Lim. "Comparison of reversible and nonreversible aqueous-soluble lipidized conjugates of salmon calcitonin". In: *Mol. pharm.* 88.5 (2008).

[21] Weiqiang Cheng, Seetharama Satyanarayanajois, and Lee-Yong Lim. "Aqueous-soluble, non-reversible lipid conjugate of salmon calcitonin: synthesis, characterization and in vivo activity." In: *Pharm. Res.* 24.1 (Jan. 2007), pp. 99–110. ISSN: 0724-8741. DOI: 10.1007/s11095-006-9128-9.

[22] D. H. Copp et al. "Evidence for Calcitonin–A New Hormone from the Parathyroid That Lowers Blood Calcium". In: *Endocrinology* 70.5 (May 1962), pp. 638–649. ISSN: 0013-7227. DOI: 10.1210/endo-70-5-638.

[23] A Cudd et al. "Enhanced potency of human calcitonin when fibrillation is avoided". In: *J. Pharm. Sci.* 84.6 (1995), pp. 717–719. DOI: 10.1002/jps.2600840610.

[24] Alan W. Cuthbert and Harry S. Margolius. "Kinins stimulate net chloride secretion by the rat colon". In: *Br. J. Pharmacol.* 75.4 (1982), pp. 587–598. ISSN: 1476-5381. DOI: 10.1111/j.1476-5381.1982.tb09178.x.

[25] M P DaCambra et al. "Structural determinants for activity of glucagon-like peptide-2." In: *Biochemistry* 39.30 (Aug. 2000), pp. 8888–94. ISSN: 0006-2960.

[26] Piyali Dasgupta, Anu Singh, and Rama Mukherjee. "N-terminal acylation of somatostatin analog with long chain fatty acids enhances its stability and anti-proliferative activity in human breast adenocarcinoma cells." In: *Biol. Pharm. Bull.* 25.1 (Jan. 2002), pp. 29–36. ISSN: 0918-6158.

[27] Marco Diociaiuti et al. "Calcitonin forms oligomeric pore-like structures in lipid membranes." In: *Biophys. J.* 91.6 (Sept. 2006), pp. 2275–81. ISSN: 0006-3495. DOI: 10.1529/biophysj.105.079475.

[28] Daniel J Drucker. "Glucagon-like Peptide 2". In: *Trends in Endocrinology & Metabolism* 10.4 (May 1999), pp. 153–156. ISSN: 10432760. DOI: 10.1016/S1043-2760(98)00136-2.

[29] Alice W. Du and Martina H. Stenzel. "Drug Carriers for the Delivery of Therapeutic Peptides". In: *Biomacromolecules* 15.4 (Apr. 2014), pp. 1097–1114. ISSN: 1525-7797. DOI: 10.1021/bm500169p.

[30] Thomas Etzerodt et al. "Selective acylation enhances membrane charge sensitivity of the antimicrobial peptide mastoparan-x." In: *Biophys. J.* 100.2 (Jan. 2011), pp. 399–409. ISSN: 1542-0086. DOI: 10.1016/j.bpj.2010.11.040.

[31] Keld Fosgerau and Torsten Hoffmann. "Peptide therapeutics: Current status and future directions". In: *Drug Discovery Today* 20.1 (Oct. 2014), pp. 122–128. ISSN: 13596446. DOI: 10.1016/j.drudis.2014.10.003.

[32] Mélanie Gagnon et al. "Comparison of the Caco-2, HT-29 and the mucus-secreting HT29-MTX intestinal cell models to investigate Salmonella adhesion and invasion." In: *J Microbiol Methods* 94.3 (Sept. 2013), pp. 274–9. ISSN: 1872-8359. DOI: 10.1016/j.mimet.2013.06.027.

[33] S Gangwar, GM Pauletti, and B Wang. "Prodrug strategies to enhance the intestinal absorption of peptides". In: *Drug discovery today* 2.4 (1997), pp. 148–155.

[34] D. Goodwin, P. Simerska, and I. Toth. "Peptides As Therapeutics with Enhanced Bioactivity". In: *Current Medicinal Chemistry* 19.26 (Sept. 2012), pp. 4451–4461. ISSN: 09298673. DOI: 10.2174/092986712803251548.

[35] I Gozes et al. "Neuroprotective strategy for Alzheimer disease: intranasal administration of a fatty neuropeptide." In: *Proc. Natl. Acad. Sci. U. S. A.* 93.1 (Jan. 1996), pp. 427–32. ISSN: 0027-8424.

[36] Vivek Gupta et al. "Mucoadhesive intestinal devices for oral delivery of salmon calcitonin." In: *J. Control. Release.* 172.3 (Dec. 2013), pp. 753–62. ISSN: 1873-4995. DOI: 10.1016/j.jconrel.2013.09.004.

[37] Ivan Guryanov et al. "Innovative chemical synthesis and conformational hints on the lipopeptide liraglutide". In: *J. Pept. Sci.* (2016). ISSN: 10752617. DOI: 10.1002/psc.2890.

[38] B Hartmann et al. "Structure, measurement, and secretion of human glucagon-like peptide-2." In: *Peptides* 21.1 (Jan. 2000), pp. 73–80. ISSN: 0196-9781.

[39] Svend Havelund et al. "The mechanism of protraction of insulin detemir, a long-acting, acylated analog of human insulin." In: *Pharm. Res.* 21.8 (Aug. 2004), pp. 1498–504. ISSN: 0724-8741.

[40] Rose Hayeshi et al. "Comparison of drug transporter gene expression and functionality in Caco-2 cells from 10 different laboratories." In: *European journal of pharmaceutical sciences : official journal of the European Federation for Pharmaceutical Sciences* 35.5 (Dec. 2008), pp. 383–96. ISSN: 0928-0987. DOI: 10.1016/j.ejps.2008.08.004.

[41] J R Henriksen and T L Andresen. "Thermodynamic profiling of peptide membrane interactions by isothermal titration calorimetry: a search for pores and micelles." In: *Biophys. J.* 101.1 (July 2011), pp. 100–9. ISSN: 1542-0086. DOI: 10.1016/j.bpj.2011.05.047.

[42] Ina Hubatsch, Eva G E Ragnarsson, and Per Artursson. "Determination of drug permeability and prediction of drug absorption in Caco-2 monolayers." In: *Nature protocols* 2.9 (Jan. 2007), pp. 2111–9. ISSN: 1750-2799. DOI: 10.1038/nprot.2007.303.

[43] Tetsumi Irie and Kaneto Uekama. "Cyclodextrins in peptide and protein delivery". In: *Adv. Drug Delivery Rev.* 36 (1999), pp. 101–123.

[44] Palle Bekker Jeppesen. "Teduglutide, a novel glucagon-like peptide 2 analog, in the treatment of patients with short bowel syndrome." In: *Therap Adv Gastroenterol* 5.3 (May 2012), pp. 159–71. ISSN: 1756-2848. DOI: 10.1177/1756283X11436318.

[45] Ib Jonassen et al. "Design of the novel protraction mechanism of insulin degludec, an ultra-long-acting basal insulin." In: *Pharm. Res.* 29.8 (Aug. 2012), pp. 2104–14. ISSN: 1573-904X. DOI: 10.1007/s11095-012-0739-z.

[46] M A Karsdal et al. "Lessons learned from the development of oral calcitonin: the first tablet formulation of a protein in phase III clinical trials." In: *J. Clin. Pharmacol.* 51.4 (Apr. 2011), pp. 460–71. ISSN: 1552-4604. DOI: 10.1177/0091270010372625.

[47] M A Karsdal et al. "Treatment of symptomatic knee osteoarthritis with oral salmon calcitonin: results from two phase 3 trials." English. In: *Osteoarthr. Cartil.* 23.4 (Apr. 2015), pp. 532–43. ISSN: 1522-9653. DOI: 10.1016/j.joca.2014.12.019.

[48] Morten Asser Karsdal et al. "Lessons learned from the clinical development of oral peptides." In: *Br. J. Clin. Pharmacol.* 79.5 (May 2015), pp. 720–32. ISSN: 1365-2125. DOI: 10.1111/bcp.12557.

[49] Hyun Jung Kim and Donald E Ingber. "Gut-on-a-Chip microenvironment induces human intestinal cells to undergo villus differentiation." In: *Integr Biol* 5.9 (2013), pp. 1130–40.

[50] Sandra Klein. "The use of biorelevant dissolution media to forecast the in vivo performance of a drug." In: *AAPS J* 12.3 (Sept. 2010), pp. 397–406. ISSN: 1550-7416. DOI: 10.1208/s12248-010-9203-3.

[51] L B Knudsen et al. "Potent derivatives of glucagon-like peptide-1 with pharmacokinetic properties suitable for once daily administration." In: *J. Med. Chem.* 43.9 (May 2000), pp. 1664–9. ISSN: 0022-2623.

[52] SD Krämer. "Absorption prediction from physicochemical parameters." In: *Pharm. Sci. Technol. To.* 2.9 (Sept. 1999), pp. 373–380. ISSN: 1461-5347.

[53] Kasper Kristensen, Jonas R Henriksen, and Thomas L Andresen. "Adsorption of cationic peptides to solid surfaces of glass and plastic." In: *PloS ONE* 10.5 (Jan. 2015), e0122419. ISSN: 1932-6203. DOI: 10.1371/journal.pone.0122419.

[54] Peter Kurtzhals et al. "Albumin binding of insulins acylated". In: *Biochem. J.* 312 (1995), pp. 725–731.

[55] Jack Kyte and Russell F. Doolittle. "A simple method for displaying the hydropathic character of a protein". In: *J Mol Biol* 157.1 (May 1982), pp. 105–132. ISSN: 00222836. DOI: 10.1016/0022-2836(82)90515-0.

[56] a S Ladokhin, S Jayasinghe, and S H White. "How to measure and analyze tryptophan fluorescence in membranes properly, and why bother?" In: *Anal. Biochem.* 285.2 (Oct. 2000), pp. 235–45. ISSN: 0003-2697. DOI: 10.1006/abio.2000.4773.

[57] Alexey S. Ladokhin, Michael E. Selsted, and Stephen H. White. "Bilayer Interactions of Indolicidin, a Small Antimicrobial Peptide Rich in Tryptophan, Proline, and Basic Amino Acids". In: *Biophys. J.* 72.2 (Feb. 1997), pp. 794–805. ISSN: 00063495. DOI: 10.1016/S0006-3495(97)78713-7.

[58] Jesper Lau et al. "Discovery of the Once-Weekly Glucagon-Like Peptide-1 (GLP-1) Analogue Semaglutide." In: *J Med Chem* 58.18 (Sept. 2015), pp. 7370–80. ISSN: 1520-4804. DOI: 10.1021/acs.jmedchem.5b00726.

[59] Kjeld Madsen et al. "Structure-activity and protraction relationship of long-acting glucagon-like peptide-1 derivatives: importance of fatty acid length, polarity, and bulkiness." In: *J. Med. Chem.* 50.24 (Nov. 2007), pp. 6126–32. ISSN: 0022-2623. DOI: 10.1021/jm070861j.

[60] Sam Maher et al. "Safety and efficacy of sodium caprate in promoting oral drug absorption: from in vitro to the clinic." In: *Adv. Drug Delivery Rev.* 61.15 (Dec. 2009), pp. 1427–49. ISSN: 1872-8294. DOI: 10.1016/j.addr.2009.09.006.

[61] Gretchen J Mahler, Michael L Shuler, and Raymond P Glahn. "Characterization of Caco-2 and HT29-MTX cocultures in an in vitro digestion/cell culture model used to predict iron bioavailability." In: *J. Nutr. Biochem.* 20.7 (July 2009), pp. 494–502. ISSN: 1873-4847. DOI: 10.1016/j.jnutbio.2008.05.006.

[62] Abdallah Makhlof et al. "Nanoparticles of glycol chitosan and its thiolated derivative significantly improved the pulmonary delivery of calcitonin." In: *Int. J. Pharm.* 397.1-2 (Sept. 2010), pp. 92–5. ISSN: 1873-3476. DOI: 10.1016/j.ijpharm.2010.07.001.

[63] Dmitry Malkov et al. "Oral delivery of insulin with the eligen technology: mechanistic studies." In: *Curr. drug delivery* 2.2 (Apr. 2005), pp. 191–7. ISSN: 1567-2018.

[64] Fiona McCartney, John P. Gleeson, and David J. Brayden. "Safety concerns over the use of intestinal permeation enhancers: A mini-review". en. In: *Tissue Barriers* (Apr. 2016), pp. 00–00. ISSN: 2168-8370. DOI: 10.1080/21688370.2016.1176822.

[65] Daniela Meleleo et al. "Acetyl-[Asn30,Tyr32]-calcitonin fragment 8-32 forms channels in phospholipid planar lipid membranes." In: *European biophysics journal : EBJ* 36.7 (Sept. 2007), pp. 763–70. ISSN: 0175-7571. DOI: 10.1007/s00249-007-0150-6.

[66] Fwu-Long Mi et al. "Oral delivery of peptide drugs using nanoparticles self-assembled by poly(gamma-glutamic acid) and a chitosan derivative functionalized by trimethylation." In: *Bioconjugate Chem.* 19.6 (June 2008), pp. 1248–55. ISSN: 1520-4812. DOI: 10.1021/bc800076n.

[67] Silvia Micelli et al. "Effect of nanomolar concentrations of sodium dodecyl sulfate, a catalytic inductor of alpha-helices, on human calcitonin incorporation and channel formation in planar lipid membranes." In: *Biophysical journal* 87.2 (Aug. 2004), pp. 1065–75. ISSN: 0006-3495. DOI: 10.1529/biophysj.103.037200.

[68] S Micelli et al. "Effect of pH-variation on insertion and ion channel formation of human calcitonin into planar lipid bilayers". In: *Front Biosci* 8 (2006), pp. 2035–2044.

[69] Mariko Morishita and Nicholas A Peppas. "Is the oral route possible for peptide and protein drug delivery?" In: *Drug discov today* 11.19-20 (Oct. 2006), pp. 905–10. ISSN: 1359-6446. DOI: 10.1016/j.drudis.2006.08.005.

[70] Elena Moroz, Simon Matoori, and Jean-Christophe Leroux. "Oral delivery of macromolecular drugs: Where we are after almost 100years of attempts." In: *Adv. Drug Delivery Rev.* (Jan. 2016). ISSN: 1872-8294. DOI: 10.1016/j.addr.2016.01.010.

[71] Nazanin Navabi, Michael A McGuckin, and Sara K Lindén. "Gastrointestinal cell lines form polarized epithelia with an adherent mucus layer when cultured in semi-wet interfaces with mechanical stimulation." In: *PLOS ONE* 8.7 (Jan. 2013), e68761. ISSN: 1932-6203. DOI: 10.1371/journal.pone.0068761.

[72] Line Hagner Nielsen et al. "Polymeric microcontainers improve oral bioavailability of furosemide." In: *Int. J. Pharm.* 504.1-2 (Mar. 2016), pp. 98–109. ISSN: 1873-3476. DOI: 10.1016/j.ijpharm.2016.03.050.

[73] C Orskov et al. "Glucagon-Like Peptides GLP-1 and GLP-2, Predicted Products of the Glucagon Gene, Are Secreted Separately from Pig Small Intestine but Not Pancreas". In: *Endocrinology* 119.4 (Oct. 1986), pp. 1467–1475. ISSN: 0013-7227. DOI: 10.1210/endo-119-4-1467.

[74] J Perez-Vilar. "Gastrointestinal mucus gel barrier". In: *Oral Delivery of Macromolecular Drugs*. 2009, pp. 21–48. ISBN: 9781441902009. DOI: 10.1007/978-1-4419-0200-9.

[75] Daniel Persson et al. "Application of a novel analysis to measure the binding of the membrane-translocating peptide penetratin to negatively charged liposomes". In: *Biochemistry* 42 (2003), pp. 421–429. ISSN: 00062960. DOI: 10.1021/bi026453t.

[76] Signe Beck Petersen et al. "Evaluation of alkylmaltosides as intestinal permeation enhancers: Comparison between rat intestinal mucosal sheets and Caco-2 monolayers". In: *European Journal of Pharmaceutical Sciences* 47.4 (2012), pp. 701–712. ISSN: 09280987. DOI: 10.1016/j.ejps.2012.08.010.

[77] Signe Beck Petersen et al. "Colonic absorption of salmon calcitonin using tetradecyl maltoside (TDM) as a permeation enhancer." In: *Eur. J. Pharm. Sci.* 48.4-5 (Mar. 2013), pp. 726–34. ISSN: 1879-0720. DOI: 10.1016/j.ejps.2013.01.009.

[78] Charlotte Pinholt et al. "Influence of acylation on the adsorption of GLP-2 to hydrophobic surfaces." In: *Int. J. Pharm.* (Jan. 2012), pp. 1–9. ISSN: 1873-3476. DOI: 10.1016/j.ijpharm.2012.01.040.

[79] B. W. Purdue, N. Tilakaratne, and P. M. Sexton. "Molecular Pharmacology of the Calcitonin Receptor". en. In: *Receptors Channels* 8 (Dec. 2002), pp. 243–255.

[80] M R Rekha and Chandra P Sharma. "Oral delivery of therapeutic protein/peptide for diabetes - Future perspectives." In: *Int. J. Pharm.* 1 (Apr. 2012), pp. 1–15. ISSN: 1873-3476. DOI: 10.1016/j.ijpharm.2012.03.056.

[81] Anne des Rieux et al. "Targeted nanoparticles with novel non-peptidic ligands for oral delivery." In: *Adv. Drug Delivery Rev.* 65.6 (June 2013), pp. 833–44. ISSN: 1872-8294. DOI: 10.1016/j.addr.2013.01.002.

[82] J.A. Rogers and A. Wong. "The temperature dependence and thermodynamics of partitioning of phenols in the n-octanol-water system". In: *Int. J. Pharm.* 6.3-4 (Sept. 1980), pp. 339–348. ISSN: 03785173. DOI: 10.1016/0378-5173(80)90117-9.

[83] Catherine A. Royer. "Probing Protein Folding and Conformational Transitions with Fluorescence". In: *Chem. Rev.* 106.5 (May 2006), pp. 1769–1784. ISSN: 0009-2665. DOI: 10.1021/cr0404390.

[84] Hyuk Sang Yoo and Tae Gwan Park. "Biodegradable nanoparticles containing protein-fatty acid complexes for oral delivery of salmon calcitonin." In: *Journal of pharmaceutical sciences* 93.2 (Mar. 2004), pp. 488–95. ISSN: 0022-3549. DOI: 10.1002/jps.10573.

[85] Norbert Sewald and Hans-Dieter Jakubke. *Peptides: Chemistry and Biology*. Vol. 19. Wiley, 2015, p. 594. ISBN: 3527802657.

[86] Rakhi B Shah and Mansoor a Khan. "Regional permeability of salmon calcitonin in isolated rat gastrointestinal tracts: transport mechanism using Caco-2 cell monolayer." In: *The AAPS journal* 6.4 (Jan. 2004), e31. ISSN: 1550-7416. DOI: 10.1208/aapsj060431.

[87] Keon-Hyoung Song, Suk-Jae Chung, and Chang-Koo Shim. "Enhanced intestinal absorption of salmon calcitonin (sCT) from proliposomes containing bile salts." In: *J. Control. Release.* 106.3 (Sept. 2005), pp. 298–308. ISSN: 0168-3659. DOI: 10.1016/j.jconrel.2005.05.016.

[88] Edith Staes et al. "Acylated and unacylated ghrelin binding to membranes and to ghrelin receptor: towards a better understanding of the underlying mechanisms." In: *Biochim. Biophys. Acta* 1798.11 (Nov. 2010), pp. 2102–13. ISSN: 0006-3002. DOI: 10.1016/j.bbamem.2010.07.002.

[89] Dorte B Steensgaard et al. "Ligand-controlled assembly of hexamers, dihexamers, and linear multihexamer structures by the engineered acylated insulin degludec." In: *Biochemistry* 52.2 (Jan. 2013), pp. 295–309. ISSN: 1520-4995. DOI: 10.1021/bi3008609.

[90] Wendy Tavares, Daniel J. Drucker, and Patricia L. Brubaker. "Enzymatic- and renal-dependent catabolism of the intestinotropic hormone glucagon-like peptide-2 in rats". In: *Am. J. Physiol. Endocrinol. Metab.* 278.1 (Jan. 2000), E134–139.

[91] M Thanou, J C Verhoef, and H E Junginger. "Oral drug absorption enhancement by chitosan and its derivatives." In: *Adv. Drug Delivery Rev.* 52.2 (Nov. 2001), pp. 117–26. ISSN: 0169-409X.

[92] Jesper Thulesen et al. "The truncated metabolite GLP-2 (3-33) interacts with the GLP-2 receptor as a partial agonist." In: *Regul. Pept.* 103.1 (Jan. 2002), pp. 9–15. ISSN: 0167-0115.

[93] Madeline Torres-Lugo et al. "pH-Sensitive hydrogels as gastrointestinal tract absorption enhancers: transport mechanisms of salmon calcitonin and other model molecules using the Caco-2 cell model." In: *Biotechnol. Prog.* 18.3 (2002), pp. 612–6. ISSN: 8756-7938. DOI: 10.1021/bp0101379.

[94] Tomomi Uchiyama, Atsushi Kotani, and Hiroyuki Tatsumi. "Development of novel lipophilic derivatives of DADLE (leucine enkephalin analogue): Intestinal permeability characteristics of DADLE derivatives in rats". In: *Pharm. Res.* 17.12 (2000).

[95] K Wallis, J R F Walters, and a Forbes. "Review article: glucagon-like peptide 2–current applications and future directions." In: *Alimentary pharmacology & therapeutics* 25.4 (Feb. 2007), pp. 365–72. ISSN: 0269-2813. DOI: 10.1111/j.1365-2036.2006.03193.x.

[96] Jeff Wang et al. "Reversible lipidization for the oral delivery of salmon calcitonin." In: *J. Control. Release.* 88.3 (Mar. 2003), pp. 369–80. ISSN: 0168-3659.

[97] Brian P. Ward et al. "Peptide lipidation stabilizes structure to enhance biological function". In: *Molecular Metabolism* 2.4 (2013), pp. 468–479. ISSN: 22128778. DOI: 10.1016/j.molmet.2013.08.008.

[98] Pd Ward, Tk Tippin, and Dr Thakker. "Enhancing paracellular permeability by modulating epithelial tight junctions." In: *Pharm. Sci. Technol. To.* 3.10 (Oct. 2000), pp. 346–358. ISSN: 1461-5347.

[99] Søren H. Welling et al. "The role of citric acid in oral peptide and protein formulations: Relationship between calcium chelation and proteolysis inhibition". In: *European Journal of Pharmaceutics and Biopharmaceutics* 86 (2014), pp. 544–551. ISSN: 18733441. DOI: 10.1016/j.ejpb.2013.12.017.

[100] Martin Werle, Abdallah Makhlof, and Hirofumi Takeuchi. "Oral protein delivery: a patent review of academic and industrial approaches." In: *Recent patents on drug delivery & formulation* 3.2 (June 2009), pp. 94–104. ISSN: 2212-4039.

[101] Kathryn Whitehead, Natalie Karr, and Samir Mitragotri. "Safe and effective permeation enhancers for oral drug delivery." In: *Pharm. Res.* 25.8 (Aug. 2008), pp. 1782–8. ISSN: 0724-8741. DOI: 10.1007/s11095-007-9488-9.

[102] A. Wikman-Larhed and P. Artursson. "Co-cultures of human intestinal goblet (HT29-H) and absorptive (Caco-2) cells for studies of drug and peptide absorption". In: *Eur. J. Pharm. Sci.* 3.3 (June 1995), pp. 171–183. ISSN: 09280987. DOI: 10.1016/0928-0987(95)00007-Z.

[103] Yu Seok Youn et al. "Improved intestinal delivery of salmon calcitonin by Lys18-amine specific PEGylation: stability, permeability, pharmacokinetic behavior and in vivo hypocalcemic efficacy." In: *J. Control. Release.* 114.3 (Sept. 2006), pp. 334–42. ISSN: 0168-3659. DOI: 10.1016/j.jconrel.2006.06.007.

[104] Qinghua Yu et al. "The effect of various absorption enhancers on tight junction in the human intestinal Caco-2 cell line." EN. In: *Drug development and industrial pharmacy* 39.4 (Apr. 2013), pp. 587–92. ISSN: 1520-5762. DOI: 10.3109/03639045.2012.692376.

[105] Liyun Yuan, Jeff Wang, and Wei-Chiang Shen. "Reversible Lipidization Prolongs the Pharmacological Effect, Plasma Duration, and Liver Retention of Octreotide". In: *Pharm. Res.* 22.2 (Feb. 2005), pp. 220–227. ISSN: 0724-8741. DOI: 10.1007/s11095-004-1189-z.

[106] L Zhang and G Bulaj. "Converting peptides into drug leads by lipidation." In: *Curr. Med. Chem* 19.11 (Jan. 2012), pp. 1602–18. ISSN: 1875-533X.

[107] Eric Zijlstra, Lutz Heinemann, and Leona Plum-Mörschel. "Oral insulin reloaded: a structured approach." In: *J Diabetes Sci Technol* 8.3 (May 2014), pp. 458–65. ISSN: 1932-2968. DOI: 10.1177/1932296814529988.

Appendix A

Kyte-Doolittle plots [55] displaying the hydrophobic/hydrophilic character of the two employed peptides GLP-2 and sCT (native sequences).

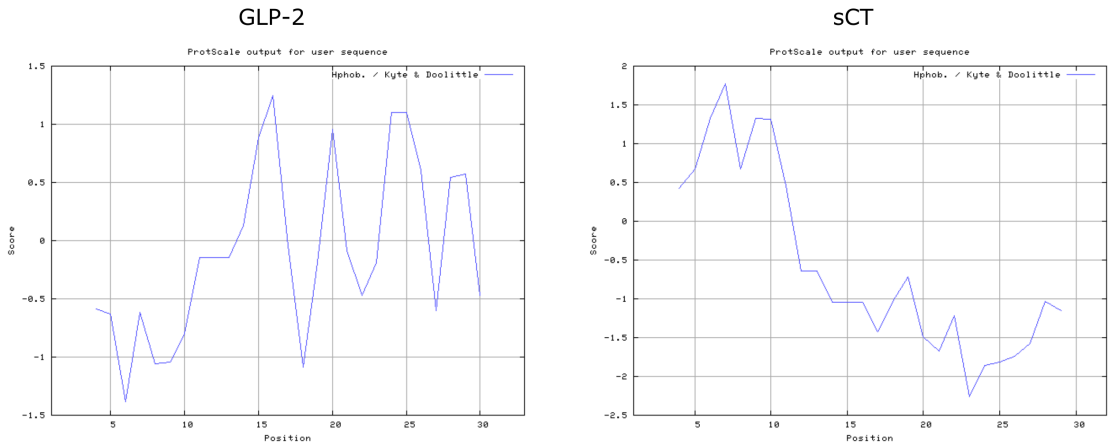

Figure A.1: Kyte-Doolittle plots for GLP-2 and sCT. Kyte-Doolittle plots display the distribution of polar and apolar residues along a protein or peptide sequence and can predict hydrophilic or hydrophobic regions. Regions with values above 0 are hydrophobic in character. Plots shown here have a window size of 7 which refers to the number of amino acids examined at a time to determine a point of hydrophobic character and is appropriate for finding hydrophilic regions that are likely exposed on the surface. (Note the different scale for the two graphs.) Figures created from http://web.expasy.org/cgi-bin/protscale/protscale.pl?1

Appendix B

Unpublished results for caco-2 absorption enhancers Tetradecyl maltoside (TDM) and Lauryol carnitine (LC) were previously investigated for their permeability enhancement of mannitol and human insulin, and for their effects on caco-2 cell monolayers. Microscopy images following immunocytochemistry are shown in fig. B.1, and for live cells in fig. B.2.

The employed concentrations of TDM and LC caused caco-2 permeability enhancement of mannitol and insulin, and reversible TEER decreases.

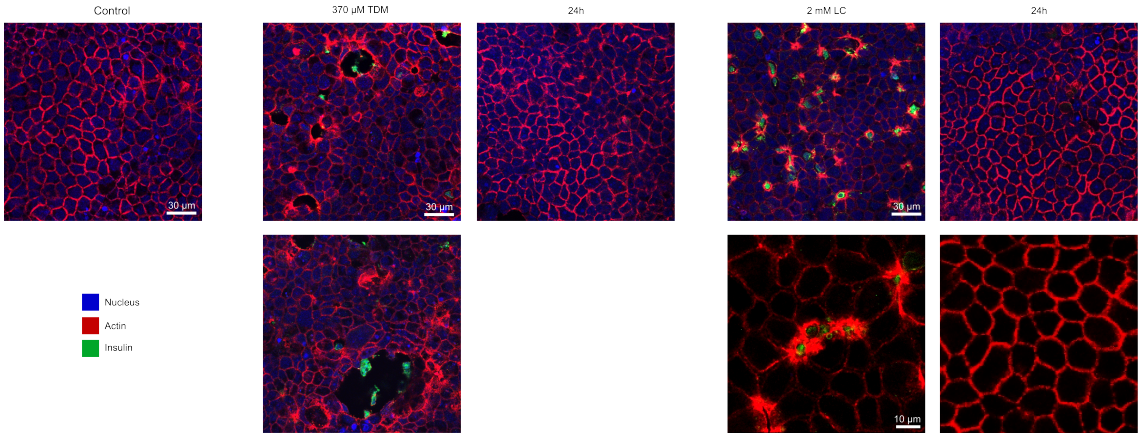

Figure B.1: Caco-2 cell interaction of TDM and LC. Microscopy images of caco-2 cell monolayers following permeability experiments with human insulin and TDM or LC, where cells are fixed and stained for nucleus (blue), filamentous actin (red), and insulin (green).

For TDM, holes where apparent in the cell layer, with small amounts of insulin visible at the edges. (Incidently, previous experiments with higher TDM concentrations caused even larger holes.) Interestingly, the cell layers recovered completely after 24 h in medium, both regarding TEER values and visible appearence. However, cell layer holes (although reversible) are likely not ideal, and may not correctly represent the *in vivo* absorption mechanism for TDM. Other studies have demonstrated both paracellular and transcellular components of TDM enhancement [76].

For LC, widespread actin reorganization is observed, with insulin mostly visible at the paracellular cell junctions. In the higher magnification image (bottom), the actin cell boundaries may have disbanded, as previously observed for paracellular enhancers [5]. However, as for TDM the cell layer recovers completely after 24 h in medium.

For live caco-2 monolayers addition of TDM and LC causes appearence of fluorescence between adjacent cells, indicative of paracellular permeability enhancement, which is slightly more pronounced for the smaller fluorophore CF.

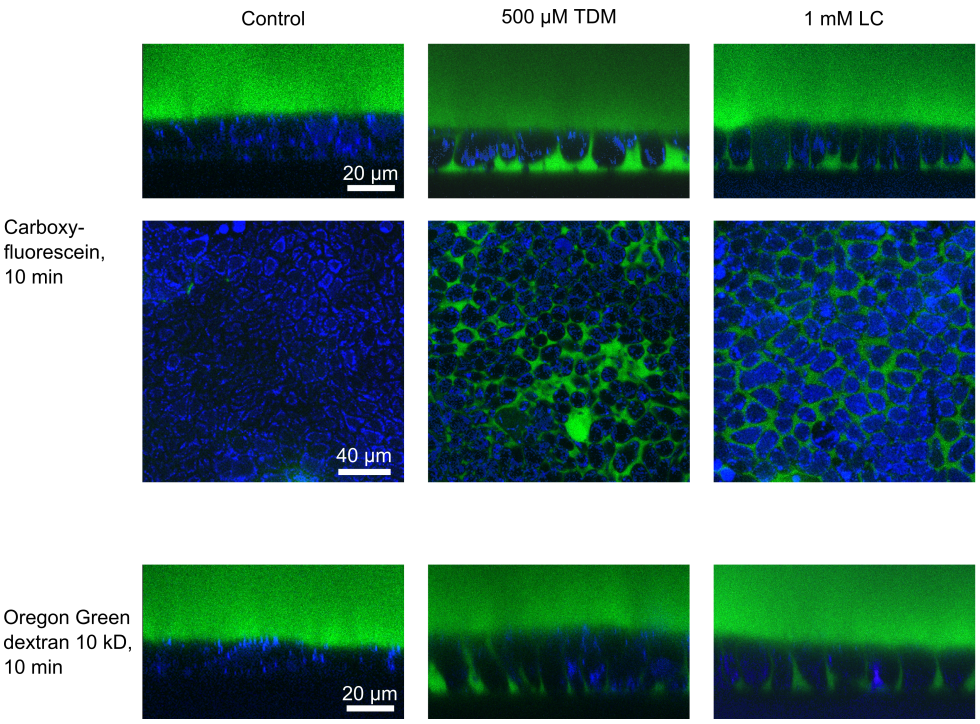

Figure B.2: Live-cell imaging with TDM and LC. Microscopy images of caco-2 cell monolayers following exposure to Carboxyfluorescein (CF) or Oregon Green dextran (10 kDa) and TDM or LC, in side-view or cross-section. Cells are stained for nucleus (blue) and fluorescence is depicted in green.

Appendix C

The following manuscript draft was prepared in collaboration with Hsih-Yin Tan and concerns the development of a microfluidic setup for culturing and studying caco-2 cells. The manuscript and its supplementary information will shortly be submitted to *PNAS*, and is typeset according to the journal guidelines.

The manuscript was primarily written by Hsih-Yin Tan, where my contribution consists of fig. 6, partially fig. 5, and experimental details for Transwell permeability experiments.

A multi-chamber microchip platform for studying drug transport across tissue barriers

Hsih-Yin Tan[a,b], Sofie Trier [a,b,d], Martin Dufva[a], Jörg P. Kutter[c], Thomas Lars Andresen[a,b,1]

[a] Technical University of Denmark, Department of Micro and Nanotechnology, Ørsteds Plads, 2800 Kgs. Lyngby, Denmark [b] Technical University of Denmark, Center for Nanomedicine and Theranostics, Ørsteds Plads, 2800 Kgs. Lyngby, Denmark [c] Department of Pharmacy, University of Copenhagen, Universitetsparken 2, 2100 Copenhagen, Denmark [d] Global Research, Novo Nordisk A/S, 2760 Maaloev, Denmark

Submitted to Proceedings of the National Academy of Sciences of the United States of America

This paper presents the design and fabrication of a multi-layer and multi-chamber microchip system using thiol-ene 'click chemistry' aimed for drug transport studies across tissue barrier models. The tissue barrier model employed to test the device was based on Caco-2 intestinal model and mannitol, dextrane and insulin were used as drug molecules (in the presence or absence of membrane permeability enhancers) to investigate transport in the microfluidic barrier system in comparison to the conventional Transwell system. The developed fabrication process allows for rapid prototyping of multi-layer microfluidic chips using different thiol-ene polymer mixtures. We incorporated porous Teflon support membranes to accommodate cell growth by masked sandwiching thiol-ene-based fluid layers. Electrodes for TEER measurements were incorporated using low melting soldering wires melted into channels as in combination with platinum wires. We demonstrated that the thiol-ene-based microchip material including the electrodes does not induce adverse effects on the cells. The Caco-2 cells cultured on the thiol-ene microchip differentiated and showed signs of producing mucus within 9 - 10 days of cell culture, indicating theformation of a robust barrier at a much faster rate than in conventional Transwell models. The presented microdevice for cell culture is useful for carrying out real-time studies of cellular barriers under optical monitoring, and enables transport studies of drugs, chemicals, and pathogens. The system may have additional uses in toxicological assessments.

thiol-ene microchip | Caco-2 cell culture | membrane barrier studies | drug permeability

Manuscript Text

Introduction

Covering the inner walls of the intestines is a single layer of epithelial cells that forms a rate limiting barrier to the absorption of drugs. Numerous experimental models have been developed for the prediction of intestinal permeability - including *in situ* isolated perfused intestinal systems (1–4). However, the use of animal models is time consuming, labour intensive and costly. Furthermore, animal models also raise ethical issues and are often not able to accurately predict the results in humans (5). Culturing and differentiation of epithelial cells derived from the intestine can provide relevant *in vitro* models for prediction of drug absorption in humans (6, 7). Caco-2 cells constitute a gold standard of intestinal model when cultured under specific conditions, i.e., grown on Transwell permeable filter supports, the cells will form a monolayer (8). They will further spontaneously differentiate and proliferate, thus exhibiting many features of the small intestinal villus epithelium (9, 10). Some of the most prominent features of Caco-2 cells cultured in this way are the formation of brush border microvilli (10) on the upper side of the cells, development of intercellular tight junctions (11), and the presence of various metabolic enzymes present in the intestinal epithelium (10, 12). Due to the formation of a tight monolayer of Caco-2 cells, this provides a physical and biochemical barrier to the passage of ions and small molecules through the Caco-2 cell layer. Therefore, it is one of the most well-established human intestinal epithelial cell lines and has been extensively used as an *in vitro* intestinal model for pharmaceutical studies, e.g., ADME-Tox (adsorption, distribution, metabolism, excretion, and toxicology) studies. About three weeks are required for Caco-2 cells to fully differentiate and form confluent and tight monolayers in Transwell inserts (8). However, this *in vitro* model does not allow to recreate the presence of continuous fluid flow nor the presence of fluid shear stresses on the epithelial cells as can be found in their natural environment. It has been postulated that the fluid shear stress in the intestinal tract varies depending on the exact location and fluid shear stresses from 1 to 5 dyn/cm^2 have been reported (13).

By using micro total analysis system technology, various functional microfluidic systems can be developed to provide integrated microenvironments for cell maintenance, continuous perfusion and real-time monitoring of cells. Several groups have reported on the design and fabrication of polydimethylsiloxane (PDMS) based microdevices for Caco-2 cell culture (14–18). Kim et al. have reported that with the combination of peristaltic motion and fluid flow in the microfluidic device, the Caco-2 cells displayed intestinal villi with physiological growth up to several hundreds of microns in height, as well as increased expression of intestine-specific functions, including mucus production (17). However, the reported microfluidic devices are only capable of culturing one set of Caco-2 monolayers for analysis at any one time. In biological cell analysis studies or drug transport studies across Caco-2 monolayers, or other model tissue barriers, it is highly desirable to investigate different conditions in the same

Significance

Transwell culture system is the gold standard *in vitro* model for assessing and predicting permeability and absorption of oral drugs in pharmaceutical industry. However, this platform cannot support any form of luminal flow conditions on the cells to more closely mimick *in vivo* conditions. Relevance of this study lies in engineering an eight chamber multi-layer microchip to support long-term studies of tissue barriers by using the Caco-2 cell intestinal model. We demonstrate the feasibility of using the *in vitro* intestinal model culture in the thiol-ene-based microchip for transport studies by using three different test compounds. Such a platform paves the way towards advanced *in vitro* intestinal model for high throughput screening of drugs, chemicals, pathogens as well as toxicological studies.

Reserved for Publication Footnotes

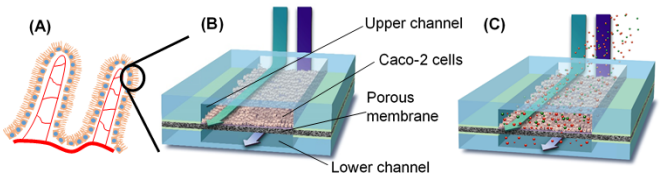

Fig. 1. Schematic illustration of the thiol-ene based microfluidic chip for intestinal transport studies. (A) Cross-sectional view of human intestinal microvilli. (B) Microarchitecture of one microchamber on the thiol-ene microfluidic chip consisting of upper and lower cell culture chambers separated by an ECM coated Teflon membrane. (C) Presence of membrane enhancer causing compounds to be transported across Caco-2 monolayer

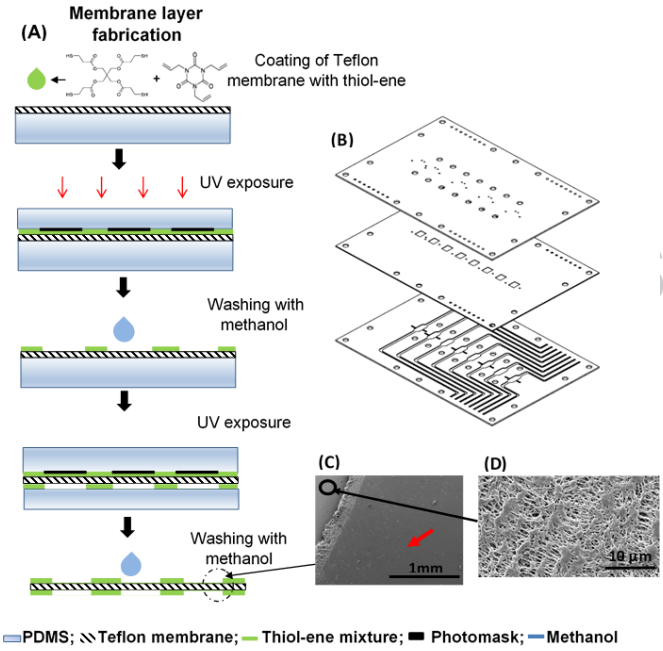

Fig. 2. (A) Schematic process of fabricating the thiol-ene coated membrane. (B) Exploded view of the high throughput multi-layer thiol-ene microchip for cell culture (*Dimension of microchip: 76 mm x 52 mm x 2.7 mm*). Thickness of the modified membrane is 0.3 mm. The membrane is coated with a thiol-ene mixture on both sides to ensure good bonding between the chip layers. Fluids were pumped in the upper and lower layers. (C) SEM images of Teflon membrane (Top view). Surface morphology was changed significantly after coating a layer of thiol-ene. The surface of the membrane has become very smooth after coating and curing a layer of thiol-ene (as indicated by red arrow). (D) Expanded view of Teflon membrane that was masked off and rinsed with methanol, thus maintaining its porous structure in these areas.

experimental system in a high throughput manner (19). Scaling up the number of cell culture microchambers on the microfluidic chip provides the possibilityfor analyzing more than one sample in parallel under controlled conditions, therefore allowing for controlled parameter comparisons. Although PDMS is an excellent material choice for fabricating microfluidic devices for cell culture, it may pose some challenges in studies that involve chemicals and drugs (20). Furthermore, PDMS has a tendency to absorb small hydrophobic molecules and this may compromise accurate measurements of drug efficacy and toxicity (21–23).

To pursue the goal of developing an alternative *in vitro* model of the human intestines for high throughput transport studies (Fig. 1), we have explored the use of thiol-ene chemistry and a novel membrane system for cell support within a microfluidic system to develop a multi-chamber microchip. The developed microchip contains eight micro-chambers, thus allowing parallel culturing of Caco-2 cells or other tissue models. The design of eight channels allows for significant controls during drug transport studies and allowed us to employ the previously reported microfluidic flow system developed by some of the authors (24). To quantitatively evaluate the integrity of the Caco-2 monolayer, two pairs of electrodes were embedded in the microchambers on the microchip to acquire trans-epithelial electrical resistance (TEER). To further assess the rate-limiting barrier of the Caco-2 monolayers cultured in the microfluidic device, transport studies using three different test compounds were examined (mannitol, dextrane and insulin). Mannitol and dextrane were used as model drugs. Insulin was used due to the interest in oral delivery of this drug in the pharmaceutical industry to provide a proof of concept of the Caco-2 monolayers cultured in the thiol-ene microchip for drug permeability studies. Insulin is usually administered by the subcutaneous route (25, 26); however, orally delivered insulin is attracting considerable attention due to the improved compliance this would provide for diabetic patients (25). Oral delivery of insulin has major limitations, due to the degradation of insulin by proteolytic enzymes in the gastrointestinal tract and poor intestinal barrier permeability due to its molecular weight (26). To increase the oral bioavailability, various strategies have been made to investigate to facilitate the absorption and transportation of insulin. One of the more successful methods is to co-administer membrane permeability enhancers (27–31) (Fig. 1c) together with the drug. For this reason, we chose to investigate the use of permeability enhancers for aiding insulin transport to further demonstrate the usability of microfluidic-based tissue barrier platforms for investigating drug transport.

Results and discussion

Development of thiol-ene-based microchip for Caco-2 cell culture. We designed and developed a thiol-ene based microchip that consists of eight cell culture micro-chambers where each cell culture chamber has two compartments (to become the apical and basal side of the cell layer, respectively) (Fig. 1). Thiol-ene was chosen since thiol-ene polymers have been reported to show low affinity to absorb molecules, have low volume shrinkage (32, 33), and are biocompatible for use in cell culture (34). The thiol-ene-based microchip has an external dimension of 76 mm x 52 mm x 2.7 mm and consists of three layers. The top and bottom layers of the microchip were fabricated via the method reported by Lafleur et. al. (35) using a two-step UV exposure (36, 37) (*SI Text Fabrication of microfluidic device*). The middle layer was a porous Teflon membrane (BGCM 00010; Millipore, Denmark) (0.4 µm in pore size; 40 µm in thickness). This porous Teflon membrane was suitable for cell culturing and it became transparent to visible light when wetted (Fig. S2), thus allowing real-time and fluorescence microscopic monitoring of the Caco-2 cells cultured on it. The bonding of the thiol-ene top and bottom fluidic layers with the Teflon membrane required a dedicated modification of the membrane. The porous Teflon membrane was coated with a thiol-ene mixture and exposed to UV radiation with a plastic mask that protected the part of the membrane to be used for cell cultures. Methanol was used to rinse the entire membrane to remove any traces of uncured thiol-ene. The end result was a thiol-ene modified membrane with regions, which were not coated with thiol-ene and thus allowed the porous Teflon membrane to be used for cell culturing. When examined with a scanning electron microscope (SEM), a smooth surface was observed in regions where the porous Teflon membrane was coated with thiol-ene and exposed to UV light. In regions that were masked and rinsed with methanol, the porous structure of the Teflon membrane was preserved (Fig. 2D). This procedure clearly demonstrated that thiol-ene 'click' chemistry can be exploited to functionalise and pattern the membrane surface (36, 37). In our pressure burst studies of the microfluidic chip, the multi-layer microchip could withstand burst pressures of more than 6 bars (*SI*

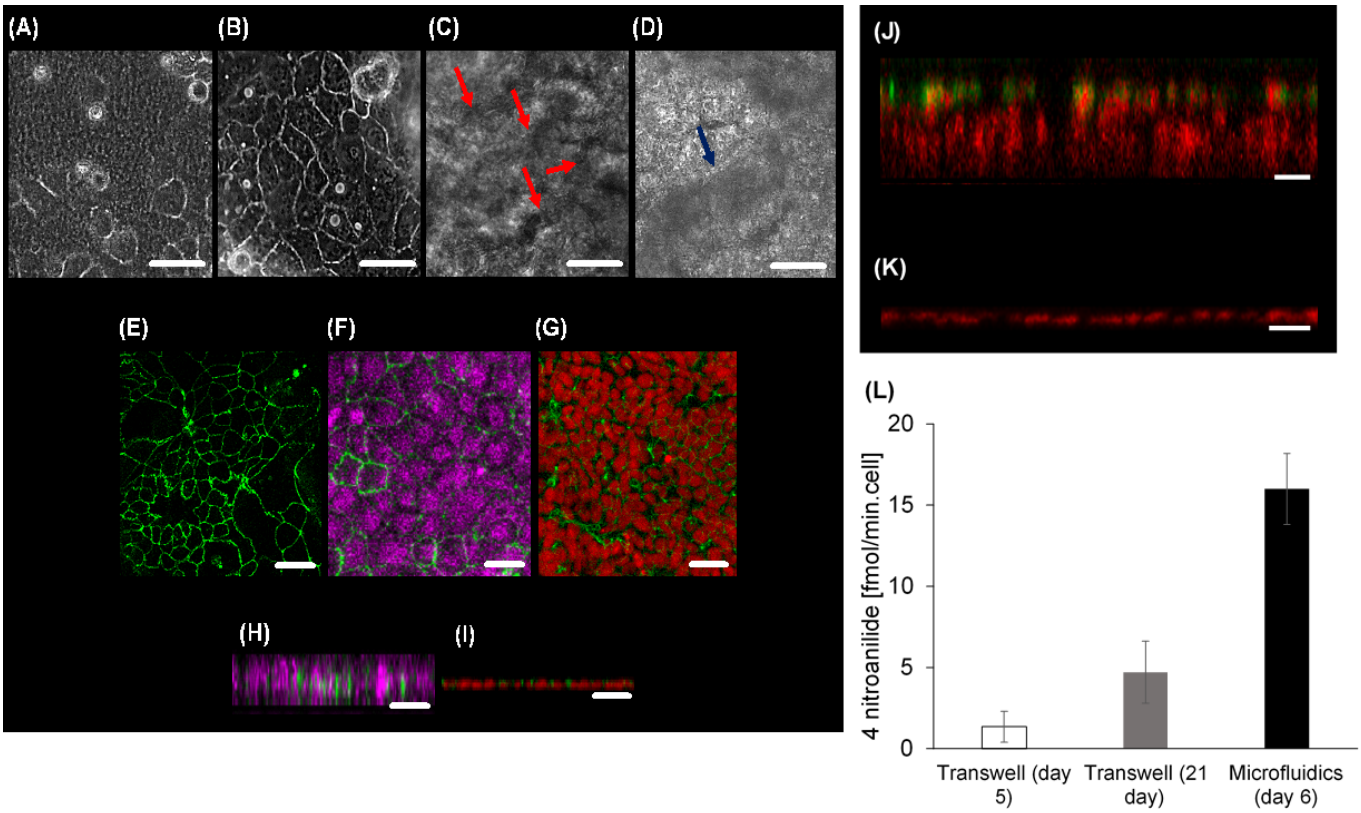

Fig. 3. Caco-2 cells cultured in microfluidic system (A-F and H). Caco-2 cells cultured in Transwell system (G and I). Phase contrast images of the Caco-2 cells cultured in the microchambers on the thiol-ene microchip over 10 days. (A) Day 1; (B) Day 2; (C) Day 5; (D) Day 8. Cells multiply and differentiate over the days of culture. Folds in the monolayer of Caco-2 cells start appearing from day 4 of cell culture. The folds in the Caco-2 monolayers are more prominent from day 5 onwards (indicated by red arrows). Dark 'patches' also start appearing on the Caco-2 monolayers from day 7 onwards. They become more prominent from day 8 of cell culture (indicated by white arrow). (E) Immunofluorescence image showing the distribution of the tight junction protein, occludin (green) at day 3. (F) Immunostaining of tight junctions (green) and nuclei (magenta). (G) Caco-2 cells cultured in Transwell stained for nucleus and tight junctions (Nuclei in red and tight junctions in green) (Day 21). (H) Vertical cross-section view of the Caco-2 monolayer (nuclei in magenta, tight junctions in green). The Caco-2 cells are ≈ 40 µm – 50 µm in height on day 3 of cell culture in the thiol-ene microfluidic chip. (I) Vertical confocal image of Caco-2 cells in Transwell (Nuclei in red and tight junctions in green). Immunofluorescence staining of nucleus and mucus on Caco-2 cells cultured in: (J) Thiol-ene microchip on day 10 of cell culture (nucleus in red, mucoprotein 2 (MUC-2) in green). The fluorescent images of the cells demonstrate that the cells have polarised into columnar cells of about 100 µm in height and formed villious-like structures. (K) Cells in the Transwell inserts were stained for nucleus and mucoprotein 2 at day 21. Only the nuclei could be fluorescently imaged but not MUC-2. Height of cells were about 25 -30 µm at day 21. (L) Differentiation of Caco-2 cells cultured in Transwell inserts and thiol-ene microchip as indicated by the activity of the brush border enzyme aminopeptidase. (n = 3, mean ± SD). Magnification 10 x. (Scale bar = 50 µm)

Table ST1). The presented method of fabricating the microfluidic chip is rapid and can easily be carried out at room temperature and in standard laboratory environments, therefore eliminating the need for costly or specialized cleanroom facilities.

Caco-2 cell culture in microfluidic system. To investigate the feasibility of culturing Caco-2 cells in the microchambers of the thiol-ene microfluidic chip, Caco-2 cells were seeded into the microchamber at a density of 8.5 x 10^6 cells/ml. Cell culture medium was perfused through the upper and lower fluidic layers at a flow rate of 3 µl/min for 9 – 10 days. Caco-2 cells were observed to adhere onto the extracellular matrix (ECM) coated Teflon membrane (*SI Text Cell culture in microfluidic system*) within 30 min after cell seeding. During the phase of active growth, it was observed that once the flow of cell culture media was started (first 24 hrs of cell culture), the Caco-2 cells spread out (38). Yet, in some regions on the ECM coated Teflon membrane, they had the affinity to grow as clusters. However, over the days of cell culture, with the constant supply of cell culture medium, the Caco-2 cells were observed to multiply and differentiate. By day 2 (Fig. 3B), distinct polygonal shapes with clear, sharp boundaries between the Caco-2 cells were observed in all the microchambers. The shape and morphology of the Caco-2 cells in the microfluidic device was similar to the cells cultured in a microplate (results not shown). Confluent monolayers of Caco-2 cells were observed in the microfluidic device typically around day 3-5 of cell culture. Folds started appearing in the monolayers around day 5 (a suggestion of villous formation) and it became more challenging to observe the cells through an optical microscope (Fig. 3C). From day 7 onwards, the appearance of 'dark' patches (Fig. 3D) were observed on the cells. As the cell culture period progressed, these 'dark' patches increased in area, or more 'dark' patches started appearing on the Caco-2 monolayers. However, these 'dark' patches were not observed when the cells were cultured at a flow rate of 0.5 µl/min (results not shown). It is suspected that these dark patches are the result of mucus produced by the Caco-2 monolayers under shear stress from the flow.

Caco-2 cell morphological studies. The establishment of apical tight junctions determines the integrity of the human intestinal epithelial cell monolayer (8). To visualise and validate the presence of apical tight junctions in the Caco-2 cells cultured in the microfluidic device, immunofluorescence staining using antibodies directed at the tight-junction protein, occludin, was carried out (*SI Text Morphological studies of Caco-2 cells in microfluidic and Transwell cultures*).

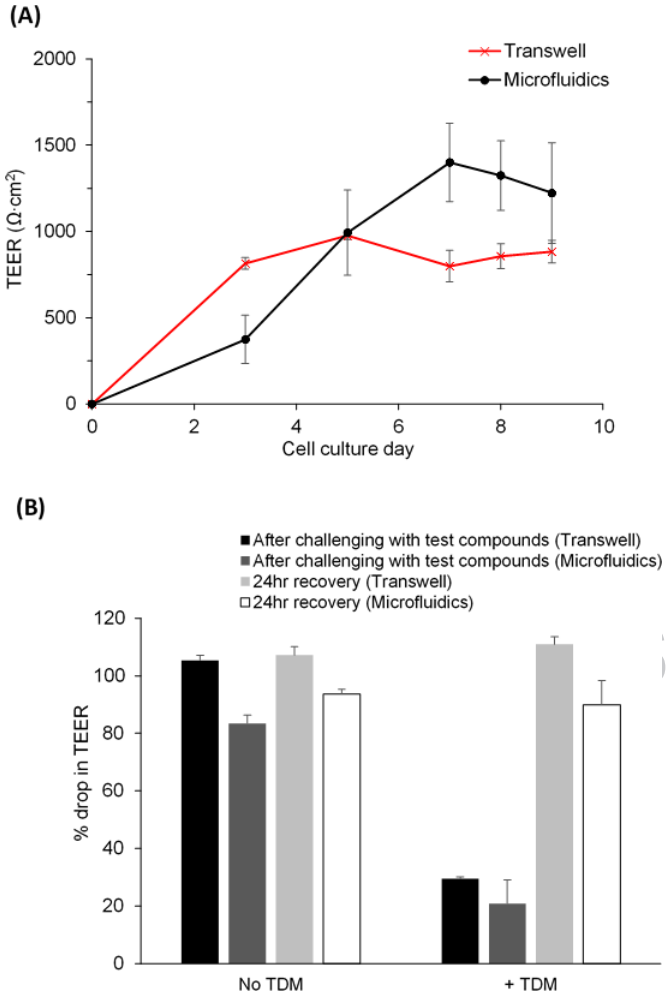

Fig. 4. (A) TEER measurements of Caco-2 cells cultured in thiol-ene microchip and Transwell inserts for the same cell concentration of 2.55 x 10^5 cells/cm^2. (Here, number of measurements per data point n = 12 for microfluidic device; and n = 5 for Transwell inserts). (B) Effect of test compounds alone or with TDM on Caco-2 TEER in the Transwell or microfluidic system, immediately after the experiment or following 24 h recovery in medium.

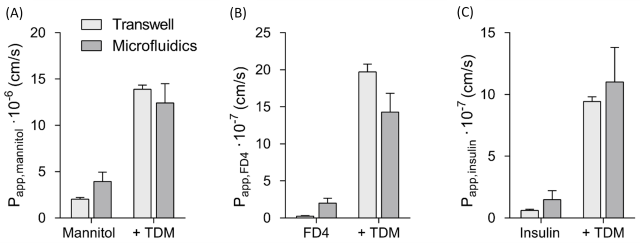

Fig. 5. Permeability of (A) mannitol, (B) FD4 and (C) insulin, alone or with TDM, across Caco-2 monolayers grown in the Transwell or microfluidic system. Data points represent mean ± SD (n = 4 for all Transwell inserts), (n = 4 for each of the experiments carried out with the microfluidic device)

The immunofluorescence images confirmed the formation of confluent Caco-2 monolayers, expressing tight junctions (Fig. 3E-F). Analysis of the vertical sections of the confocal images of the Caco-2 cells (Fig. 3H) revealed that the tight-junction proteins were situated between neighbouring cells at the apical side of the Caco-2 cells (Fig. 3F and 3H). Images of the cells cultured in the Transwell inserts at day 21 appeared cuboidal with heights of 14 – 20 µm (Fig. 3I). However, the Caco-2 cells cultured in the thiol-ene microfluidic device (three days of cell culture) were observed to appear columnar in shape with heights of ≈ 40 – 50 µm (Fig 3H). Our data is consistent with a previous report (17). The Caco-2 cells cultured in the microfluidic device is about the same columnar size and shape (40-50µm) as reported in healthy human intestinal epithelial cells (39). It is believed that the presence of continuous perfusion of cell culture medium in the microfluidic device may be responsible for stimulating the Caco-2 cells to polarise into columnar cells that were almost 2 fold taller than the cells from Transwell inserts.

In our microfluidic device, over the days of cell culture in the microfluidic device, from microscopic phase contrast images, there were observable regions of 'dark' patches (Fig. 3D). These 'dark' patches started appearing from day 7 of cell culture, but became more prominent from day 8 onwards. We observed that these dark patches were absent when the cells were cultured at a low flow rate of 0.5 µl/min (results not shown). To further investigate the nature or origin of these 'dark' patches, the Caco-2 monolayers were stained for the muco-protein, Mucin-2 (Mucin-2 is commonly found in human intestines) on day 10 of cell culture. Our immunofluorescence staining directed towards the protein Mucin-2 showed positive stains at the apical surfaces of the villous Caco-2 monolayers (Fig. 3J). This is surprising as in an earlier study (17, 40) the authors claimed the production of mucus on the Caco-2 cells cultured in a microfluidic device was due to fluid flow and cyclic peristaltic motions. However, the Caco-2 cells cultured in the thiol-ene microfluidic device were only exposed to low fluidic stresses (≈ 0.008 dyn/cm^2). It was also reported the gastrointestinal tract has a tendency to protect itself from mechanical and other stresses by producing and secreting a layer of lubricating mucus onto epithelial surfaces (41). Therefore, we hypothesise the exposure to low fluidic shear stresses (≈ 0.008 dyn/cm^2) may have resulted in the Caco-2 cells exhibiting some protective function by producing mucus on the apical side of the cells. To further confirm our observation, we also performed the same staining procedure on cells cultured in the Transwell inserts. Past studies have reported that Caco-2 cells do not produce mucus when cultured in static culture conditions (19). As expected the images of our Transwell cultures did not show the presence of Mucin-2 on the Caco-2 monolayers (Fig. 3K).

From the fluorescent images (Fig. 3J), it can also be observed that the Caco-2 cells cultured in the microfluidic device form folds and are capable of growing up to a height of ≈ 100 µm when they are cultured for a longer term (day 9 – 10). These results are consistent with an earlier study which showed fluid flow can encourage the formation of villous structures in the Caco-2 monolayers (17, 40).

Differentiation of Caco-2 cells. Another characteristic of differentiated Caco-2 cells is the high level expression of brush border enzymes that are commonly found in small intestinal epithelial cells (10, 12). To evaluate the differentiation of the Caco-2 cells that were cultured in our thiol-ene microchip, we measured the level of aminopeptidase activity by using the substrate L-alanine-4-nitroaniline hydrochloride (L-A4N). The aminopeptidase experiments were also carried out in the static Transwell inserts. The Transwell studies were carried out on day 5 and 21 of cell culture. In the microfluidic device, the aminopeptidase studies were carried out on day 5 of cell culture. Our analysis of data from the Transwell cultures showed that the aminopeptidase activity increased by more than 5-fold between Caco-2 cells cultured for 5 days and 21 days, respectively. These data are consistent with earlier findings (12, 17). Interestingly, analysis of the samples collected from our microfluidic device, with only 5 days of cell culture, showed that the aminopeptidase activity was 4 times higher than the aminopeptidase activity in the Transwell inserts at day 21 (Fig. 3L). Our results are comparable to earlier findings (14, 17). These results clearly confirmed that cells cultured in

the presence of continuous flow (as in the microfluidic device) required a shorter time to polarise and differentiate.

Trans-epithelial electrical resistance (TEER) measurements. Trans-epithelial electrical resistance (TEER) is a widely used technique for quantifying the integrity of the tight junctions present between cells that govern the solute transport across the paracellular space of epithelial monolayers (10). To ensure as much as possible an equal potential drop over the entire membrane (42), the electrodes were embedded directly above and below the membrane in our microfluidic device. The electrodes embedded in the thiol-ene microfluidic chip were produced in-house using a low-melting indium alloy (InBiSn) (*SI Fabrication of microfluidic device*) for the bottom electrodes and platinum wires for the top electrodes. TEER measurements were obtained by coupling the electrodes to a multi-meter (Keithley, USA) that supplied DC signals (constant current = 10 μA). TEER measurements of the Caco-2 monolayer cultured in the thiol-ene microchip were taken from day 3 onwards of cell culture and monitored over the remaining days of the experiments. Importantly, the TEER measurements of the Caco-2 cells cultured in the thiol-ene microchip showed a significant increase over the days of cell culture (Fig. 4A). TEER values for the microfluidic system reached a maximum of about 1400 $\Omega \cdot cm^2$ and the high values could be maintained from day 7-9. The standard deviation (SD) of the TEER values from the microfluidic device is much larger compared to the SD of the data from the Transwell inserts. This is attributed to the difference in electrode designs. Furthermore, the positions of the electrodes on the microfluidic device may vary slightly from microchamber to microchamber, and this may contribute to differences in measured resistances (43).

Effect of membrane permeability enhancer on TEER values. To validate the accuracy of the TEER values acquired from the electrodes on the microfluidic chip, a membrane enhancer, tetradecyl-β-D-maltoside (TDM), was introduced to the Caco-2 monolayers for two hours. TDM, is a compound that interacts with lipid cell membrane to permeabilise it, therefore increasing the transcellular pathway (28, 30, 44). It also modifies the tight junctions between adjacent cells, hence causing a drop in the TEER values. Consequently, this also causes an increase in the paracellular transport of compounds across the Caco-2 monolayer (28, 30, 44). The concentration of TDM used in this study is within the range that was reported previously (29). The concentration of TDM used in this study would disrupt the integrity of the Caco-2 monolayer while allowing it to recover when subjected to 24 hours of recovery with cell culture medium (Fig. 4B). Therefore, one will expect the TEER values to drop after exposing the Caco-2 monolayers to TDM, and then an increase of TEER values after 24 hours recovery period in cell culture medium. Interestingly, with the introduction of TDM to the Caco-2 monolayers cultured in the microfluidic device, the TEER data acquired in the absence and presence of membrane permeability enhancers showed distinct differences. It could be clearly seen that in the presence of TDM, the TEER values measured in the microfluidic device dropped to 20.6 % of their initial values (Fig. 4B). When the Caco-2 monolayers were subsequently subjected to 24 hours of continuous perfusion with cell culture medium, the TEER values recovered to 90 % of the initial values (Fig. 4B). This significant drop in TEER values with the introduction of TDM and an increase in the TEER values during the 24 hour recovery in cell culture medium was consistent with the data acquired from the static Transwell cultures (Fig. 4B). The TEER results recorded from the microfluidic device were also an indication that the electrodes fabricated on the microfluidic device were sensitive to detect dynamic changes in the integrity of the Caco-2 monolayers.

Permeability studies of FITC–dextran (FD-4), mannitol and insulin in the presence or absence of membrane permeability enhancer. Paracellular transport of compounds across the Caco-2 monolayers is governed by the presence of the tight junctions between adjacent cells. To assess if the Caco-2 monolayers cultured in the thiol-ene microchip exhibit a rate-limiting barrier, the behavior of three different test compounds (mannitol, fluorescein isothiocyanate (FITC)-labeled-dextran (FD 4) and insulin) was studied.

Permeability studies were carried out on day 9 or day 10 of cell culture. We measured the permeabilities (P_{app}) for mannitol, FD-4 and insulin to be 3.94 x 10^{-6} cm/s, 2 x 10^{-7} cm/s and 9.43 x 10^{-7} cm/s, respectively, in the microfluidic chip. The P_{app} values of similar compounds in the static Transwell cultures were slightly lower as compared to the microfluidic device (Fig. 5). To further investigate whether the permeability of different test compounds is affected by the introduction of TDM, we next exposed the Caco-2 monolayers in both the microfluidic device and the Transwell inserts to mixtures of test compounds with TDM. In both systems, the P_{app} values for all three compounds greatly increased (Fig. 5) in the presence of TDM. In the microfluidic device, the P_{app} values for mannitol, FD-4 and insulin were 12.42 x 10^{-6} cm/s, 14.29 x 10^{-7} cm/s and 11.02 x 10^{-7} cm/s respectively (Fig. 5). While the P_{app} values of the similar test compounds from the static Transwell cultures were 13.9 x 10^{-6} cm/s, 19.72 x 10^{-7} cm/s and 9.43 x 10^{-7} cm/s. The permeability results clearly demonstrated that the addition of TDM effectively permeabilised the Caco-2 monolayers in both systems and allowed substantial transport of compounds across the Caco-2 monolayers. Additionally, the P_{app} values of the test compounds in the presence of TDM were comparable between the static Transwell cultures and the microfluidic system. Therefore, the Caco-2 monolayers cultured in the microfluidic device could be an interesting alternative *in vitro* model of the human intestines for drug transport studies.

Conclusion

A thiol-ene based multi-chamber and multi-layer microfluidic chip was engineered to provide a controlled platform to sustain long-term Caco-2 cell cultures under fluidic flow for transport studies. Characterization of the microfluidic chip revealed that the functionality of the porous Teflon membrane (sandwiched between the top and bottom fluidic layers) could be changed by coating and curing it with a thiol-ene mixture, followed by ECM coating of the porous region of the Teflon. Thus, bonding the Teflon membrane between two cured thiol-ene layers within a fluidic system formed a microchip that could support long time cell culture. The experiments with the Caco-2 cells cultured in the thiol-ene microfluidic chip revealed, the growth and differentiation of the Caco-2 cell cultures accelerated under fluidic conditions. Furthermore, under continuous flow conditions, the Caco-2 cells cultured in the microchip developed villous morphogenesis, exhibited increased differentiation and formed a tight barrier, closely mimicking the human intestine. We showed that this intestinal model was adequate for transport studies.

In summary, this work has shown that Caco-2 cells cultured in a microengineered thiol-ene microfluidic chip may serve as a promising alternative *in vitro* platform for pharmaceutical, toxicological, and cell-cell communication studies, among others. With eight chambers fabricated on the same microchip, it allows for parallel studies to be carried out on the same microfluidic chip under basically identical conditions.

Materials and methods

Fabrication of thiol-ene microfluidic chip. Pentaerythritol tetrakis-(3-mercaptopropionate) (4 thiol moieties), tri-allyl-tri-azine (3 ene moieties) and trimethylopropane tris-(2-mercaptopropionate) (3 thiol moieties) used for fabricating the fluidic layers in the thiol-ene microfluidic chips were all purchased from Sigma Aldrich, Denmark. The commercially available Teflon membrane that was modified and sandwiched between the thiol-ene layers was purchased from Milipore, Germany. Methanol (Sigma, Denmark) was used for removal of uncured thiol-ene on the modified Teflon membrane. The microelectrodes embedded in the thiol-ene microchips were fabricated

by inserting pieces of low-melting temperature indium alloy (InBiSn, In 51 % Bi 32.5 % Sn 16.5 % by weight) (Indium Corp., Utica, NY) for the bottom fluidic layer and platinum wire (Advent, UK). The detailed fabrication of the microfluidic device is reported in the *SI Text Fabrication of microfluidic device*.

Cell culture. Human Caco-2 intestinal epithelial cells used in the experiments were obtained from American Type Culture Collection ((ATCC), HTB-37, Germany). The passages of the Caco-2 cell line used in the microfluidics studies ranged from the 40^{th} to 50^{th} passages, and for the Transwell studies, passages in the range of 40^{th} to 65^{th} were used. The Caco-2 cells were cultured routinely in Dubelco's Modified Eagle Medium (DMEM; Sigma, Denmark). The culture medium is supplemented with 10 % (v/v) heat-inactivated fetal bovine serum (FBS; Sigma, Denmark), 1% (v/v) nonessential amino acids (NEAA; Gibco, Denmark) and 1% (v/v) penicillin-streptomycin (P/S; Gibco, Denmark).

Cell staining for morphological studies. To visualize the cytoskeleton and morphology of the cultured Caco-2 cell monolayers in the microchip, the Caco-2 monolayers were first fixed in 4% paraformaldehyde and permeabilied with 0.1% (v/v) Triton-X-100 (Sigma, Denmark). F-actin, tight junctions and mucin were stained using Rhodamine-Phallodin (RP; (Invitrogen, USA), anti-occludin antibodies (Z0-1-1A12 mouse monoclonal antibody-Alexa Fluor® 488, Life Technologies, USA) and anti-mucin 2 antibodies (mouse monoclonal antibody; Abcam, Denmark) respectively. 7-Aminoactinomycin D (7-AAD; Invitrogen, USA) was used to stain the nucleus. The cells were imaged with a laser scanning confocal microscope (Carl Zeiss Axio Observer, Germany).

Preparation of compounds for permeability studies. The compounds used in the permeability studies, [^{3}H]-mannitol (PerkinElmer; USA), fluorescein isothiocyanate (FITCH)-labeled dextran (FD4; 4kDa; Sigma, Denmark), insulin (Novo Nordisk, Denmark) and tetradecyl-β-D-Maltoside (TDM; Sigma, Denmark) were all prepared using buffer$^+$ as the diluent. Buffer$^+$ was prepared by mixing Hank's Buffered Saline solution (HBSS; Gibco, Denmark), 0.1% (wt/v) OVA (ovalbumin; from chicken egg white, Sigma, Denmark) and 10 mM HEPES (HEPES; Sigma, Denmark) at pH 7.4. The different compounds were prepared in various concentrations: 0.8 μCi/ml [^{3}H]-mannitol, 100 μM insulin (peptide/drug) or 540 μM FD4, and 0 or 400 μM TDM.

Acknowledgements.

This work is supported by The Danish Council for Independent Research (FTP) and the Lunbeck Foundation.

1. Stewart B, et al. (1995) Comparison of intestinal permeabilities determined in multiple in vitro and in situ models: Relationship to absorption in humans. *Pharm Res* 12(5):693–699.
2. Lozoya-Agullo I, González-Álvarez I, González-Álvarez M, Merino-Sanjuán M, Bermejo M (2015) In Situ perfusion model in rat colon for drug absorption studies: comparison with small intestine and Caco-2 cell model. *J Pharm Sci* 104(9):3136–45.
3. Svensson USH, Sandström R, Carlborg Ö, Lennernäs H, Ashton M (1999) High in situ rat intestinal permeability if artemisinin unaffected by multiple dosing and with no evidence of P-glycoprotein involvement. *Drug Metab Dispos* 27(2):227–232.
4. Zakeri-Milania P, et al. (2007) Human intestinal permeability using intestinal perfusion in rat. *J Pharm Pharm Sci* 10(3):368–379.
5. Holmes AM, Creton S, Chapman K (2010) Working in partnership to advance the 3Rs in toxicity testing. *Toxicology* 267(1-3):14–9.
6. Hilgers AR, Conradi RA, Burton PS (1990) Caco-2 cell monolayers as a model for drug transport across the intestinal mucosa. *Pharm Res* 7(9):902–910.
7. Stenberg P, Norinder U, Luthman K, Artursson P (2001) Experimental and computational screening models for the prediction of intestinal drug absorption. *J Med Chem* 44(12):1927–1937.
8. Hubatsch I, Ragnarsson EGE, Artursson P (2007) Determination of drug permeability and prediction of drug absorption in Caco-2 monolayers. *Nat Protoc* 2(9):2111–9.
9. Hidalgo IJ, Raub TJ, Borchardt RT (1989) Characterization of the human colon carcinoma cell line (Caco-2) as a model system for intestinal epithelial permeability. *Gastroenterology* 96(3):736–749.
10. Pinto M, et al. (1983) Enterocyte-like differentiation and polarization. *Biol cell* 47(323):323–330.
11. Anderson JM, et al. (1989) ZO-1 mRNA and protein expression during tight junction assembly in Caco-2 cells. *J Cell Biol* 109(3):1047–1056.
12. Howell S, Kenny AJ, Turner AJ (1992) A survey of membrane peptidases in two human colonic cell lines Caco-2 and HT-29. *Biochem J* 284(2):595–601.
13. Guo P, Weinstein AM, Weinbaum S (2000) A hydrodynamic mechanosensory hypothesis for brush border microvilli. *Am J Physiol Physiol* 10031(4):F698–F712.
14. Chi M, et al. (2015) A microfluidic cell culture device (μFCCD) to culture epithelial cells with physiological and morphological properties that mimic those of the human intestine. *Biomed Microdevices* 17(3):9966.
15. Gao D, Liu H, Lin J-M, Wang Y, Jiang Y (2013) Characterization of drug permeability in Caco-2 monolayers by mass spectrometry on a membrane-based microfluidic device. *Lab Chip* 13(5):978–85.
16. Imura Y, Asano Y, Sato K, Yoshimura E (2009) A microfluidic system to evaluate intestinal absorption. *Anal Sci Int J Japan Soc Anal Chem* 25(12):1403–1407.
17. Kim HJ, Huh D, Hamilton G, Ingber DE (2012) Human gut-on-a-chip inhabited by microbial flora that experiences intestinal peristalsis-like motions and flow. *Lab Chip* 12(12):2165–74.
18. Kimura H, Yamamoto T, Sakai H, Sakai Y, Fujii T (2008) An integrated microfluidic system for long-term perfusion culture and on-line monitoring of intestinal tissue models. *Lab Chip* 8(5):741–6.
19. Artursson P, Borchardt RT (1998) Intestinal drug absorption and metabolism in cell cultures: Caco-2 and beyond. *Pharm Res* 4(12):1655–1658.
20. Huh D, et al. (2013) Microfabrication of human organs-on-chips. *Nat Protoc* 8(11):2135–57.
21. Lee JN, Park C, Whitesides GM (2003) Solvent compatibility of poly(dimethylsiloxane)-based microfluidic devices. *Anal Chem* 75(23):6544–54.
22. Toepke MW, Beebe DJ (2006) PDMS absorption of small molecules and consequences in microfluidic applications. *Lab Chip* 6(12):1484–6.
23. Wang JD, Douville NJ, Takayama S, ElSayed M (2012) Quantitative analysis of molecular absorption into PDMS microfluidic channels. *Ann Biomed Eng* 40(9):1862–73.
24. Sabourin D, et al. (2013) The MainSTREAM component platform: a holistic approach to microfluidic system design. *J Lab Autom* 18(3):212–28.
25. Fonte P, Araújo F, Reis S, Sarmento B (2013) Oral Insulin Delivery: How Far Are We? *J Diabetes Sci Technol* 7(2):520–531.
26. Carino GP, Mathiowitz E (1999) Oral insulin delivery. *Adv Drug Deliv Rev* 35(2-3):249–257.
27. Arnold JJ, Ahsan F, Meezan E, Pillion DJ (2004) Correlation of tetradecylmaltoside induced increases in nasal peptide drug delivery with morphological changes in nasal epithelial cells. *J Pharm Sci* 93(9):2205–13.
28. Petersen SB, Nielsen LG, Rahbek UL, Guldbrandt M, Brayden DJ (2013) Colonic absorption of salmon calcitonin using tetradecyl maltoside (TDM) as a permeation enhancer. *Eur J Pharm Sci* 48(4-5):726–34.
29. Petersen SB, et al. (2012) Evaluation of alkylmaltosides as intestinal permeation enhancers: comparison between rat intestinal mucosal sheets and Caco-2 monolayers. *Eur J Pharm Sci* 47(4):701–12.
30. Yang T, Arnold JJ, Ahsan F (2005) Tetradecylmaltoside (TDM) enhances in vitro and in vivo intestinal absorption of enoxaparin, a low molecular weight heparin. *J Drug Target* 13(1):29–38.
31. Uchiyama T, et al. (1999) Enhanced permeability of insulin across the rat intestinal membrane by various absorption enhancers: their intestinal mucosal toxicity and absorption-enhancing mechanism of n-Lauryl-β-D-maltopyranoside. *J Pharm Pharmacol* 51(11):1241–1250.
32. Carlborg CF, Haraldsson T, Öberg K, Malkoch M, van der Wijngaart W (2011) Beyond PDMS: off-stoichiometry thiol-ene (OSTE) based soft lithography for rapid prototyping of microfluidic devices. *Lab Chip* 11(18):3136–47.
33. Hoyle CE, Lee TY, Roper T (2004) Thiol-enes: Chemistry of the past with promise for the future. *J Polym Sci Part A Polym Chem* 42(21):5301–5338.
34. Hung L-H, Lin R, Lee AP (2008) Rapid microfabrication of solvent-resistant biocompatible microfluidic devices. *Lab Chip* 8(6):983–7.
35. Lafleur JP, Kwapiszewski R, Jensen TG, Kutter JP (2013) Rapid photochemical surface patterning of proteins in thiol-ene based microfluidic devices. *Analyst* 138(3):845–9.
36. Carlborg CF, et al. (2014) Functional off-stoichiometry thiol-ene-epoxy thermosets featuring temporally controlled curing stages via an UV/UV dual cure process. *J Polym Sci Part A Polym Chem* 52(18):2604–2615.
37. Natali M, Begolo S, Carofiglio T, Mistura G (2008) Rapid prototyping of multilayer thiolene microfluidic chips by photopolymerization and transfer lamination. *Lab Chip* 8(3):492–4.
38. Jokhadar SZ, Suštar V, Svetina S, Batista U (2009) Time lapse monitoring of Caco-2 cell shapes and shape dependence of the distribution of integrin β1 and F-actin on their basal membrane. *Cell Commun Adhes* 16(1-3):1–13.
39. Bullen TF, et al. (2006) Characterization of epithelial cell shedding from human small intestine. *Lab Invest* 86(10):1052–63.
40. Kim HJ, Ingber DE (2013) Gut-on-a-chip microenvironment induces human intestinal cells to undergo villus differentiation. *Integr Biol* 5(9):1130–40.
41. Forstner G (1995) Signal transduction, packaging and secretion of mucins. *Annu Rev Physiol* 57(1):585–605.
42. Odijk M, et al. (2015) Measuring direct current trans-epithelial electrical resistance in organ-on-a-chip microsystems. *Lab Chip* 15(3):745–52.
43. Lee WG, et al. (2008) Effect of geometry on impedance of cell suspended media in electrically mediated molecule uptake using a microstructure. *Curr Appl Phys* 8(6):696–699.
44. Ward PD, Tippin TK, Thakker DR (2000) Enhancing paracellular permeability by modulating epithelial tight junctions. *Pharm Sci Technolo Today* 3(10):346–358.

Please review all the figures in this paginated PDF and check if the figure size is appropriate to allow reading of the text in the figure.

If readability needs to be improved then resize the figure again in 'Figure sizing' interface of Article Sizing Tool.

Supporting Information

SI Text

Fabrication of microfluidic device. Two sets of molds were required to fabricate the fluidic layers of the thiol-ene microchip. The first mold was fabricated on polymethylmethacrylate (PMMA). The design of this mold was the exact replica of the thiol-ene microchip design. A second mold made from PDMS was the inverse design of the PMMA mold. The designs of the top and bottom layers of the microchip were first drawn with an engineering software, Autocad (Ver 18.1). To fabricate the first master molds, the drawings were converted to codes by EZ-CAM (ver 15.0, Germany) and micromilled (Mini-Mill/3, Minitech Machinery Corporation, GA, USA) onto 5 mm PMMA blocks. The second molds were fabricated by mixing poly dimethylsiloxane (PDMS; DowCorning, Germany) in the ratio of 1:10 (curing agent: pre-polymer), degassed under vacuum and poured onto the PMMA master mold. The liquid PDMS was cured in the oven at 70 °C for more than 20 hrs. Once the PDMS molds were cured, they were de-molded from PMMA molds, bearing the replicated design of the microchip layers.

Two different mixtures of thiol-ene were prepared for the microchip fabrication. The top and bottom layers, containing the fluidic microchannels and chambers were fabricated with a mixture of pentaerythritol tetrakis-(3-mercaptopropionate) (tetra-thiol moieties; Sigma, Denmark) (and 1,3,5 trilallyl-1,3,5-triazine-2,4,6(1H,3H,5H)-trione (tri-allyl moieties; Sigma, Denmark) in stoichiometric ratios. The different components were mixed, poured onto the PDMS molds and exposed to UV (for 40 s on both sides (Dymax 5000-EC Series UV curing flood lamp, Dymax Corp., Torrington, CT, USA, ~40 mW cm−2 at 365 nm) (Fig S1A).

To fabricate the thiol-ene coated Teflon membrane, a commercially available Teflon membrane (Millipore, Denmark) (0.4 μm in pore size; 40 μm in thickness) was modified to enable better bonding of the membrane to the thiol-ene parts containing the fluidic manifolds. A thiol-ene mixture consisting of trimethylopropane tris-(2-mercaptopropionate) (tri-thiol moieties; Sigma, Denmark) and the tri-allyl component as above, in stoichiometric ratios, was prepared and used to coat the membrane. The coated membrane was exposed to UV radiation for 25 s through a plastic mask (Infinite Graphics, Singapore) that protected the cell culture regions (Step 2 in Fig S1B). Thereafter, methanol (Sigma, Denmark) was used to rinse the entire membrane to remove any uncured thiol-ene (Step 3 in Fig. S1B). Before bonding the layers, holes for the inlets, outlets and electrode ports were drilled through the partial cured thiol-ene layers. Next, the layers (thiol-ene coated membrane and thiol-ene fluidic manifolds) were aligned onto each other. Slight pressure was applied with a roller over the layers to ensure good contact between the surfaces. To finalise the bonding, the combined layers were exposed to UV radiation for an additional minute on each side (Final step in Fig S1).

The completed microchip would have two sets of electrodes (top and bottom) embedded into selected chambers for measurement of the trans-epithelial electrical resistance (TEER). The bottom electrodes were fabricated using an Indium alloy (InBiSn (In 51 % Bi 32.5 % Sn 16.5 % by weight); Indium Corp, Utica, NY). Top electrodes were fabricated using Platinum wire (Pt, Advent, UK) (diameter 0.5 mm). To fabricate the bottom electrodes, the assembled microfluidic chip was first placed onto a hot plate set at 80 °C for 10 min. Pieces of the InBiSn metal, with length of 5 mm, were inserted into the electrode ports (connecting to the lower fluidic layer) on the thiol-ene microchip. Slight pressure was applied manually to push the melted metal into the electrode groove. Once the electrodes were formed, electric wires of diameter 0.4 mm were inserted to the liquid metal to act as connecting wires to the multimeter (Keithley, USA). To fabricate the top electrodes, pieces of Pt wires (diameter of 0.5 mm, length of 5 mm) were forced fit into the electrode ports drilled through the top fluidic layer. Two connecting Cu wires were soldered to the Pt wires. To fix the electrodes in position, UV-epoxy (NOA81; Norland, USA) was applied at the junctions between connecting wires and thiol-ene chip. The entire chip was exposed to UV light for 30 s. The entire procedure of embedding the electrodes on the microchip could be carried out in ambient environment, eliminating the use of expensive, sophisticated instruments in environment-controlled cleanroom.

Pressure burst studies of thiol-ene microchip layers. The burst pressure test of the different thiol-ene microfluidic chips were carried out at two different temperatures, namely room temperature (25°C) and incubator temperature (37 °C). The bond strength between the layers were investigated at 37 °C, which was the required temperature for cell culture of Caco2 cells. Therefore, this will also be the temperature that the

microfluidic chip would be subjected to for long periods. For the studies carried out at 37 °C, the microchip was first placed into an oven set at 37 °C, then transferred to a hotplate set at 37°C during the burst pressure tests. The system and method reported by Silkane et. al. (1) was used to carry out the burst pressure studies. The microchannels were first filled with diluted red food colour dye. Red dye was used to allow better visual observations during the pressure experiments. When testing the top layer, the inlets and outlets of the bottom layer and the outlet of the top layer were sealed with a layer of cured thiol-ene. These ports were sealed to prevent any leakage of pressure during the studies. The same procedure was carried out when testing the bottom fluidic layer. The instrument for the pressure test, as well as the chip filled with dye are shown in Fig. S2. Next, the microchip was connected to a mechanical clamp, where a pressure sensor was mounted onto a polycarbonate block. Via a tube, the system was connected to two 10 ml syringes. Pressure in the microchip was increased, by using the clamp to compress the air in the syringes. The entire system for the burst pressure test is shown schematically in Fig. S2a. The output of the pressure sensor was measured with an in-house written Labview program (National Instruments, Austin, TX, USA).

Cell culture in Transwell inserts and microfluidic chip

Transwell system. Control studies were carried out using static cultures of Caco-2 cells in 12 well Transwell plates (Corning , Sigma, Denmark). The inserts in the well plate each had a porous polycarbonate membrane (1.1 cm^2, 0.4 μm pores). In the Transwell studies, the Caco-2 cells harvested with trypsin/ETDA solution (0.05 %; Sigma, Denmark) were seeded on the top surface of the porous Transwell membrane at a density of 1 x 10^5 cells/well. The Caco-2 cells were grown for 14–16 days in Dulbecco's Modified Essential Medium (DMEM; Sigma, Denmark) supplemented with 10 % (v/v) heat-inactivated fetal bovine serum (FBS; Sigma, Denmark), 1% (v/v) nonessential amino acids (NEAA; Gibco, Denmark) and 1% (v/v) penicillin-streptomycin (P/S; Gibco, Denmark). The medium was changed every second day of cell culture.

Microfluidic system. After the microchip was fabricated, it was assembled onto the platform with MAINSTREAM components (2). The Teflon tubings (inner diameter = 0.2 mm; Bola, Denmark) microcomponents and microchip were sterilised by perfusing 70 % ethanol throughout the entire system at a flow rate of 5μl/min for 2 hours. Following that, sterile water was flushed into the entire system for an additional 2 hours at a flow rate of 5μl/min. It was crucial to ensure good microenvironment in the cell culture chamber and good cell attachment during cell seeding in the microchip. To achieve this, extra cellular matrix mixtures (ECM) known to have the ability in improving the cellular microenvironment (3–5), was used to coat the Teflon membrane. An ECM mixture: 300 μg/ml matrigel (Corning, United Kingdom) and 50 μg/ml collagen (BD Bioscience, Denmark) and serum-free DMEM was flowed into the microchip to coat the porous membrane. The ECM mixture was flowed into the microchip for 2 hours at a flow rate of 5μl/min in an incubator. After the incubation, the microchip device was perfused with cell culture medium overnight in an incubator (37°C, 5 % CO_2). Following that, the harvested Caco-2 cells from the trypsin/EDTA solution was seeded into the microfluidic chip.

For cell seeding in the microfluidic microchip, the harvested Caco-2 cells was diluted with DMEM containing 60 % (v/v) FBS solution. The re-suspended cell mixture was syringed into the 'cell loading' reservoirs that were assembled onto the microfluidic platform. The peristaltic micropump on the microfluidic platform was activated at a very high flow rate (flow rate ≈ 65 μl/min) to draw the cell suspension into the cell culture chambers. The microchambers were seeded with Caco-2 cells at a concentration of 2.5 x 10^5 cells/cm^2. A normal optical microscope was utilized to observe the distribution of the cells in the chambers. Caco-2 cells attached onto the ECM-coated Teflon membrane within 30 minutes. Next, the entire system with the microchip was placed in the incubator (37°C, 5% CO_2). After 2 hours, the peristaltic micropump was activated to perfuse culture medium through the upper microchannels and microchambers at a constant flow rate of 0.5 μl/min. Cell culture medium was flowed only in the upper layer on day 1 of cell culture. This was to ensure the Caco-2 cells establish an intact monolayer. From the second day of cell culture onwards, the micropump that was perfusing through the lower microchannels and microchambers was also activated. Flow rate was set at 3 μl/min for both top and bottom channels. Over the 9 - 10 days of cell culture, phase contrast images of the cells in four different positions of each of the microchambers were taken and compared.

Trans epithelial barrier measurements (TEER)

Transwell set-up. To acquire the TEER measurements (Ω) from the Transwell inserts, a Millicell ERS-2 (Millipore, USA) coupled to a pair of chopstick Silver/SilverChloride (Ag/AgCl) electrodes was used. TEER values ($\Omega \cdot cm^2$) were determined by subtracting the baseline measurements recorded in absence of cells, then multiply the cell culture area (cm^2) (eq. 1).

Microfluidic device. TEER measurements (Ω) of the Caco-2 cells cultured in the microfluidic device were obtained by coupling the connecting wires of the electrodes to a multimeter (Keithley, USA) using alligator clips. Similar to the Transwell studies, the final TEER values were determined by subtracting the baseline measurements recorded in the absence of cells, then multiply the cell culture area of the porous Teflon membrane (area 0.1 cm^2).

TEER measurements. The final TEER values ($\Omega \cdot cm^2$) from the microfluidic device were determined by subtracting the baseline measurement in the absence of cells ($R_{baseline}$) from the read out (R_1) and multiplying with the area of cell culture (A_o) as shown in equation 1.

Eq (1): $$(R_1 - R_{baseline}) \times A_o = TEER$$

Morphological studies of Caco-2 cells cultured in microfluidic system and Transwell cultures. Phase contrast images of the Caco-2 monolayers were obtained using an inverted microscope (Carl Zeiss, Germany). Images were analysed with the imaging software (AxioVision 4.8.2, Carl Zeiss, Germany). Fluorescent confocal images of the monolayer morphology were obtained using a confocal microscope (Carl Zeiss, Germany). The procedure for cell staining and the dyes used were the same for both Transwell cultures and microfluidic device. PBS was used to rinse the cells between each processing step. The Caco-2 cells were fixed with 4% (vol/vol) paraformaldehyde for 30 min, following by permeabilisation with 0.1 % Triton X-100 for 30 min. After which, a blocking buffer (1% bovine serum albumin (BSA; Sigma, Denmark), 0.1% Tween-20 (Sigma, Denmark) in phosphate buffer saline (PBS; Sigma, Denmark)) was introduced to the cells for 1 hr. To visualize tight junctions, immunofluorescence staining was performed using mouse anti-ZO-1 (Z0-1; Life Technologies, Denmark) diluted in the blocking buffer 1:100, and introduced into the cells and left static overnight in the fridge at 4°C. Immunofluorescence staining was also carried out to stain the mucoprotein, mucin-2. Primary mouse monoclonal antibody (ab11197; AbCam, Denmark) prepared in blocking buffer (1:100), was introduced to the cells. The samples were protected from light and left static overnight in the fridge at 4°C. After which, the cells was rinsed with blocking buffer followed by introducing the secondary antibody (AlexaFluor 488 goat anti-mouse; Life technologies, Denmark) prepared in blocking buffer (1:200) and left static in room temperature for 2 hrs. Staining of the nucleus and actin were carried out by diluting 7-aminoactinomycin D (AAD; Invitrogen, Denmark) (32 μM) and rhodamin phallodin (RP; Life Technologies, Denmark)) to 1:100 in PBS and incubated with the cells for 1 hr. Lastly, mounting media (Vectashield; VWR, Denmark) was added to the cells to protect the fluorescent dyes. For the Transwell cultures, the membranes were removed from the inserts and mounted onto glass slides before microscopic imaging. Staining of cells in the microfluidic device, were performed *in situ* within the microchannels by flowing the different reagents into the microchannels and microchambers via MAINSTREAM platform. Fluorescent imaging of the stained Caco-2 cells on the thiol-ene microchip was performed through the thiol-ene layer on an upright microscope (ZEISS Axioscope; Carl Zeiss, Germany). The recorded images of the cells were analysed with an imaging process software AxioVision SE64 Rel4.8.

Aminopeptidase studies to determine differentiated Caco-2 cells. L-alanine-4-nitroaniline hydrochloride (L-4AN; Sigma, Denmark) was prepared by dissolving the L-A4N substrate in DMEM without phenol red ($DMEM^{-PR}$, Gibco, Denmark) to a concentration of 1.5 mM. In the Transwell studies, the Caco-2 cells were first rinsed with $DMEM^{-PR}$ in both the apical and basolateral sides for 3 times. 500 μl of L-A4N substrate solution was added to the apical side of the cells and 1500 μl of $DMEM^{-PR}$ was added to the basal lateral side of the cells and incubated at 37 °C. Sample aliquots of 100 μl was removed from the apical side at 30 min intervals and transferred to a 96-well microplate. Studies were carried out for a 2 hr period. Analysis of the sample aliquots were carried out with a microplate reader (Victor 3V; Perkin Elmer). $DMEM^{-PR}$ was set as the

reference. The test was calibrated with a series of dilutions of 4-nitroanilide in DMEM^{-PR}. One unit is defined as the hydrolysis of 1.0 μmol of 4-nitroanilide per minute. All of the reagents preparation and experimental studies were conducted under the protection of light. The aminopeptidase experiments in the Transwell cultures were carried out on cell culture day 5 and 21.

In the microfluidic device, the aminopeptidase studies were carried out on day 5 of cell culture. DMEM^{-PR} was first perfused to both the top and bottom fluidic channels for 45 min at a flow rate of 3 μl/min. Next, 1.5 mM of L-A4N solution was flowed into the upper microchannels and microchambers of the thiol-ene microchip at a flow rate of 3 μl/min. Sample aliquots of 120 μl were removed from the outlets of the upper microchannels at every 30 min and transferred to a 96-well microplate. Similar to the Transwell studies, the sample aliquots from the microfluidic system were analysed for the cleaved product, 4-nitroanalide with the microplate reader.

Permeability studies of fluorescein isothiocyanate–dextran (FD-4), mannitol and insulin in the presence or absence of membrane enhancer. In the Transwell studies, before carrying out the transport experiments, DMEM was changed to buffer$^+$ (*see Materials and methods for preparation of buffer*$^+$). 400 μl of buffer$^+$ was added to the apical side and 1 ml to the basolateral prior to equilibrate the Transwell plate for 60 minutes. Buffer$^+$ was replaced apically by 400 μl test solution at time zero, and the Transwell plates were incubated at 37°C and 5% CO_2 with gentle shaking. The gentle shaking is to ensure there was little unstirred diffusion layers of fluid in the basolateral region. Basolateral samples were collected every 15 minutes for 1 hour and analyzed along with apical test solutions, for [^{3}H]-mannitol content in a scintillation counter (Packard TopCount; PerkinElmer), after mixing with scintillation fluid (Microscint-40; PerkinElmer), along with a peptide and FD4 content. We chose to use the peptide, insulin, as a proof-of-concept demonstration in using the Caco-2 monolayers cultured in the thiol-ene microchip for drug permeability studies. After experiments, cells were washed twice with buffer$^+$ and replenished with medium for 24 hour recovery. In the microfluidic set-up, similar to the Transwell studies, before the start of experiment, the DMEM was replaced with buffer$^+$. Buffer$^+$ was flowed into the system for 1 hr. Subsequently, the buffer was changed to the test solutions in the top fluidic layer. Flow rate was set at 3 μl/min (in both the upper and lower layers). In the waste collection reservoirs, 200 μl of buffer was added to each of the waste reservoirs. This would enable sample aliquots of 100 μl collected at every 15 min intervals. During calculation of the permeability of the compounds across the cell monolayers, dilution of the sample aliquots were factored. Preparation of the test solutions can be found in *Materials and methods* segment.

Data analysis of permeability results. The Caco-2 translocation of peptide or [^{3}H]mannitol over Caco-2 layers is expressed as the apparent permeability (P_{app}), given by:

Eq. (E1): $$P_{app} = \frac{dQ}{dt}\,\frac{1}{A \cdot C_0}$$

Where dQ/dt is the steady-state flux across the cell layer (pmol/s), A is the surface area (1.12 cm^2 for Transwell, 0.1 cm^2 for microfluidic), and C_0 is the initial sample concentration (6) .

The basolateral samples were analyzed for insulin content using commercial insulin enzyme immunoassay kit (EIA, Phoneix Pharmaceuticals, Germany). Standards were prepared from test solutions, and were fitted to eq. 2 using Prism-6 (GraphPad).

Eq. (E2): $$Abs(450nm) = A + \frac{B-A}{1+10^{((logEC_{50}-x)\cdot C)}}$$

where *x* is log(concentration) of peptide in M, and A, B, C and EC_{50} are fitting parameters (7).

Basolateral samples were analyzed for FD4 content in a fluorescence plate reader (MD Spectramax Gemini, USA) with excitation/emission of 490/525 nm, based on standard curves prepared from test solutions. Statistical analysis was carried out using the softwares, Origin (OriginPro, Ver 9.1) and Prism (GraphyPad, Ver 6), where unpaired Students t-tests were used for comparison, and a significant difference was considered if $p < 0.05$. Results are presented as the mean ± standard deviation of the mean (SD).

SI figures

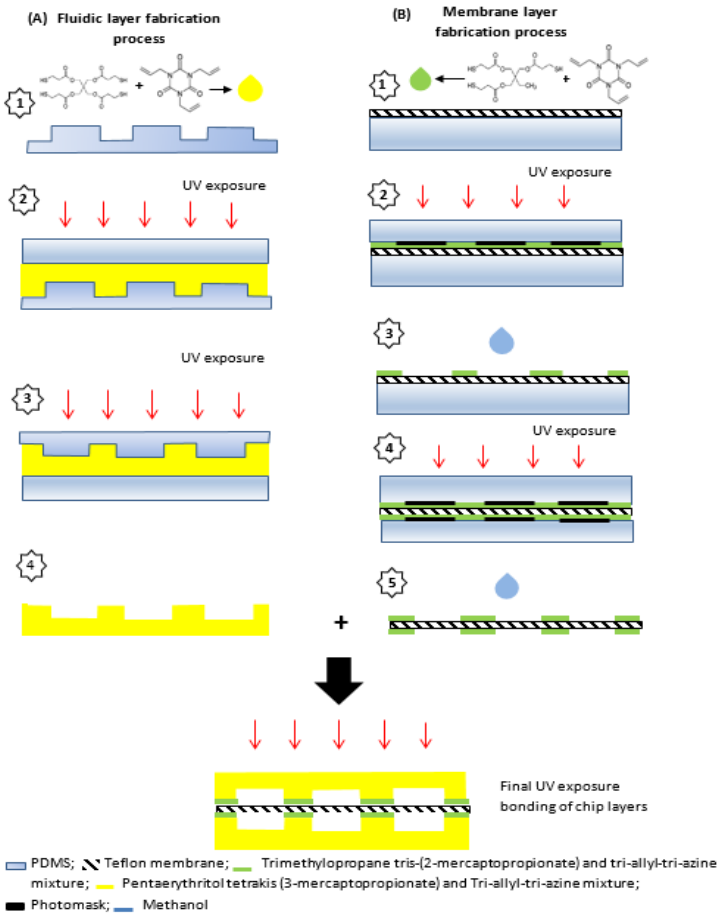

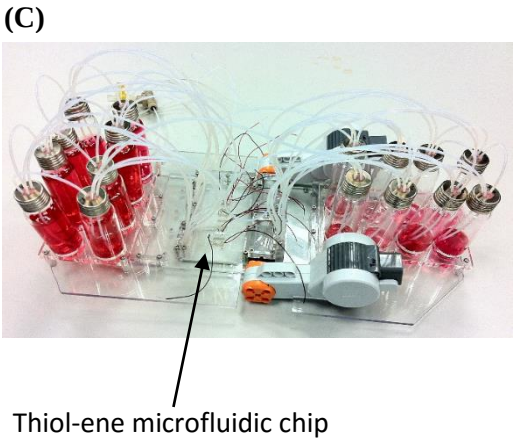

Figure S1. Schematic process of fabricating the thiol-ene microchip. (A) The upper and lower fluidic layer; (B) The thiol-ene coated Teflon membrane. (C) Final assembled system with microfluidic chip for cell culture. Microchambers on the microchip are embedded with the electrodes for acquiring TEER measurements.

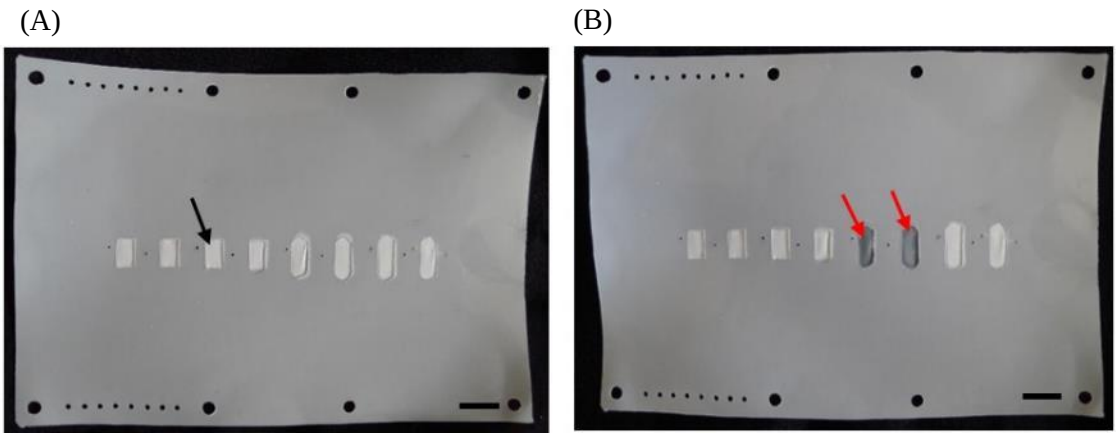

Figure S2. Porous Teflon membrane modified with a layer of cured thiol-ene mixture. Black arrow indicating the region on porous membrane that was protected by a plastic mask during UV-exposure. When dry, the region appeared white and opaque. (b) Two chambers were wetted with DI water, as indicated by red arrows. Teflon membrane becomes transparent in visible light. (Scale bar = 5 mm)

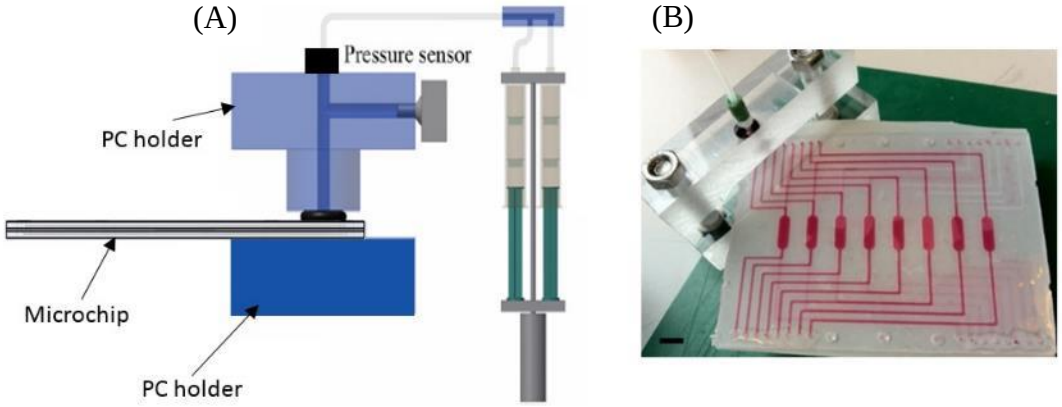

Figure S3. Burst pressure study for thiol-ene microchip. (a) Schematic view of the pressure system (1). The thiol-ene microchip was clamped between the PC holders. The pressure sensor on the top of the PC holder will measure the pressure of the set-up. The syringes are compressed to provide the pressure into the microchip. (b) Microfluidic chip filled with red dye. The inlet and outlet ports for the bottom fluidic layer and outlet for the top layer were sealed with cured thiol-ene. The inlet port of the top fluidic layer is clamped between the mechanical device.

Sample	Maximum pressure (Bars)	Temperature
3T3E + 3T3E	2.0 ± 0.66	25 °C
4T3E + 4T3E	Layers could not be bonded	
4T3E + 3T3E	> 6.0	
3T3E + 3T3E	< 0.3	37 °C
4T3E + 4T3E	Layers could not be bonded	
4T3E + 3T3E	> 6.0	

Table ST1. Tabulated data of the maximum pressure the different thiol-ene mixtures used for fabricating the microchips could withstand in different temperature conditions. All thiol-ene mixtures were prepared in stoichiometric ratios. Where 4T = tetra-thiol, 3T = tri-thiol and 3E = tri-allyl. (n = 6)

References

1. Sikanen TM, et al. (2013) Fabrication and bonding of thiol-ene-based microfluidic devices. *J Micromechanics Microengineering* 23(3):037002.
2. Sabourin D, et al. (2013) The MainSTREAM component platform: a holistic approach to microfluidic system design. *J Lab Autom* 18(3):212–28. Available at:
3. Kuschel C, et al. (2006) Cell adhesion profiling using extracellular matrix protein microarrays. *Biotechniques* 40(4):523–531.
4. Basson MD, Turowski G, Emenaker NJ (1996) Regulation of Human (Caco-2) Intestinal Epithelial Cell Differentiation by Extracellular Matrix Proteins 1. *Exp Cell Res* 305(225):301–305.
5. Zemljic Jokhadar S, Znidarcic T, Svetina S, Batista U (2007) The effect of substrate and adsorbed proteins on adhesion, growth and shape of Caco-2 cells. *Cell Biol Int* 31(10):1097–108.
6. Hubatsch I, Ragnarsson EGE, Artursson P (2007) Determination of drug permeability and prediction of drug absorption in Caco-2 monolayers. *Nat Protoc* 2(9):2111–9.
7. Borchard G (2009) The absorption barrier. *Oral Delivery of Macromolecular Drugs*, ed Bernkop-Schnürch A (Springer US, New York), pp 49–64.

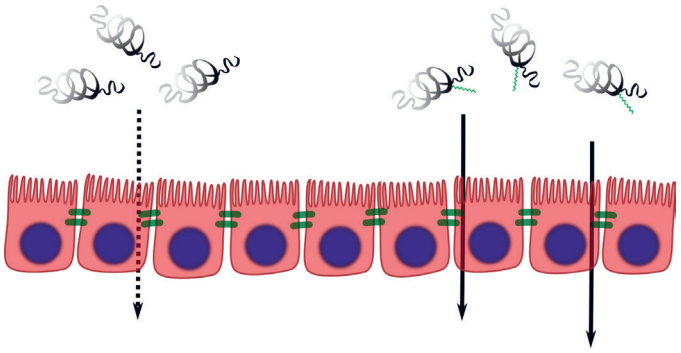

Published by:
DTU Nanotech
Department of Micro- and Nanotechnology
Technical University of Denmark
Ørsteds Plads, building 345C
DK-2800 Kgs. Lyngby